AN ABSTRACT OF THE DISSERTATION OF

Nicholas J. AuYeung for the degree of Doctor of Philosophy in Chemical Engineering presented on October 14, 2011.

Title: Hydrogen Production via a Sulfur-Sulfur Thermochemical Water-Splitting Cycle

Abstract approved: _____

Alexandre F.T. Yokochi

Thermochemical water splitting cycles have been conceptualized and researched for over half a century, yet to this day none are commercially viable. The heavily studied Sulfur-Iodine cycle has been stalled in the early development stage due to a difficult HI-H_2O separation step and material compatibility issues. In an effort to avoid the azeotropic HI-H_2O mixture, an imidazolium-based ionic liquid was used as a reaction medium instead of water. Ionic liquids were selected based on their high solubility for SO_2, I_2, and tunable miscibility with water. The initial low temperature step of the Sulfur-Iodine cycle was successfully carried out in ionic liquid reaction medium. Kinetics of the reaction were investigated by I_2 colorimetry. The reaction also evolved H_2S gas, which led to the conceptual idea of a new Sulfur-Sulfur thermochemical cycle, shown below:

$$4I_{2(l)}+4SO_{2(l)}+8H_2O_{(l)} \leftrightarrow 4H_2SO_{4(l)} + 8HI_{(l)}$$

$$8HI_{(l)} + H_2SO_{4(l)} \leftrightarrow H_2S_{(g)}+4H_2O_{(l)} + 4I_{2(l)}$$

$$3H_2SO_{4(g)} \leftrightarrow 3H_2O_{(g)}+3SO_{2(g)}+1½O_{2(g)}$$

$$H_2S_{(g)}+2H_2O_{(g)} \leftrightarrow SO_{2(g)}+3H_{2(g)}$$

The critical step in the Sulfur-Sulfur cycle is the steam reformation of H_2S. This highly endothermic step is shown to successfully occur at temperatures in excess of 800˚C in the presence of a molybdenum catalyst. A parametric study varying the H_2O:H_2S ratio, temperature, and residence time in a simple tubular quartz reactor was carried out and Arrhenius parameters were estimated.

All reactive steps of the Sulfur-Sulfur cycle have been either demonstrated previously or demonstrated in this work. A theoretical heat-to-hydrogen thermal efficiency is estimated to be 55% at a hot temperature of 1100 K and 59% at 2000 K. As a highly efficient, all-fluid based thermochemical cycle, the Sulfur-Sulfur cycle has great potential for feasible process implementation for the transformation of high quality heat to chemical energy.

Hydrogen Production via a Sulfur-Sulfur Thermochemical Water-Splitting Cycle

by Nicholas J. AuYeung

A DISSERTATION

Submitted to

Oregon State University

in partial fulfillment of

the requirements for the

degree of

Doctor of Philosophy

Presented October 14, 2011

Commencement June 2012

Doctor of Philosophy Dissertation of Nicholas AuYeung presented on October 14, 2011

APPROVED:

_____

Major Professor, representing Chemical Engineering

_____

Head of the School of Chemical, Biological, and Environmental Engineering

_____

Dean of the Graduate School

I understand that my dissertation will become part of the permanent collection of Oregon State University libraries. My signature below authorizes release of my dissertation to any reader upon request.

_____

Nicholas J. AuYeung, Author

ACKNOWLEDGEMENTS

I first would like to acknowledge the financial support for the project. Early work was funded by the California Energy Commission. This material is based upon work supported by the National Science Foundation under Grant No. 0748280.

I would like to thank my advisor, Alex Yokochi, who has invested so much time, effort, and patience into my experience as a graduate student. His philosophy is to motivate through inspiration and because of him I will always set my goals high. Always approachable, his enthusiasm and optimism is always contagious and has made graduate school a wonderful experience for me. I am also grateful that he allowed me to pursue interests outside of school and live a balanced life.

My graduate committee has been very helpful throughout my studies. In addition to having them serve on my committee, I have also had the honor being a student in classes taught by my committee Professors Chih-hung Chang, Richard Peterson, and Michael Lerner. Special thanks go to committee member Roger Ely for convincing me to attend Oregon State and welcoming me to his research meetings early on. His research group would spearhead the OSU Hydrogen Club, which has been a major outlet for me in the past few years.

I also would like to acknowledge my labmates in the Yokochi lab-Alex Bistrika, Kevin Caple, Matt Delaney, Nathan Coussens, Malachi Bunn, Victoria Johnson, and Anees Sardari who have always been supportive sounding boards for many ideas and issues that have come up throughout my studies here.

Thanks also go to Andy Brickman for his countless pieces of practical advice; Manfred Dittrich for his willing help in many machining tasks; and Mohammad Azizian, Alan Milligan, and Glenn Watson for their consultation on various analytic issues.

I must also thank Skip Rochefort, who gave me excellent advice upon meeting him at an AIChE conference as an undergraduate: "Well, I hope you're considering graduate school". Both Skip and my influential high school chemistry teacher Stan Bebyn would agree with my worldview that chemists should also be runners. Professors Jim Stuart, Richard Parnas, Michael Cutlip, Ben Wilhite, and Joe Helble were all wonderful mentors at UConn who invested many outside-the-classroom hours into the biodiesel project and gently pushed me into pursuing an advanced degree.

Most importantly, I would like to thank my parents, brothers Ben and Nate, and my wonderful partner Aida for all their unwavering love and support. My parents both instilled in me the principles of hard work and never giving up. Through all these years they have always believed in me and have shared my emotional investment in whatever I decided to pursue. They have both made countless sacrifices for me and I will forever be grateful. Without them I would not be here.

Table of Contents

1 INTRODUCTION 1
1.1 Background 1
1.2 Literature Review 4
2 INVESTIGATION OF THE BUNSEN REACTION IN IONIC LIQUIDS 22
2.1 Screening of commercially available ionic liquids as to their ability to release hydrogen iodide ($HI_{(g)}$) from the Bunsen reaction. 24
2.2 Investigation of Bunsen Reaction Kinetics 27
2.3 Investigation into the evolution of hydrogen sulfide via the side reaction: 34
2.4 Demonstration of sulfur trioxide/sulfuric acid separation from ionic liquid 36
3 DEMONSTRATION OF STEAM REFORMATION OF H_2S 37
3.1 Preliminary Proof of Concept 37
3.2 Investigation of Thermal Splitting of Hydrogen Sulfide in a Quartz Reactor 43
3.3 Parametric Study of Steam Reformation of Hydrogen Sulfide 48
4 PROCESS DESIGN OF SULFUR-SULFUR CYCLE 68
4.1 Estimation of Overall Thermal Efficiency of the Sulfur-Sulfur Cycle 68
4.2 Process Considerations 73
5 CONCLUSION AND FUTURE WORK 76
5.1 Conclusion 76
5.2 Future Work 77
BIBLIOGRAPHY 81
APPENDICES: 90
APPENDIX A: Physical and Chemical Properties of Sulfur-Sulfur Cycle Species 93
APPENDIX B: Kinetics of the Bunsen Reaction 95
APPENDIX C: Preliminary Investigation into Steam Reformation of Hydrogen Sulfide 101
APPENDIX D: Steam Reformation of Hydrogen Sulfide 103

LIST OF FIGURES

FIGURE PAGE

Figure 1.1: A thermochemical cycle conceptualized as a heat engine. 2
Figure 2.1: Structures of some imidazolium ionic liquids 25
Figure 2.2: Spectral differences of iodine in dichloromethane with and without ionic liquid [BMIM][OTf]. 29
Figure 2.3: Spectral variation of iodine in ionic liquid [BMIM][OTf]with temperature (diluted in dichloromethane). 30
Figure 2.4: Normalized iodine concentration profile over time for small-scale batch reactions. 32
Figure 2.5: Arrhenius Plot of Bunsen Reaction in Ionic Liquid 33
Figure 2.6: Conversion of SO_2 to H_2S, measured as H_2S concentration in reactor headspace. 35
Figure 2.7: Detection of sulfur trioxide in headspace of heated ionic liquid at 160˚C 36
Figure 3.1: Gibbs free energy change, ΔG, from 800-2000K. 38
Figure 3.2: Theoretical equilibrium composition of system with feed of 1 mole H_2S and 2 mol H_2O. 38
Figure 3.3: Steam reformation apparatus 39
Figure 3.4: Hydrogen evolution from water heated in stainless steel tube at high temperature. 40
Figure 3.5: Hydrogen sulfide conversion to sulfur dioxide via steam reformation at various temperatures. 41
Figure 3.6: Hydrogen production via steam reformation of hydrogen sulfide at various temperatures 42
Figure 3.7: Hydrogen to SO_2 ratio for preliminary steam reformation of hydrogen sulfide trials. 42
Figure 3.8: Conversion of H_2S to H_2 in quartz tube in presence of Mo wire. 45
Figure 3.9: Fraction of initial H_2S remaining after thermal decomposition in presence of Mo wire 45
Figure 3.10: Hydrogen sulfide decomposition in quartz reactor 46
Figure 3.11: Hydrogen production in quartz tube 47
Figure 3.12: Comparison of thermodynamic predictions of equilibrium concentrations based upon minimization of Gibbs Free Energy and stoichiometric methods. 49
Figure 3.13: Quartz tube reactor with catalyst wire 51
Figure 3.14: Experimental apparatus for steam reformation of H_2S. 52
Figure 3.15: Normalized concentrations H_2 at various H_2O:H_2S ratios. 54

Figure 3.16 Normalized concentrations H_2S at various H_2O:H_2S ratios. 54
Figure 3.17 Normalized concentrations of SO_2 at various H_2O:H_2S ratios. 55
Figure 3.18 H_2:SO_2 ratio at various H_2O:H_2S ratios. 55
Figure 3.19: Mass Balance on sulfur at various H_2O:H_2S ratios. 56
Figure 3.20: Normalized concentration of H_2S at various residence times. 57
Figure 3.21: Normalized concentration of SO_2 at various residence times. 58
Figure 3.22: Normalized concentration of H_2S at various residence times. 58
Figure 3.23: H_2:SO_2 ratio at various residence times. 59
Figure 3.24: Mass balance on sulfur at various residence times. 60
Figure 3.25: Hydrogen yield from steam reformation over other surfaces. 61
Figure 3.26: Sulfur dioxide yield from steam reformation over other surfaces. 62
Figure 4.1: Sensitivity of overall thermal efficiency to H_2O:H_2S ratio using in the steam reformation step. Thermal efficiency is based on the HHV of H_2O (286 kJ/mol). .. 71
Figure 4.2: Dependence of extent of reaction for both thermal splitting (ε_1) and steam reformation (ε_2) on temperature and H_2O:H_2O ratio. 71
Figure 4.3: Conceptual Diagram of Sulfur-Sulfur Cycle Process 75
Figure 5.1: Gas-liquid contacting reactor for H_2S production 78
Figure 5.2: Conceptual diagram of membrane reactor 79
Figure 5.3: Predicted outlet composition from steam reformation reactor operating at 1500°C with a 20:1 H_2O:H_2S ratio, based on kinetic parameters obtained in this work. 80

LIST OF TABLES

TABLE PAGE

Table 2.1: Ionic liquids studied and their conjugate acids 23
Table 2.2: Parameters for hydrogen sulfide generation 34
Table 3.1: Apparent Arrhenius parameters from steam reformation of H_2S studies in presence of molybdenum wire and thermal splitting of H_2S as determined by Karan et al. without catalyst. Reported variance is ± 1 standard error. 66
Table 4.1: Energy inputs for a Sulfur-Sulfur Cycle operating at ~1100 K, with a 2:1 H_2O:H_2S ratio in the steam reformation section. 69

NOMENCLATURE AND ABBREVIATIONS USED IN THE TEXT

Symbol	Description	[units]
[BMIM][OTf]	1-Butyl-3-methylimidazolium tetrafluoroborate	
[BMIM][PF_6]	1-Butyl-3-methylimidazolium Hexafluorophosphate	
[BMIM][OTf]	1-Butyl-3-methylimidazolium trifluoromethanesulfonate	
[BMPL][FAP]	1-Butyl-1-methylpyrrolidinium tris(pentafluoroethyl)trifluorophosphate	
C_i	Concentration of species i	Varies, M, ppm, etc
C_r	Concentration ratio for solar concentrator	
E_a	Activation Energy	J/mol or kJ/mol
[EMIM][HSO_4^-]	1-Ethyl-3-methylimidazolium hydrogensulfate	
[FAP]	tris(pentafluoroethyl)trifluorophosphate	
ΔG	Gibbs Free Energy Change	kJ/mol
ΔH	Enthalpy Change	kJ/mol
HI	Hydrogen Iodide	N/A
HMIM.Tf_2N	1-Hexyl-3-methylimidazolium bis(triflluoromethylsulfonyl)imide	
I	Solar intensity	W/m^2
k	Bunsen reaction rate constant	s^{-1}-M^{-2}
K	Equilibrium Constant	
k’	Pseudo-first order Bunsen rate constant	s^{-1}
k_1	Irreversible rate constant thermal decomposition of H_2S	s^{-1}
K_1	Equilibrium constant, thermal decomposition of H_2S	
k_1’	Pseudo-first order irreversible rate constant thermal Decomposition of H_2S	s^{-1}
$k_{1,0}$	Pre-exponential term (frequency factor)	s^{-1}

	for thermal decomposition of H_2S	
$k_{1,m}$	Reparameterized pre-exponential term (frequency factor) for thermal decomposition of H_2S	s^{-1}
k_2	Irreversible rate constant for steam reformation of H_2S	s^{-1}
K_2	Equilibrium constant for steam reformation of H_2S	
k_2'	Pseudo-first order irreversible rate constant for steam reformation of H_2S	s^{-1}
$k_{2,0}$	Pre-exponential term (frequency factor) for steam reformation of H_2S	s^{-1}
$k_{2,m}$	Reparameterized pre-exponential term (frequency factor) for steam reformation of H_2S	s^{-1}
N	Number of samples	
[OTf]	trifluoromethanesulfonate	
Q	Heat	kJ/mol
R	Ideal Gas Constant	8.314 J/mol-K
s	Standard deviation	varies
SE	Squared Error	varies
SSE	Sum of the Squared Error	varies
T	Temperature	K, °C
T_m	Median temperature used in reparameterization	K
TBA.OTf	Tetrabutylammonium trifluoromethanesulfonate	
[TMPP]		
W	Work	kJ/mol
y_i	Mole fraction	
ε_1	Extent of reaction for thermal decomposition of H_2S	
ε_2	Extent of reaction for steam reformation of H_2S	
η	Overall thermal efficiency	
η_{abs}	Collector absorption efficiency	
σ	Stephan-Boltzmann Constant	5.6705×10^8 W/m^2-K^4
ν	Degrees of freedom	
χ_ν^2	Reduced chi-squared function	

For Vic Sandone, my late grandfather, who paved the way from Connecticut to Corvallis in 1949 and watches over me from a firetower somewhere in the Oregon woods…

1 INTRODUCTION

1.1 Background

Hydrogen has been identified as the energy carrier of the future since hydrogen fuel cells, the ideal end use application, emit only water. From a production point of view, hydrogen is the most abundant element in the universe, and can be harnessed from relatively abundant feedstocks such as water or biomass. Besides being environmentally benign, hydrogen fuel cells offer greater efficiencies when compared to traditional methods of electricity generation.[1] Although fuel cell development, hydrogen storage, and hydrogen infrastructure are all areas of concern, the overwhelming limiting factor in development of a hydrogen economy is a reliable, efficient, and sustainable method of hydrogen production. A sustainable hydrogen production method is one that excludes fossil fuels (both in the production steps and the feedstock itself), uses a readily available feedstock (water), does not generate hazardous waste, and most importantly, has a favorable energy balance.

While today hydrogen is primarily produced via the steam reformation of methane,[2] a production route using water as a feedstock would be more desirable. Electrolysis of water suffers from reliance on electricity, which is either derived from cheap fossil sources or currently expensive, renewable sources such as wind or solar. Although water can also be thermally decomposed, the temperatures required make it an unfeasible process due to material constraints.[2]

In light of the shortcoming of materials of construction suitable for high temperature direct thermal decomposition, a thermochemical cycle using energy derived from a solar concentrator has the potential to be a realistic and feasible method of carbon-free hydrogen production.[3] A thermochemical cycle can be conceptualized as a heat engine, which can convert heat into work (see Figure 1.1).[4] In a thermochemical cycle, heat is used to drive endothermic reactions and produce chemical energy in form of H_2. In contrast to the thermal decomposition of water which requires temperatures greater

than 2500°C, thermochemical cycles can be carried out at temperatures that are currently attainable using solar concentrators (nearly 2000°C) or high temperature nuclear reactors (~850°C).[5]

Thermochemical cycles are evaluated by their overall thermal efficiency, which is a metric for how efficiently a cycle can convert heat into work. This primary heat, however, always has a production efficiency associated with it. For instance, a solar thermal concentrator must optimize optical efficiency and minimize radiative losses. After hydrogen is produced, hydrogen is most efficiently used in fuel cells to produce electricity. Taking everything into account, it would much more efficient to simply produce electricity from heat via a Rankine, Brayton, or combined cycle, however storage of this electricity is problematic. Unlike batteries, flywheels, or compressed air, hydrogen has the ability to be a pathway for energy storage in form of a fluidic chemical fuel.

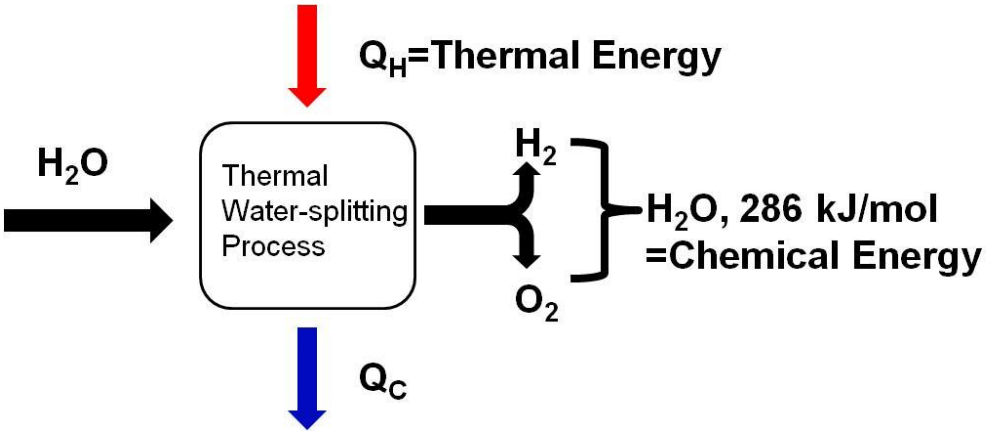

Figure 1.1: A thermochemical cycle conceptualized as a heat engine.

The limiting factor in thermochemical cycle development is development of a working thermochemical cycle itself. Among proposed cycles of the last 40 years, the Sulfur-Iodine cycle appears to be the most heavily researched. The Sulfur-Iodine cycle uses heat and water to produce hydrogen and oxygen with intermediate species containing sulfur or iodine being recycled. Nevertheless, the current sulfur-iodine cycle is plagued by high heat loads involved in the concentration, purification, and decomposition of intermediate acid products (HI and H_2SO_4), which may be mitigated by

removing excess water.[6] Less residual water would result in less energy being expended into separation processes. Furthermore, an alternative reaction medium other than water such as an ionic liquid has the potential to make the sulfur iodine cycle a viable process for hydrogen production.

Relatively new to the chemical industry, ionic liquids are non-volatile solvents typically composed of an organic cation and an inorganic anion. The term "ionic liquid" stems from the class of compounds which exist in the liquid phase for a wide range of temperatures; typical boiling points are over 400°C and typical melting points below 150°C. With over 10^{18} identified possible organic salts, ionic liquids can be "tailor-made" for specific applications.[7] The low temperature, liquid-phase reaction (more commonly known as the Bunsen reaction) between iodine, sulfur dioxide, and water performed in an ionic liquid would require only a stoichiometric or near stoichiometric amount of H_2O, and the resulting HI and H_2SO_4 would no longer be in an aqueous phase. This opens up the possibility of reactions involving the two product acids, such as generation of H_2S:

$$H_2SO_4 + 8HI = H_2S + 4I_2 + 4H_2O \qquad \text{Eq. 1.1}$$

As detailed in the following document, the results of using an ionic liquid reaction medium led to the conceptualization of a new "Sulfur-Sulfur" thermochemical cycle that has distinct advantages over the traditional sulfur-iodine cycle and other thermochemical cycles in general. The generation of H_2S affords facile in situ regeneration of I_2, avoiding HI-H_2O separation and subsequent threat of I_2 solidification downstream. The H_2S can then be steam reformed at high temperature. Proof of concept experiments and a kinetic model that describes the H_2S-H_2O system at high temperature will be shown. The cycle has an estimated upper bound thermal efficiency of roughly 55% (heat-to-H_2). In short, an all-fluid thermochemical cycle has been shown to be feasible based on theoretical thermodynamic calculations as well as key preliminary experiments.

This work is an improvement to the process chemistry of the Sulfur-Iodine thermochemical cycle. From the very beginning, the motivation for this project has come

from the principles of green chemistry and green engineering, especially with respect to energy efficiency.

1.2 Literature Review

Hydrogen production encompasses many facets of physics and engineering, many of which will be covered very briefly, if at all, by this literature review. This literature review encompasses past research efforts concerning the sulfur family of thermochemical cycles, the decomposition of hydrogen sulfide (H_2S), and ionic liquids due to their importance in this project.

1.2.1 Thermochemical cycles

The most straightforward approach to splitting water is the thermal decomposition of water itself. Temperatures must approach at least 2500 K to facilitate this process, however since the Gibbs free energy (ΔG) value for water dissociation to H_2 and O_2 does not reach zero until 4310 K, higher temperatures are desirable. The unfortunate problem with direct solar hydrogen production is that few materials will withstand the high temperatures required. Even when this approach is successful, the resulting H_2 and O_2 must still be separated.[3]

Thermochemical cycles present theoretical thermal efficiencies on the order of 50%.[8] One of the most promising routes to producing hydrogen is thermochemical water splitting, which uses multiple reactions to avoid the high temperatures associated with direct solar hydrogen production. There are many inevitable losses in efficiency associated with undergoing multiple reactions and separations.[3] Nevertheless, since thermochemical cycles produce O_2 and H_2 in separate steps, they avoid recombination, which is an important advantage.[2]

The simplest cycles are metal oxide cycles and consist of only two steps:

$$M_xO_y = M_xO_{y-1} + \tfrac{1}{2}O_2 \qquad \text{Eq. 1.2}$$

$$MxO_{y-1} + H_2O = M_xO_y + H_2 \qquad \text{Eq. 1.3}$$

Numerous metal/metal oxide couples have been proposed however only the Zn/ZnO and FeO/Fe_3O_4 couples have been seriously considered due to their

thermodynamic feasibility at temperatures under 2500 K. Apart from the sheer magnitude of high temperatures required, the Zn/ZnO cycle suffers from Zn-O_2 recombination at high temperature. Rapid quenching of the metal vapor and O_2 must occur to avoid this, which is speculated to be a surface-driven reaction by Steinfeld.[9] Reducing agents have also been considered as additives to reduce oxygen and avoid recombination.[2] Recently, mixtures of different metals such as Zn, Sn, Mn, Fe and their oxides have been tested by Bhosale et al. and synthesized using sol-gel techniques to produce porous, nanostructured networks for maximum surface area. Over the course of several cycles, however, this morphology was observed to decrease due to grain growth and sintering occurring at high temperatures.[10]

1.2.2 Heat sources

Thermochemical cycles such as the sulfur-iodine and hybrid-sulfur cycle require process heat at temperatures on the order of 1200 K. In 1966, Funk cited nuclear reactors as a good candidates for generating high quality process heat for water splitting[11]. In the following decade the High Temperature Gas-cooled Reactor (HTGR) saw much development.[12] Harth and Hoelein simulated the HTGR by heating helium at 40 bar via electrically resistive heating to 1273 K. The endothermic steam reformation of methane was successfully carried out in a tubular reactor exposed to this circulating hot helium gas.[13]

The concentration of sunlight can also be used to generate the high temperatures necessary for thermochemical hydrogen production. This is achieved by use of a heliostat that directs sunlight to a well insulated receiver cavity.[14] Light is emitted through an opening called an aperture. Inside the cavity, the light is reflected multiple times to increase absorbance of energy. There is always a tradeoff between having a large aperture and larger radiation losses.[15]

The key disadvantage of solar versus nuclear is the variation of sunlight with weather, time of day, and time of year. This can be overcome over short timeframes by storing excess thermal energy.[16] Although thermochemical cycles have higher Carnot

efficiencies as temperature increases, Perkins et al. point out that the lower temperature solar cycles would not suffer radiative losses to the same extent of a higher temperature solar cycle.[2] If a solar concentrator has a concentration ratio of C_r; solar intensity of I, [W/m^2]; and temperature T, [K]; the absorption efficiency, η_{abs}, is

$$\eta_{abs} = 1 - \frac{\sigma T^4}{IC_r}, \qquad \text{Eq. 1.4}$$

where σ is the Boltzmann constant 5.6705 x 10^8 W/m^2-K^4. For each solar concentrator, there exists a stagnation temperature, T_{stag}, which is the highest temperature attainable by the concentrator for a given concentration ratio:

$$T_{stag} = \left(\frac{IC_r}{\sigma}\right)^{\frac{1}{4}} \qquad \text{Eq. 1.5}$$

The maximum efficiency of a thermochemical cycle is this absorption efficiency multiplied by the Carnot efficiency:

$$\eta_{max} = \left(1 - \frac{\sigma T^4}{IC_r}\right) * \left(1 - \frac{T_C}{T}\right) \qquad \text{Eq. 1.6}$$

Where T_c is the temperature that heat is rejected to, [K]. From Eq. 1.5, an optimal temperature can be found by taking the derivative with respect to T and setting equal to 0:[15]

$$T_{opt}^5 - (0.75T_L)T_{opt}^4 - \frac{T_C IC_r}{\sigma} = 0 \qquad \text{Eq. 1.7}$$

1.2.3 Sulfur Family of Thermochemical Cycles

Significant worldwide interest in thermochemical water splitting was evident at the 1969 International Round Table on Direct Production of Hydrogen with Nuclear Heat held in Ispra, Italy. This meeting resulted in the creation of 24 cycles, which can loosely be grouped in three categories: mercury, iron-chloride, and sulfur.[17] Another screening survey was done by Brown for General Atomics in 2000, which took into account the number of elements, number of steps, phases of matter, and the chemical compatibility of species involved among other criteria. The work of Brown included hybrid cycles, which

are both thermochemical and electrochemical in nature. The five highest rated cycles in descending order were: the Westinghouse (Hybrid Sulfur), Mark 13, UT-3 (Br,Ca, Fe), sulfur-iodine, and Julich Center EOS (iron sulfates).[18]

1.2.3.1 The Sulfur-Iodine cycle

The sulfur-iodine cycle in particular has undergone much investigation, not only in academia but also by corporations such as General Atomics.[19] Using state of the art decomposition and separation strategies, Goldstein et al. estimated the upper bound total cycle efficiency to be 51% (higher heating value).[20] The sulfur-iodine cycle consists of three reactions, the first of which is the exothermic Bunsen Reaction (Eq. 1.8). In the Bunsen reaction, H_2O reacts with dissolved SO_2 and I_2 to form two aqueous phase acids (H_2SO_4 and HI) that partition gravimetrically. The Bunsen reaction is commonly carried out in an excess of H_2O to make the reaction spontaneous.[21]

Once separated, the acids are each purified and then thermally decomposed, the products of HI decomposition being H_2 and I_2 and the products of H_2SO_4 decomposition being H_2O, SO_2, and O_2.[20] The sulfuric acid decomposition is actually two reactions, with H_2SO_4 first forming SO_3 and H_2O, followed by SO_3 decomposing to form O_2 and SO_2, the latter of which is recycled. The sulfur-iodine reaction scheme is as follows:

$$I_{2(s)} + SO_2(g) + 2H_2O = H_2SO_{4(aq)} + 2HI_{(aq)} \qquad \text{Eq. 1.8}$$

$$2HI(g) = I_{2(g)} + H_{2(g)} \qquad \text{Eq. 1.9}$$

$$H_2SO_{4(g)} = SO_{3(g)} + H_2O_{(g)} \qquad \text{Eq. 1.10}$$

$$SO_{3(g)} = SO_{2(g)} + \tfrac{1}{2}\, O_{2(g)} \qquad \text{Eq. 1.11}$$

Kubo et al. managed to run the sulfur iodine cycle continuously at a production rate of 32 liters per hour for 20 hrs.[22]

Two side reactions have been known to occur in the Bunsen reactor:

$$H_2SO_4 + 6HI = S + 3I_2 + 4H_2O \qquad \text{Eq. 1.12}$$

$$H_2SO_4 + 8HI = H_2S + 4I_2 + 4H_2O \qquad \text{Eq. 1.1}$$

Sakurai reports that the sulfur formation reaction is dominant as opposed to the H_2S formation reaction. These side reactions occur with increasing acid content and decreasing I_2 content, which can be explained by mass action. In addition to side reactions, Sakurai et al. also observed that higher temperatures may lead to the reverse of the Bunsen reaction.[23] Lee et al. did an extensive study on the reactant ratios and found that a 4-6 molar excess of I_2 (with respect to SO_2) and 11-13 molar excess of water were optimal in order to avoid either of these side reactions.[24] Goldstein used a 9:1 ratio of H_2O to I_2 for his efficiency calculations.[25] Norman et al. at General Atomics advocated using 7 times as much I_2 as H_2O by weight to facilitate the two-phase separation of Bunsen products, which corresponds roughly to the same molar ratios as prescribed by Lee.[26] Giaconia et al. and Kubo et al., found that increased reactor temperature allowed for increased loading of I_2, which ultimately led to a lower proportion of the H_2SO_4 contaminating the $HI_{(aq)}$ phase.[6, 22]

1.2.3.1.1 Acid Purification and decomposition

Due to the two products (HI and H_2SO_4) being in an aqueous state, separations are needed to remove excess water. The most energetically costly parts of the cycle are the decompositions of hydroiodic and sulfuric acids.[20] The decomposition of hydroiodic acid requires temperatures of 300-450ºC.[27] Nomura reports selectivities of H_2 greater than 80% from HI using an active carbon catalyst and silica membrane, however they also calculated the use of such a device did not significantly improve the overall thermal efficiency of the sulfur-iodine cycle.[28]

Decomposition of sulfuric acid is a two-step process; sulfuric acid is first decomposed to SO_3 and H_2O, then the SO_3 is cracked to produce O_2 and reform SO_2. Huang and T'Raissi carried out flowsheet simulations using ASPEN software in which H_2SO_4 was concentrated and decomposed using 2 plug-flow reactors in series and found that 100% conversion H_2SO_4 of was possible at a temperature of only 750 K. Catalysts can be used to reduce the high temperatures required to decompose sulfuric acid.[21] Barbarossa found a 300 °C decrease in onset decomposition temperature (500 ˚C vs. 800 ˚C) using both Ag–Pd/PdO and Fe_2O_3 as catalysts.[29] Sandia National Laboratory has

been active in developing a silicon carbide "bayonet" reactor in which H_2SO_4 is heated within the second of two concentric tubes, reacts with catalysts, reaches the end of the outer tube, and returns via the inner tube. Since all connections can be made prior to heating acid and after the products (SO_2, O_2, H_2O) have cooled down substantially, PTFE fittings can be used. Silicon carbide bayonet reactors are also commercially available.[30]

Giaconia et al. advocates minimizing the water excess in the Bunsen reaction, for a higher heat input is required in these later separation processes.[6] The Fischer reaction converts SO_2 (with base), I_2, and H_2O in a 1:1:1 molar ratio respectively (as opposed to a 1:1:2 ratio) to form SO_3 (with base) and HI, in the presence of methanol (or equivalent):

$$I_2 + SO_2 + H_2O = SO_3 + 2HI \qquad \text{Eq. 1.13}$$

It is known that the Fischer reaction is first order with respect to each reactant (SO_2, I_2, and H_2O) in either acidic (pH<7) or basic conditions (pH>9), and that the rate constant is highly dependent on pH.[31] Common bases used are pyridine and imidazole.[32] The reaction is typically carried out in an alcoholic solvent. Although the exact mechanism of the reaction is unknown, Sherman observed that the lower pKa of the solvent, the greater participation of water in the reaction.[33] W. Fischer was able to isolate SO_3 as an intermediate in the Bunsen reaction, and speculated that the Bunsen and Fischer reactions share the same mechanisms.[34] Reaction rate constant for the Fischer reaction are on the order of $10^{11} cm^6\text{-}min^{-1}\text{-}mol^{-2}$.[32] Rate constants for the Bunsen reaction were not found, however on a qualitative basis, Kubo et al. , do report a rapid reaction.[22]

In an effort to decrease the amount of excess water, Stewart et al. used a Nafion-117® membrane to concentrate HI from H_2O by separation factors of 200-700. However, due to the corrosive nature of acids, membrane lifetime is of significant concern.[35]

Mason and Bowman created a variation of the sulfur-iodine cycle using magnesium oxide in a minimum amount of water:

$$MgO_{(s)} + SO_{2(g)} = MgSO_{3(s)} \qquad \text{Eq. 1.14}$$

$$MgO(s) + MgSO_3(s) + I_2 = MgSO_{4(s)} + MgI_{2(s)} \qquad \text{Eq. 1.15}$$

$$MgI_{2(s)} + H_2O_{(l)} = MgO_{(s)} + 2HI_{(g)} \quad \text{Eq. 1.16}$$

$$2HI_{(g)} = H_{2(g)} + I_{2(g)} \quad \text{Eq. 1.9}$$

$$MgSO_{4(s)} = MgO_{(s)} + SO_{2(g)} + ½\ O_{2(g)} \quad \text{Eq. 1.17}$$

This approach has largely been overlooked, however due to the participation of solids and not fluids. Mason and Bowman recommended tantalum and lanthanum as possible other choices for metals, since their respective sulfates decompose at lower temperatures than $MgSO_4$ (1350K).[36]

In 2009, Giaconia et al. attempted a similar strategy by adding $PbSO_4$(s) to the Bunsen reaction mixture to precipitate PbI_2:[37]

$$PbSO_{4(s)} + 2HI_{(aq)} \rightarrow PbI_{2(s)} + H_2SO_{4(aq)} \quad \text{Eq. 1.18}$$

Dehydrated phosphoric acid (HPO_3) is then added to release anhydrous HI gas and form $Pb(PO_3)_2$, which is then treated with the $H_2SO_{4\ (aq)}$ created previously in Eq. 1.18 to regenerate $PbSO_{4(s)}$ and $H_3PO_{4(aq)}$:

$$PbI_{2(s)} + 2HPO_3 \rightarrow 2HI_{(g)} + Pb(PO_3)_2 \quad \text{Eq. 1.19}$$

$$Pb(PO_4)_2 + 3H_2SO_{4(aq)} \rightarrow 3PbSO_{4(s)} + 2H_3PO_{4(aq)} \quad \text{Eq. 1.20}$$

1.2.3.1.2 Material compatibility

The acidic HI-I_2-H_2O mixture, collectively known as "HIx", is known to be extremely corrosive. Wong et al. did high temperature immersion tests on two refractory metals, a reactive metal, a superalloy, and a ceramic. The niobium and tantalum-based refractory metals showed little to no corrosion (mass change) due to a uniform passivation layer forming. Although forming a similar passivation layer, the reactive zirconium metals showed pit formation, and the superalloy C-276 (nickel-based) saw significant mass change. Ceramic mullite showed minimal mass change and was recommended for interconnect components.[27]

R.L. Ammon at the Westinghouse Electric Corporation carried out extensive study on materials suitable for their hybrid-sulfur cycle. For the H_2SO_4 vaporizer,

silicon, silicon nitride, and silicon carbide showed good corrosion resistance in high temperature 1000-hr exposure testing. For the decomposition reactors, stainless steel 444 along with alonized Hastelloy G and Incoloy 800 were identified as possible candidate materials after 1000 hr exposure to both inlet (H_2O/SO_3) and outlet (H_2O, SO_2, O_2, and SO_3) environment at 1144 K.[38]

1.2.3.1.3 Alternative Reaction Media

There have been attempts to solve problems associated with excess water by using alternative reaction media. De Beni et al. attempted to increase separation of the two acidic phases by using liquid SO_2 as a solvent, which acts as an intermediate phase between the HIx phase and the H_2SO_4 phase. Water is consumed by the upper H_2SO_4 phase, as well as the HIx phase during the reaction. Once all I_2 has reacted in the SO_2 phase, it rises above the H_2SO_4 aqueous phase, leading to contamination of the aqueous phase by HI. Side reactions between HI and SO_2 like those described by Sakurai between HI and H_2SO_4, are known to occur.[23, 39, 40] De Beni et al. advocated carrying the reaction out to the point where not all I_2 was consumed, then removing the upper H_2SO_4 aqueous phase and allowing the SO_2 evaporate to yield a nearly azeotropic HIx phase. To enable a complete reaction, addition of low boiling and high boiling organic solvents (with liquid SO_2) was also investigated. Low boiling solvents (dimethylether, diethylether, and acetone) were found to increase concentration of the H_2SO_4 phase up to 45% acid, however an actual process would require cooling to avoid solvent evaporation from the liquid phase. Tributylphosphate (TBP), a higher boiling liquid, enabled an HIx phase with 70% HI, which is higher than the azeotropic point. However, this concentrated HIx cannot be separated from the TBP since the TBP degraded above 320 K and extraction using water resulted in dilution of HI to 20%.[40] More recently, Giaconia et al. revisited using TBP and was also unsuccessful in extracting an HI-rich HI-H_2O mixture from the TBP.[37]

Taylor et al. investigated using ionic liquids as extraction agents to remove HI from the reaction mixture. Several imidazolium, morphonium, phosphonium and pyrollidinium based cations with either tris(pentafluoroethyl)trifluorophosphate [FAP],

bis(trifluoromethylsulphonyl)imide [Tf_2N^-], and trimethylpentyl)phosphinate [TMPP] hydrophobic anions were tested. The bis(trifluoromethylsulphonyl)imide [Tf_2N^-] anion performed the best and removed upwards of 25% of HI into the organic phase, compared to 15.9% observed when the authors used TBP to evaluate these new solvents compared to DeBeni. Taylor el al. reason that although a hydrophobic anion, the [Tf_2N^-] anion is a better choice for an extracting agent since it more hydrophilic than the [FAP] anion and can accept more water, which is usually in equilibrium with HI and thus co-extracting. Unfortunately, organic cations from the ionic liquid were detected in the aqueous Bunsen phase, signaling poor solvent stability. It is thought that I- anions from HI match up with organic cations and migrate to the aqueous phase.[41]

1.2.3.2 Hybrid Sulfur Cycle

The hybrid sulfur cycle, also known as the Westinghouse Cycle, consists of one electrochemical step and one thermochemical step. The electrochemical step achieves reduction of water in the presence of sulfur dioxide to form hydrogen and sulfuric acid at a theoretical voltage of 0.17 V, which is significantly lower than that of water electrolysis (1.23 V). The second step is the thermal decomposition of sulfuric acid at high temperatures, a step which is identical to that of the sulfur-iodine cycle:[42]

$$2H_2O_{(l)} + SO_{2(g)} = H_2SO_{4(aq)} + H_{2(g)} \qquad 0.16\ V \qquad \text{Eq. 1.21}$$

$$H_2SO_{4(g)} = SO_{2(g)} + \tfrac{1}{2}\ O_{2(g)} + H_2O(g) \qquad \text{Eq. 1.22}$$

Gorensek et al., carried out flowsheet models using a PEM electrolyzer operating at 0.6V/500 mV/cm^2 and a bayonet reactor for H_2SO_4 decomposition, where the high temperature heat source was a high temperature gas cooled reactor (HGTR). The overall thermal efficiency was found to be 35% (lower heating value (LHV)) and 41% (higher heating value (HHV)) assuming an efficiency for the available electrical power of 45%. A PEM conventional (water) electrolysis plant operating under the same conditions and assumptions would have a 30% (LHV) overall thermal efficiency, while conventional alkaline electrolysis would fare even worse (28% LHV).[30]

In an economic investigation of potential routes to hydrogen utilizing high temperature solar thermal heat, Graf et al. estimated the hybrid sulfur cycle had the lowest conservative price ($8.0/ kg H_2)) compared to a metal oxide thermochemical cycle ($18.8/ kg H_2) and electrolysis ($6.8/ kg H_2). In optimistic scenarios, the hybrid sulfur cycle actually had the highest price ($3.9/kg H_2) versus $3.5/kg H_2 for the metal oxide cycle and $2.1/kg H_2 for the electrolysis plant.[43]

The electrolysis section of the hybrid sulfur cycle has been recognized as being especially suited to using solar photovoltaic electricity due to the low voltage required relative to conventional electrolysis. Lower voltage requires less solar cells, and hence lower costs. Hinkley et al. predicted that a hybrid sulfur plant operating with a grid powered electrolyzer and solar thermal driven acid decomposer would have a lower H_2 price ($5.16/kg H_2) than a conventional alkaline electrolyzer running off grid electricity ($5.57/kg H_2). This illustrates the economic and efficiency advantage of using solar thermal heat to drive chemical reactions directly in comparison to a purely electrochemical process. A hybrid solar cycle operating with grid buffered PV and PV-only increased the price to $7.05 and $7.27 per kg H_2 respectively. It should be noted, however, that the PV-only scenario assumed only ~5 hours of intermittent operation per day, which is undesired from the standpoint of electrode lifetime. The grid-buffered PV case also would suffer from non-steady state operation.[44]

1.2.4 Thermal Methods of Hydrogen Sulfide Decomposition

Hydrogen production from hydrogen sulfide is receiving increased attention in the energy community due to its prevalence in proximity to natural gas wells and geothermal features. An estimated 4.2 million tons of H_2S are produced each year from natural gas wells (1.8 million tons) and oil refineries (2.4 million tons), the latter of which primarily from sweetening and desulfurization processes.[45] The traditional method of dealing with H_2S is the Claus process, which consists of two exothermic steps:

$$2H_2S+3O_2 = 2SO_2+2H_2O \quad (1000\text{-}1200^{\circ}C) \quad \text{Eq. 1.23}$$

$$SO_2+2H_2S=2H_2O+3S \quad (\text{Claus Reaction}) \quad \text{Eq. 1.24}$$

The first step uses roughly 1/3 of the H_2S available, while after the second step approximately 60-70% of H_2S has been converted to solid sulfur. More modern plants use additional catalytic reactors to increase H_2S conversion up to 98%. The Claus process is the most common way of dealing with toxic H_2S since it produces relatively high purity sulfur and steam.[46]

1.2.4.1 Solar Thermal Decomposition of Hydrogen Sulfide

Due to the increasing need to produce energy from high-sulfur feedstocks, alternative methods for desulfurization of fossil fuels are being investigated. Additionally, since H_2 is receiving increased attention as an energy carrier, the thermal decomposition of H_2S is being considered as an alternative pathway for desulfurization:

$$H_2S=H_2+½\ S_2 \qquad \text{Eq. 1.25}$$

Villasmil and Steinfeld carried out economic analyses based on detailed flowsheets comparing a pure solar decomposition process, a hybrid solar/natural gas decomposition process, and finally the Claus process, finding that the pure solar process would introduce 45% cost savings over the traditional Claus process. Two heliostat models were considered: 1) a tower mounted reactor and a concentration of 2500 suns; and 2) a beam down approach where concentrated sunlight focused on a central tower sent to a ground level reactor via a compound parabolic concentrator equivalent to 5000 suns. Both approaches were quite comparable in terms of H_2 cost, capital cost, and process efficiency. The hybrid solar/natural gas process had an estimated H_2 price of \$0.058/kWh, which while somewhat less expensive that the estimated \$0.061-0.086/kWh for a pure solar H_2S splitting process, is significantly more complex since the process accommodates two high temperature heat sources.[45]

Recently, Baykara et al. have proposed a solar-thermal process to decompose H_2S into hydrogen and solid sulfur via catalytic thermolysis of hydrogen sulfide naturally emitted from the Black Sea, where H_2S concentrations are roughly 9.5 mg/L at depths of 1500 m or greater. Seawater containing H_2S would be pumped from a depth of 2000 m

and the escaping H_2S gas would be captured and sent to a solar parabolic concentrator dish. The dish would be equipped with a reactor operating at 1000 K, 1 atm, and employ a Co-Mo catalyst. Such a configuration also lends itself to mobile operation on a large barge or ship that could tap into different areas of the Black Sea so as to not deplete any single area.[47]

1.2.4.2 Kinetic Investigations of Hydrogen Sulfide Decomposition

Despite being heavily studied, the kinetics of H_2S decomposition remain an enormous question mark. There are still significant disagreements in literature as to whether the forward reaction rate order is first or second order with respect to H_2S concentration, and the associated activation energies reported range from as low as 50 kJ/mol with catalysts to nearly 300 kJ/mol without.[48] Kaloidas and Papyannakos studied the intrinsic kinetics of the decomposition reaction and concluded that the rate determining step is the cleavage of the H-S bonds of the H_2S molecule adsorbed on the catalytic surface.[49] Karan et. al, reasoned that the decomposition reaction can be modeled as follows:

$$-r_{H_2S} = k_1 C_M C_{H_2S} \qquad \text{Eq. 1.26}$$

where $-r_{H_2S}$ is the rate of H_2S decomposition; k_1 is the rate constant [m^3/kmol-s]; C_M is the concentration of other species, M, facilitating collisions [kmol/m^3]; and C_{H_2S} is the concentration of H_2S [kmol/m^3]. Karan et. al reconciled several literature values[49, 50] of the forward reaction rate constant, k_1, to arrive at an expression of k_1 [m^3/kmol-s] = (1.12±0.11) x10^{11} exp[(28,360±200)/T], valid for temperatures (T) from 800-3100 ˚C.[51] Bishara et al. observed kinetics showing second-order dependence with respect to H_2S concentration while conducting the reaction in a catalytic, solar thermal setting.[52]

The heterogeneity of the H_2S decomposition reaction has been found to be extremely significant. Harvey et al. investigated the reaction from 1350-1600 K in alumina tubes of varying surface area and derived two global reaction rate expressions that include the reverse reaction. The homogeneous reaction was found to have an

activation energy of 286 kJ/mol, while that of the heterogeneous reaction was only 186 kJ/mol.[53] Such results agree well with previous studies carried out by Tesner et al and Kappauf et al, which similarly concluded that surface reactions must have high contribution.[54]

Catalysis plays an important role in achieving high yields in many of these processes. Raymont et al. observed higher conversion under presence of a variety of surfaces including silica, cobalt-molybdate, and 1% pre-sulfided platinum up to a temperature of 1250 K, however once this temperature was reached, equilibrium could be reached without catalyst. Cobalt-molybdate was found to have the most effect on increasing reaction rate.[55] Fukudo et al. achieved 95% conversion of H_2S to S_2 and H_2O in the presence of MoS_2 at 800˚C with continuous removal of products, while FeS, NiS, and CoS_2 exhibited negligible activity. The actual sulfur product formed is speculated to be a function of temperature, however above 900 K, primarily S_2 is formed.[56, 57] Bishara et al. studied several catalysts in a solar thermal setting and found Ni-Mo, Ni-W, and Co-Mo based catalyst all successful, with Ni-Mo based catalysts having the highest conversion (14.5%) at a temperature of 973 K (temperature range studied was only 873-1073 K).[52]

Nearly complete conversion to H_2 was achieved by Edlund and Pledger who developed a membrane reactor to continuously remove H_2, ultimately reaching conversions of 99.4%. The reactor featured a composite metal membrane composed of a vanadium base, platinum feed section, palladium permeate section, and SiO_2 intermetallic layers to improve thermal stability of the device.[58]

1.2.4.3 Other Processes Using Hydrogen Sulfide

Kotera et al. conceptualized an actual thermochemical cycle based on H_2S decomposition:[59]

$$H_2S = H_2 + \tfrac{1}{2} S_2 \qquad \text{Eq. 1.25}$$

$$1\tfrac{1}{2} SO_2 + H_2O = H_2SO_4 + \tfrac{1}{2} S \qquad \text{Eq. 1.27}$$

$$H_2SO_4 = H_2O + SO_2 + ½\ O_2 \qquad \text{Eq. 1.22}$$

$$¾\ S_2 + H_2O = H_2S + ½\ SO_2 \qquad \text{Eq. 1.28}$$

Another route to hydrogen production from H_2S is using O_2 in the presence of a metal catalyst to produce H_2 and SO_2, which has been demonstrated by Yang and Koon with platinum:

$$H_2S+O_2=H_2+SO_2 \quad [60] \qquad (1.1)$$

A thermochemical process for hydrogen sulfide decomposition has been proposed in a multi-step process by Herrington and Kohl [61], as well as Bowman :[62]

$$H_2S+CO_2=COS+H_2O \qquad \text{Eq. 1.29}$$

$$COS+O_2=CO+SO_2 \qquad \text{Eq. 1.30}$$

$$\underline{CO+H_2O=CO_2+H_2} \qquad \text{Eq. 1.31}$$

$$\text{Net: } H_2S+O_2=H_2+SO_2 \qquad \text{Eq. 1.32}$$

Huang and T-Raissi have simulated reformation of hydrogen sulfide using methane:[63]

$$H_2S + CH_4 = CS_2 + 3H_2 \qquad \text{Eq. 1.33}$$

Wang has proposed an open-cycle by adding H_2S-containing acid gas from fossil fuel processing to sulfuric acid produced in the sulfur-iodine thermochemical cycle:[64]

$$I_{2(s)}+SO_{2(g)}+2H_2O=H_2SO_{4(aq)}+2HI_{(aq)} \qquad \text{Eq. 1.8}$$

$$2HI_{(g)}=I_{2(g)}+H_{2(g)} \qquad \text{Eq. 1.9}$$

$$1½\ SO_2+H_2O=H_2SO_4+½\ S \qquad \text{Eq. 1.34}$$

$$2H_2S+H_2SO_4=S+2SO_2+3H_2 \qquad \text{Eq. 1.35}$$

Sulfur (S) can then be further oxidized to reform SO_2:

$$S+O_2=SO_2 \qquad \text{Eq. 1.36}$$

Steam Reformation of Hydrogen Sulfide

Rostrup-Nielsen investigated the steam reformation of sulfur deposited on supported Ni for the purpose of catalyst regeneration in natural gas reforming processes:

$$H_2S+H_2O = SO_2+3H_2O \qquad \text{Eq. 1.37}$$

Regeneration was achieved by treatment of Ni sintered with sulfur by exposure to H_2O:H_2 at ratios of 2 to 1000 at 700˚C. At H_2O:H_2 ratios less than 250, 60% of the sulfur remained after 4 h, and at ratios greater than 250 the sulfur remaining quickly decreased to an asymptotic value achieved using pure steam (roughly 15% of the initial amount). Rostrup-Nielson concluded that H_2 produced via this steam reformation reaction would greatly inhibit the steam reformation reaction. Removal of chemisorbed H_2S on Ni also was only found to be successful when enough steam was present to fully oxidize the Ni:

$$Ni+H_2O = NiO + H_2. \qquad \text{Eq. 1.38}$$

Rostrup-Nielson also observed formation of sulphates using steam treatment of sulfided, alkali-promoted, Ni catalysts.[65]

1.2.5 Ionic Liquids as reaction media

Ionic liquids are becoming popular substitutes for organic solvents in chemical processing. Ionic liquids are available commercially or can be synthesized easily from two starting substances containing the organic cation and inorganic anion. Since they have no volatility they do not emit harmful fumes like traditional organic solvents. They are highly versatile and can be engineered for specific needs by changing their ionic nature or substituents.[66] Most importantly, their high boiling points make separation and recovery procedures much easier[67]. Ionic liquids have virtually no vapor pressure, which is ideal for separation processes such as distillation.[68] Since the convenience and benefits of ionic liquids are still being discovered, much of the physical and chemical property data traditionally determined experimentally is not available.[69]

1.2.5.1 Solubility of Gases

Many ionic liquids enjoy high SO_2 solubility. Jiang et al. report SO_2 saturation mole fractions at 298K for [BMIM][BF_4] and [BMIM][Tf_2N] of 0.570 and 0.552 respectively[70], which agree with studies done by Huang et al. [19] Anderson et al. report much higher saturation mole fractions (0.74) for both 1-n-hexyl-3-methylimidazolium

bis(trifluoromethylsulfonyl)imide [HMIM][Tf_2N] and 1-n-hexyl-3-methylpyridinium, [HMPY][Tf_2N].[71] Lee and Huang et al. both concluded that the cation does not have strong effects on absorption capacity.[72, 73] Lee et al. investigated the use of ionic liquids in thermochemical water splitting via the sulfur-iodine and hybrid sulfur cycles as absorbents for SO_2 following the H_2SO_4 decomposition process. All ionic liquids chosen had the same [BMIM] cation, and among the various anions investigated, [BMIM][Cl] and 1-Butyl-3-methylimidazolium acetate, [BMIM][OAc], had the highest absorption capacity, however in a desorption study not all SO_2 was able to be desorbed, even at 400K. These observations led the authors to speculate that SO_2 was bonded with the anions, and they found that a more appropriate choice for an absorbent was 1-Ethyl-3-methylimidazolium methylsulfate [BMIM][$MeSO_4$], which although not possessing the absorption capacity of the aforementioned solvents, did show favorable absorption/desorption kinetics. Huang et al. performed ^{1}H NMR and FTIR and concluded that SO_2 is not chemically bonded in any way to the [BF_4] or [Tf_2N] ionic liquids.[72]

Shokouhi et al. investigated H_2S solubility in various [BF_4] ionic liquids and found that H_2S was more soluble than CO_2, leading to the possibility that ionic liquids could be suitable for separating gases in oil and natural gas fields. Ab initio calculations performed by Pomelli et al. reveal strong H_2S interaction with [Cl], [BF_4], [Tf_2N], and [OTf] anions and weak interactions with the [PF_6] anion.[74] The mole fraction of H_2S in 1-(2-hydroxyethyl)-3-methylimidazolium tetrafluoroborate, [HEMIM][BF_4], ranged from 0.039 at 303K and 136 kPa to 0.247 at 303K and 1027 kPa, corresponding to a Henry's Law constant of 3.13 MPa for H_2S.[75] Rahmati-Rastrami et al. determined a relative order for H_2S solubility among the three ionic liquids studied: [HMIM][BF_4] > [HMIM][PF_6] ≈ [HMIM][Tf_2N], with Henry's Law constants at 303 K found to be 1.25, 1.74, and 1.79 MPa respectively. Using NMR spectroscopy, Pomelli et al. determined mole fractions at 1400 kPa and 298K followed the order [Cl] > [BF_4]> [OTf]> [Tf_2N] >[PF_6], however with the exception of [Cl] (mole fraction of 0.86), all others were between 0.72 and 0.79.[74] Jou et al. found high pressure dependence on

solubility, determining H_2S mole fractions in ionic liquid [BMIM][PF_6]of 0.077 at 298 K and 115 kPa all the way up to 0.875 at 298 K and 2120 kPa, with a Henry's law constant of 1.43 MPa at 298 K. Because of this pressure dependence, Jou et al. argue that ionic liquids are likely to be used only as bulk acid gas removal absorbents, when acid gas partial pressures are significant enough to result in high solubility, as opposed to cleaning dilute streams.[76]

1.2.5.2 Thermal Stability

In general, ionic liquids have negligible vapor pressure and essentially do not evaporate.[66] Rebelo et al. speculate that boiling points are high in ionic liquids due to the Coloumb interactions of ionic species preventing formation of a gas phase.[77] In a screening of ionic liquids as to their potential use as a thermal fluid in solar energy applications, Valkenburg et al. observed that the [BMIM][BF_4] ionic liquid has a thermal stability onset temperature of 423 °C.[78] Lee et al. measured thermal ranges for ionic liquids using TGA-DTA and report [BMIM][BF_4] and [BMIM][PF_6] stabilities from room temperature to over 673 K.[72] Rebelo, Taylor, and others have demonstrated reduced pressure distillation of [Tf_2N] ionic liquids.[77, 79]

1.2.5.3 Acid Dissociation

The dissociation of 3 weak organic acids in [BMIM][BF_4] was observed by visible spectroscopy by MacFarlane et al. and in all three cases [BMIM][BF_4] lead to less dissociation than in acidic water. Depending on the ionic liquid, they concluded that acids can become relatively weaker or stronger in ionic liquids than in water. In other words, a more basic ionic liquid would make an acidic solute more acidic, and a less basic ionic liquid would make an acidic solute less acidic. An equivalent explanation is to compare the pKa of the conjugate acid of the anion (ie. triflic acid for 1-butyl, 3-methylimidizolium trifluoromethane sulfonate) to that of the hydronium ion; ionic liquids containing lower pKa conjugate acids will see less acid dissociation for the same acidic solute in water.[80] This provides a semi-quantitative framework for choosing ionic

liquids. Roberts et al. investigated Hammett acidity of strong acids (triflic acid and bistriflic acid) in ionic liquids 1-butyl-3-methylimidazolium tetrafluoroborate, [BMIM][BF_4], 1-butyl-3-methylimidazolium triflate [BMIM][OTf], 1-butyl-3-methylimidazolium hexafluorophosphate [BMIM][PF_6], triethylammonium bistrifluoromethylsulfonyl imide [$HNEt_3$][Tf_2N]. Robert et al. added identical amounts of acids and found that acidity follows the order of ionic liquid anion: PF_6^->BF_4^->Tf_2N^- >OTf^-. Also noted by Robert et al. was higher acidity for ionic liquids containing the SbF_6^- anion than those of PF_6^-.[81] This observation contradicts the theory of MacFarlane et al. , since HPF_6 and $HSbF_6$ have much lower pKa's in water than HBF_4, HTf_2N, or HOTf. D'Anna et al. determined acid strength in ionic liquids 1-butyl-2, 3-dimethylyimidizolium bis(trifluoromethylsulfonylimide), [BM_2IM][Tf_2N]; and N-butyl-N-methylpyrrolidinium bis(trifluoromethylsulfonylimide), [BMPYRR][Tf_2N]; using p-Nitrophenolate. For each of some 11 carboxylic acids, all had higher pKa's in the ionic liquids chosen than in water.[82]

Studies have also investigated effect of cation choice on acid dissociation. Robert et al. observed that for ionic liquids of the same anion but different cations, there was found to be no significant difference in Hammett acidity.[81] Thomazeau et al. observed nearly identical Hammett acidities for strong acid HTf_2N in [BM_2IM][BF_4] and [BMIM][BF_4].[83] In experiments carried out by D'Anna et al. , acidity was consistently lower in [BMPYRR][Tf_2N] when compared to [BM_2IM][Tf_2N], however this may be more of a result of an increased proton transfer due to aromatic acids interacting with the BM_2IM^+ cation through π-bond interaction.[82]

2 INVESTIGATION OF THE BUNSEN REACTION IN IONIC LIQUIDS

The Sulfur-Iodine cycle suffers from the difficult task of separating H_2SO_4 and HI from H_2O, the latter of which requires reactive distillation or membrane separation due to the HI/H_2O azeotrope. Several approaches have been attempted to free HI from H_2O, including alternative solvents[37, 39] and solid separations[37, 84]. Recently, Taylor et al. attempted to extract HI from the aqueous phase using hydrophobic ionic liquids, however it was found that a co-extraction was occurring that simultaneously took organic cations from the ionic liquid into the aqueous phase.[41]

The original aim of this investigation was to release HI vapor from a liquid phase reaction without resorting to distillation or membrane techniques presently employed in current process schemes. Since HI is usually dissociated in aqueous setting, it is unable to vaporize, despite having a normal boiling point of -35°C in a molecular state. The approach in this study was to use an ionic liquid as a reaction medium and evaluate their ability to facilitate the Bunsen reaction and release HI vapor. As is discussed below, HI was never detected in the gas phase in any significant amount, however H_2S was found to elute readily from the liquid phase reaction, which lead to the development of the Sulfur-Sulfur cycle.

Table 2.1: Ionic liquids studied and their conjugate acids

Ionic Liquid	**Abbreviation**	**Anion (A^-)**	**Hydrophilic/ Hydrophobic**	**pKa of HA in H_2O**
1-Butyl-3-methylimidazolium tetrafluoroborate	BMIM.BF_4	BF_4^-	Hydrophilic	-0.44
1-Butyl-3-methylimidazolium Hexafluorophosphate	BMIM.PF_6	PF_6^-	Hydrophobic	-20
1-Hexyl-3-methylimidazolium bis(triflluoromethylsulfonyl)imide	HMIM.Tf_2N	$N(CF_3SO_3)^-$	Hydrophobic	-4
1-Ethyl-3-methylimidazolium hydrogensulfate	EMIM.HSO_4	HSO_4^-	Hydrophilic	-3
1-Butyl-3-methylimidazolium trifluoromethanesulfonate	BMIM.OTf	$CF_3SO_3^-$	Hydrophilic	-13
1-Butyl-1-methylpyrrolidinium tris(pentafluoroethyl)trifluorophosphate	BMPL.FAP	$(C_2F_5)_3PF_3^-$	Hydrophobic	unknown
Tetrabutylammonium trifluoromethanesulfonate	TBA.OTf	$CF_3SO_3^-$	Hydrophilic	-13

2.1 Screening of commercially available ionic liquids as to their ability to release hydrogen iodide ($HI_{(g)}$) from the Bunsen reaction.

Small-scale batch reactions were carried out by adding stochiometric, sub-stoichiometric, and excess amounts of water and sulfur dioxide to a solution of iodine in anywhere from 1-5 mL of ionic liquid. Reactions were carried out at atmospheric pressure from 25-200˚C. Initial trials used [BMIM][BF_4] ionic liquid due the non-coordinating nature of the anion. Unfortunately, no significant amount of HI was found to elute from the liquid phase in any conditions. Ionic liquids were chosen on the criteria of anion inertness and pKa of the conjugate acid. The hexafluorophosphate anion was found to produce white fumes, which were assumed to be hydrogen fluoride vapor due to the etching of glass reaction vials. Other unsuccessful solvents include the bis(trifluorosulfonyl)imide and tris(pentafluoroethyl)trifluorophosphate anion containing ionic liquids. It was then realized that these anions would not be sufficient based upon the pKa argument as outlined by MacFarlane et al.[80] As a result, two triflate anion ionic liquids, [BMIM][OTf] and tributylammonium trifluoromethanesulfonate, [TBA][OTf], were used as solvents, due to their corresponding conjugate acid being stronger in water than hydrogen iodide. Figure 2.1 shows some common ionic liquid structures.

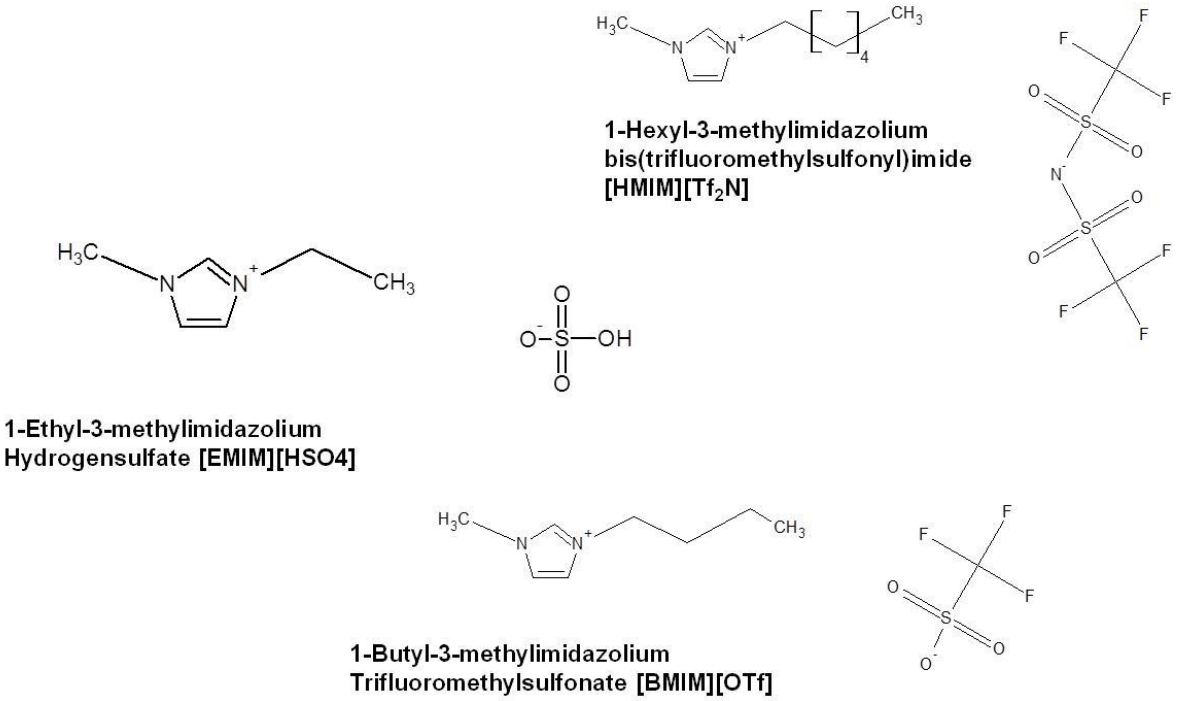

Figure 2.1: Structures of some imidazolium ionic liquids

Gas-phase product analysis was explored by a variety of methods. Initial batch Bunsen syntheses involved purging the headspace gas with an inert carrier (helium or nitrogen), bubbling this product gas into water, and then measuring the resultant conductivity. Although this approach showed that there was a conductive species formed, there was no way of differentiating between an iodine-species and a sulfur-species. The next approach was to use an ion selective electrode (ISE) specific to iodide. Unfortunately, this instrument also responded to sulfur-species, invalidating any possibility of a unique response from hydrogen iodide vapor.

Compound-specific techniques were then explored as a characterization method to identify hydrogen iodide vapor. Gas chromatography via a Helium Ionization Detector and an Agilent GasPro capillary column were used to analyze for HI. Hydrogen iodide standard was prepared by drying azeotropic HI-H_2O over P_2O_5 as described by Dillon and Young[85]. Although arriving at this method was the result of considerable time and effort, it still had drawbacks in that hydrogen sulfide eluted with similar retention times even at

low column temperatures (30-40 ˚C). Furthermore, the column lost significant retention ability after 2-3 months of use. Throughout these trials, hydrogen sulfide had been noticed as a vapor product quite readily. Unfortunately, none of the solvents listed in Table 2.1 were found to successfully liberate HI vapor. Additional analytical steps were taken to identify hydrogen iodide, including using a purge-and-trap unit to concentrate any hydrogen iodide vapor swept from the reaction flask, as well as using a residual gas analyzer to sample headspace gas products. Neither approach was successful throughout the wide range of reaction conditions investigated.

2.1.1 Purification of ionic liquids

Although the sulfur-sulfur cycle is designed to be a continuous process, it is foreseeable that ionic liquids will need to be purified and tested periodically. Experimentation in the lab resulted in a waste stream of ionic liquids with various iodine and sulfur species. Purification of these ionic liquids generally follows the methods of Earle et al. , however the iodine species cause very obvious discoloration, which does not disappear with simple liquid-liquid extraction using water and an organic phase.[86] Although no quantitative study has been done, I_2 is much more soluble in the ionic liquids used in this project than in water, since the amount of I_2 that is easily dissolved per unit volume of ionic liquid is 2-3 orders of magnitude greater than that of water. Since the iodine species were remaining the organic phase, a solution of water and sodium thiosulfate ($Na_2S_2O_3$) was used to reduce the iodine, in a similar fashion to the actual Bunsen reaction. This process was then followed with additional water washes, treatment with $MgSO_4$ and/or activated charcoal, and finally, evaporation of the light organic species (in this case dichloromethane) as prescribed by Earle et al. [86]

For hydrophobic ionic liquids such as [HMIM][Tf_2N], this process resulted in no iodine-related absorbance in the UV-visible range. Persistent difficulties arise, however when the ionic liquid is hydrophilic in nature, since it will partition in to the aqueous phase during extraction. In many cases significant amounts, if not all, of the ionic liquid were lost using this method, and it is vital that minimal amounts of water are used in extraction.

2.2 Investigation of Bunsen Reaction Kinetics

Upon the unsuccessful attempts to liberate HI vapor, it was desired to measure the kinetics of the Bunsen reaction. Since iodine has a high extinction coefficient, UV-visible spectroscopy was used to measure the disappearance of iodine (reaction progress). No formal investigations of Bunsen reaction kinetics are reported in literature, though the Karl Fischer reaction has been studied extensively.[31, 32, 87] Since the Bunsen reaction is usually carried out in water (in this case a reactant in huge excess), the kinetics are immeasureably fast. By limiting the amount of water, the reaction can be carried out at a measurable rate.

2.2.1 Materials and Methods

A hydrophilic ionic liquid, 1-Butyl-3-methylimidazolium trifluoromethanesulfonate [BMIM][OTf] was obtained from Sigma-Aldrich (BASF, 98%). It was diluted using dichloromethane then filtered to remove solids in suspension from production. The resulting liquid was clear with a slight brown color. To remove the dichloromethane, the liquid was put in a rotary evaporator for 2 h and treated en vacuo for at least 3 h. Iodine was obtained from Fluka (99.5%). Sulfur Dioxide (Airgas) was bubbled into [BMIM][OTf] and assumed to have a saturation mole fraction of 0.5 based on studies on other ionic liquids done by Jiang et al. [70] All water used was both deionized and distilled on site.

Solutions of I_2 (0.012M) in [BMIM][OTf] were made in small 2 mL brown glass vials and heated to the specified temperature (50, 70, or 100 ˚C) in a silicon oil bath. A reactant solution of SO_2 and H_2O in a 2:1 molar ratio was prepared in [BMIM][OTf] Pre-reaction (i.e. t=0) concentrations were measured prior to adding in the other reactants. The reaction was started by adding in an 18-fold excess of SO_2 and H_2O in ionic liquid. Reaction progress was tracked by extracting liquid samples out of the reaction vessel and measuring the absorbance of the sample diluted in a quartz cuvette of dichloromethane using an Avantes Avaspec 3648 UV-Vis spectrophotometer and Avantes Avalight DHc

(halogen and deuterium) light bulb. Room temperature air was used as a reference. Due to small sample volumes (10 uL), it was assumed that the liquid volume of the reactor was essentially constant.

A point of major confusion in UV-Vis spectroscopy of iodine-containing species is determining what compounds are actually absorbing. In dichloromethane, I_2 dissolves easily to form a violet colored solution as is shown in Figure 2.2. The maximum extinction coefficient for I_2 was found to be 807 M^{-1} cm^{-1} at 504 nm, which agrees reasonably well with past literature.[88] Smaller peaks are also seen at 265, 294, and 365 nm, however the peak at 265 nm was found to be very temperature unstable, while the others have been previously attributed to I_3^-, which has extinction coefficients in the 294 and 365 nm vicinities of approximately 40,000 and 26,000 M^{-1} cm^{-1} respectively[89]. As an excess of ionic liquid [BMIM][OTf] is added, the spectrum quickly shifts and the principal iodine peak at 504 nm disappears and a new maximum is found at 397 nm. Simply using the naked eye, it is evident that ionic liquids have a drastic effect on the I_2/ I_3^- equilibrium, as the violet color immediately disappears and the solution becomes orange in color. As more iodine is added to the mixture, the peak then begins to shift back to the right, and a peak shoulder begins to appear around 500 nm. The broad absorption band from roughly 250-400 nm is most likely a combination of the ionic liquid and I_3^- spectra. This qualitative experiment shows the preference of I_2 to equilibrate to I_3^- in ionic solvents.

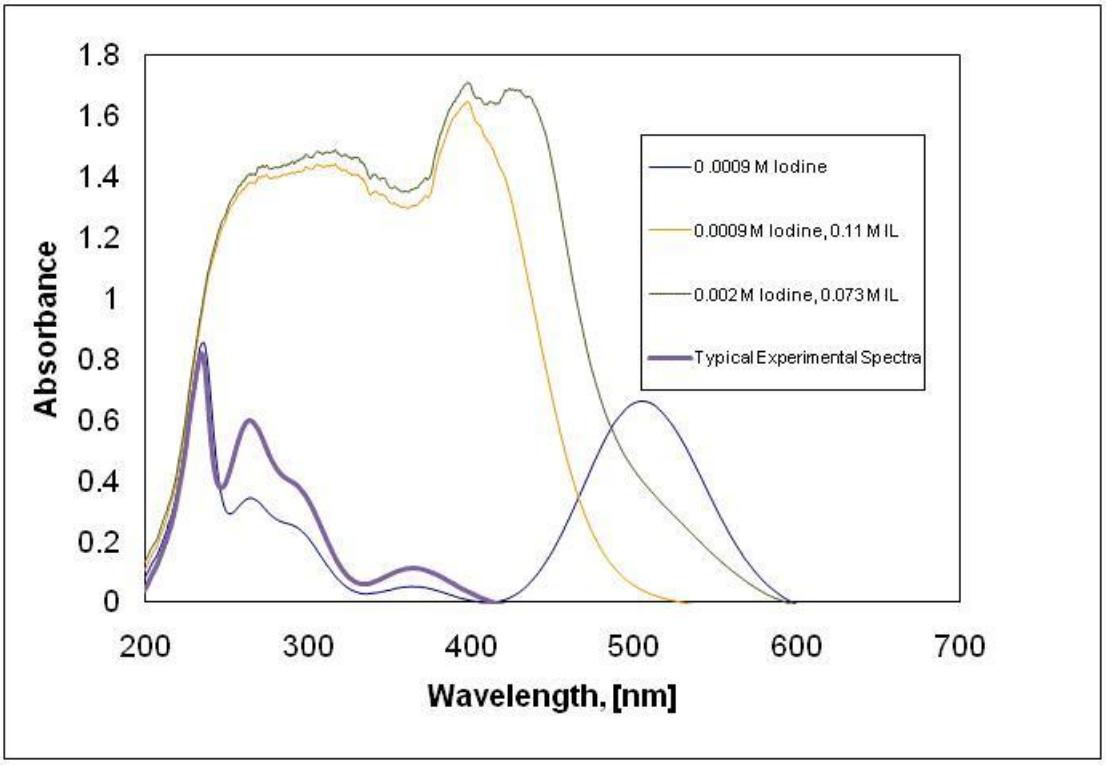

Figure 2.2: Spectral differences of iodine in dichloromethane with and without ionic liquid [BMIM][OTf]. The typical experimental spectra are that of a reaction occurring in ionic liquid. Notice the absence of the peak ca. 500 nm due to the ionic liquid solvent. The peak ca. 234 nm is CH_2Cl_2.

In the kinetic experiments performed here, the peaks took positions exclusively in line with the I_3^- spectra, and the peak occuring in the vicinity of 500 nm corresponding to I_2 was not seen. Therefore, it was decided that the disappearance of iodine species would be tracked via monitoring the I_3^- peaks. Considerable difficulty was encountered in deciding the appropriate peak to track, since all the iodine-containing species were continually seeking equilibrium with every change in concentration or temperature (see Figure 2.3). Of the three peaks that were readily measurable under the given experimental conditions, the peak at 294 nm seemed to be the most stable in response to changes in temperature. As a result, this wavelength was used for calibration and tracking purposes (see Appendix B, Figure B.1-Figure B.2).

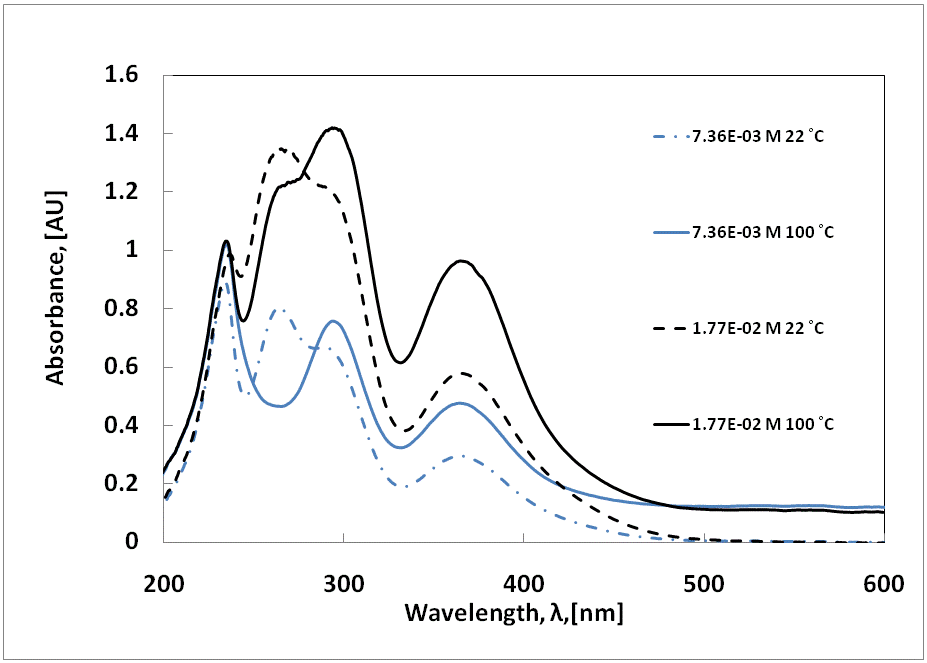

Figure 2.3: Spectral variation of iodine in ionic liquid [BMIM][OTf]with temperature (diluted in dichloromethane).

2.2.2 Results and Discussion

Iodine concentration was extrapolated from the absorbance measurements at the chosen wavelength and then fitted to a pseudo first-order (with respect to I_2) equation for reaction progress as it was consumed:

$$\frac{dC_{I_2}(t)}{dt} = k'C_{I_2} \qquad \text{Eq. 2.1}$$

with initial condition: $C_{I_2}(0) = C_{I_{2,0}}$,

where C_{I_2} is iodine concentration, [M]; $C_{I_2,0}$ is the initial iodine concentration, [M]; k' is the pseudo-first order reaction rate constant [s^{-1}], and t is time [s^{-1}]. This model assumes that the Bunsen reaction is first order with respect to I_2 and that the concentrations of H_2O and SO_2 remain essentially constant (0.43 M and 0.13 M respectively) due to initially being present in roughly 10-fold excess. If unimolecular kinetics are also assumed with

respect to both H_2O and SO_2, the pseudo first order reaction rate constant can be defined as follows:

$$k' = kC_{H_2O}C_{SO_2} \quad \text{Eq. 2.2}$$

where k is the actual rate constant, $[M^{-2}s^{-1}]$.

Values for reaction rate constants were found by two methods: first graphically determining slope of a linearized $\ln(C_{I_2}/C_{I_2,0})$ versus time plot; and secondly, solving the equation for $C_{I_2}(t)$ at each timepoint explicitly for the rate constant, k. Arrhenius parameters were obtained by direct fitting the pseudo-first order model directly to the data via a least squares approximation. The form of the Arrhenius equation used in the model fitting is shown here:

$$k = k_m \exp\left[-\frac{E_a}{R}\left(\frac{1}{T} - \frac{1}{T_m}\right)\right] \quad \text{Eq. 2.3}$$

where k_m is the pre-exponential term, $[s^{-1}]$; Ea is the activation energy, [J/mol]; T is temperature, [K]; T_m is a median temperature (in this case 343 K); R is the ideal gas law constant, 8.314 $J\text{-}mol^{-1}K^{-1}$. This form was chosen to avoid correlation between the pre-exponential term and activation energy.[90] Conversion to the more heavily used form of the equation,

$$k = k_0 \exp\left[-\frac{E_a}{RT}\right] \quad \text{Eq. 2.4}$$

can be done by using the following relation:

$$k_0 = k_m \exp\left[\frac{E_a}{RT_m}\right], \quad \text{Eq. 2.5}$$

where k_0 also has units of $[M^{-2}s^{-1}]$.

In Figure 2.5, rate constants from both methods are compared to a linear curve constructed from the directly obtained Arrhenius parameters. Although there is deviation from Arrhenius behavior at 100˚C, the Arrhenius equation appears to describe the

behavior of the reaction. Furthermore, direct fitting of the Arrhenius parameters to the data via a least squares method resulted in a lower sum of the squared error of the residuals than both alternative approaches of either explicitly determination for or graphically determining rate constant (k) values (See Appendix B, Table B. 1). The Arrhenius pre-exponential term, k_0, and activation energy, E_a, estimated from directly fitting were found to be 24,400 ± 1800 M^{-2}-s^{-1} and 32.9 ± 3.0 kJ-mol^{-1} respectively.

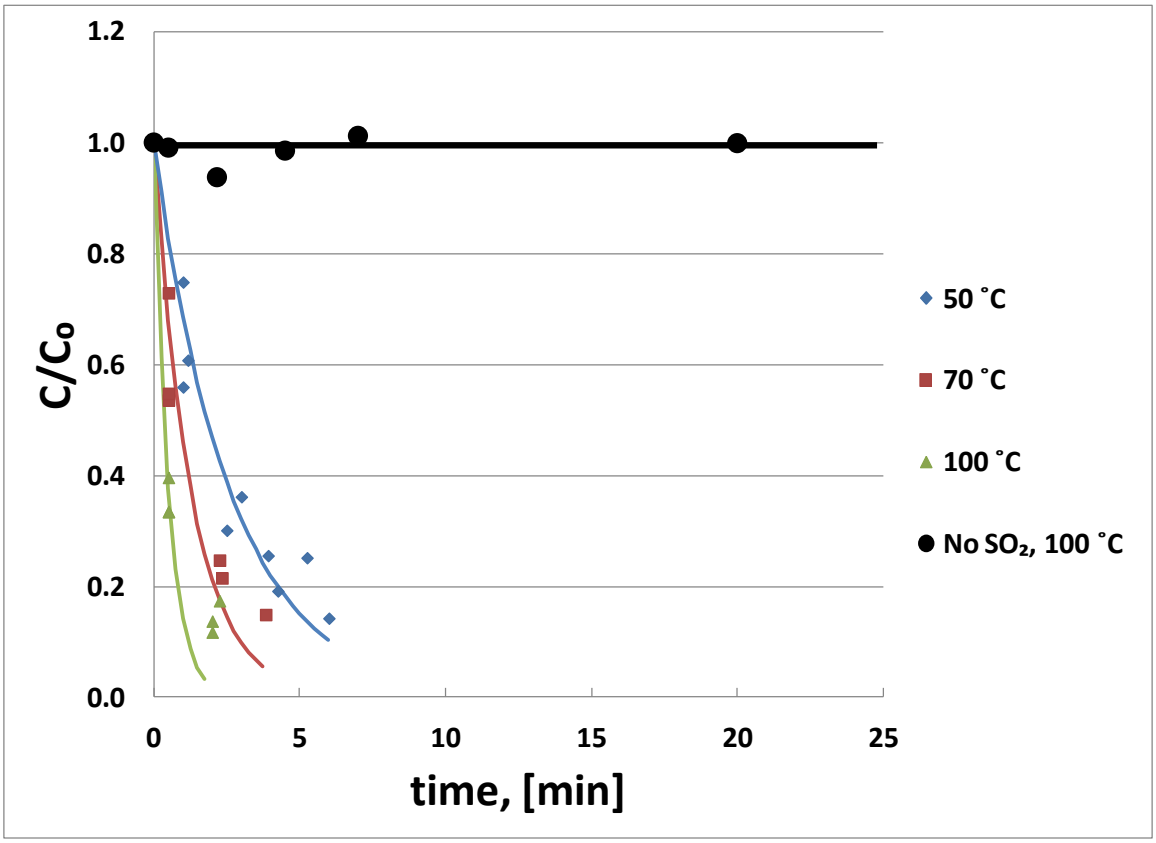

Figure 2.4: Normalized iodine concentration profile over time for small-scale batch reactions. Note: Excluding the blank, each data set is a culmination of multiple runs at a given temperature.

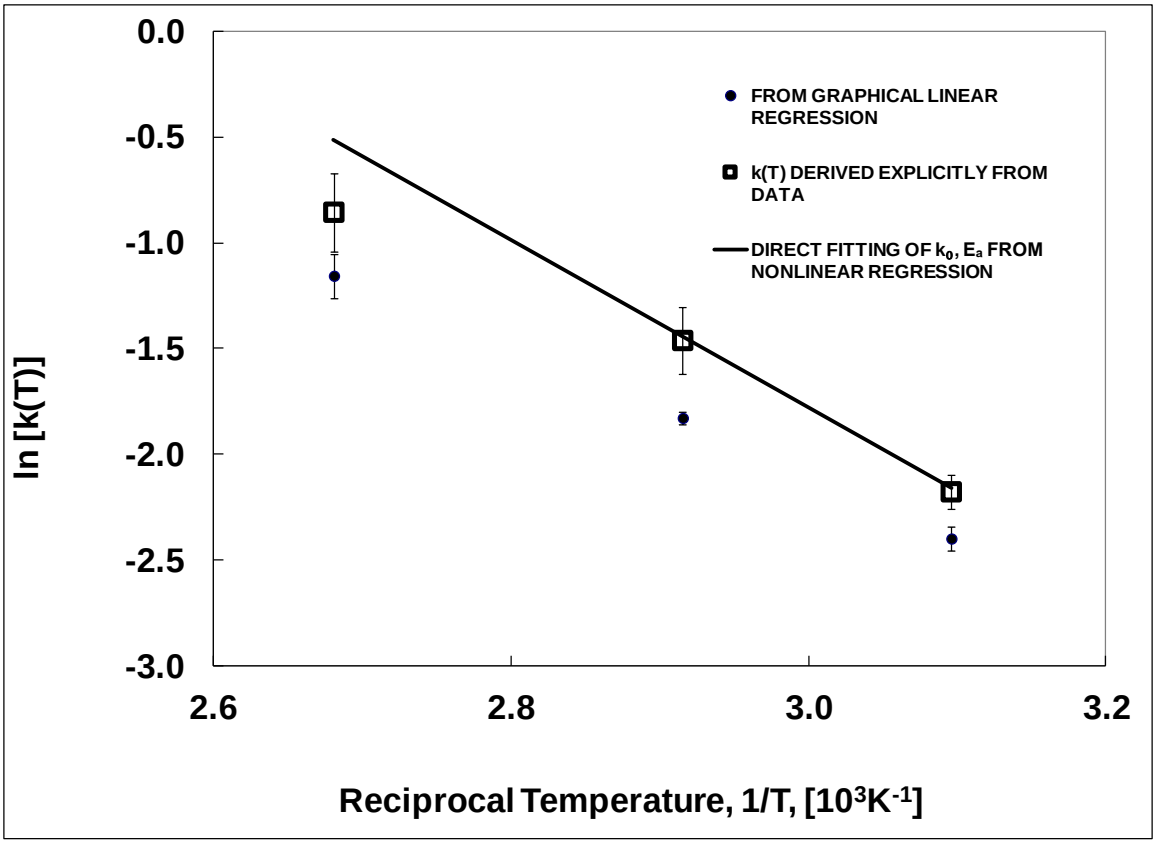

Figure 2.5: Arrhenius Plot of Bunsen Reaction in Ionic Liquid

2.3 Investigation into the evolution of hydrogen sulfide via the side reaction:

$$8HI_{(l)} + H_2SO_{4(l)} \leftrightarrow H_2S_{(g)} + 4H_2O_{(l)} + 4I_{2(l)}$$

Table 2.2: Parameters for hydrogen sulfide generation

Parameter	**Low Value**	**High Value**
Temperature	75˚C	100˚C
Water	1.85 M	3.70 M
Iodine	19.6 mM	39.3 mM
Sulfur Dioxide	0.1 M	0.2 M

A preliminary half-factorial experiment where iodine, water, and sulfur dioxide concentrations were varied in addition to temperature variations was carried out to explore these phenomena. The reaction parameter settings are summarized in

Table 2.2. Headspace concentration was monitored via syringe and injection into an SRI 8610 GC equipped with an FPD (Flame Photometric Detector) and a 2m Restek Rt-XLSulfur micropacked column. Figure C. 1-Figure C. **3** in Appendix C show calibration curves for gas chromatography measurements. In order to let the system reach equilibrium, no sampling was done before 20 minutes. As shown in Figure 2.6, trials with high temperatures had reached equilibrium after 20 min while low temperature trials did not reach equilibrium until 80 minutes or more. Sulfur dioxide concentration was not found to be an important factor, although it can clearly be seen that iodine concentration increases reaction rate. In these trials, water concentration was found to be the most significant parameter, as those trials that did not have a "high" concentration of water did not produce hydrogen sulfide in excess of 1% conversion.

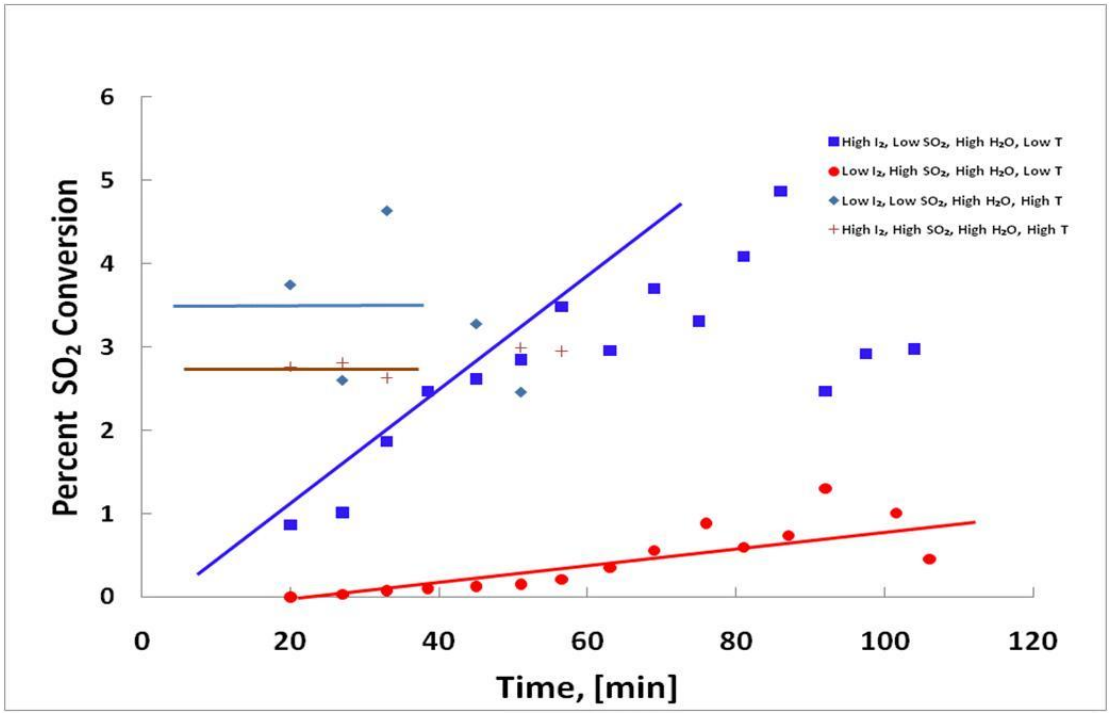

Figure 2.6: Conversion of SO_2 to H_2S, measured as H_2S concentration in reactor headspace.

It is apparent that higher temperatures lead to faster reactions. Similarly, higher iodine concentrations lead to faster reaction rates. The reaction appears to occur quite slowly, on the order of ~1 hr. Nevertheless, with H_2S evolving from the liquid phase reaction mixture, a new "Sulfur-Sulfur" thermochemical cycle has been conceptualized:

$$4I_{2(l)}+4SO_{2(l)}+8H_2O_{(l)} \leftrightarrow 4H_2SO_{4(l)} + 8HI_{(l)} \qquad \text{Eq. 1.8}$$

$$8HI_{(l)} + H_2SO_{4(l)} \leftrightarrow H_2S_{(g)}+4H_2O_{(l)} + 4I_{2(l)} \qquad \text{Eq. 1.1}$$

$$3H_2SO_{4(g)} \leftrightarrow 3H_2O_{(g)}+3SO_{2(g)}+1\tfrac{1}{2}O_{2(g)} \qquad \text{Eq. 1.22}$$

$$H_2S_{(g)}+2H_2O_{(g)} \leftrightarrow SO_{2(g)}+3H_{2(g)} \qquad \text{Eq. 1.37}$$

The most important step in the cycle is the highly endothermic steam reformation of hydrogen sulfide, which produces 3 moles of H_2 for every mole of H_2S, thereby counterbalancing the energy expenditures of decomposing 3 moles of H_2SO_4.

2.4 Demonstration of sulfur trioxide/sulfuric acid separation from ionic liquid

Facile separation of sulfur trioxide and/or sulfuric acid from the solvent is necessary if ionic liquids are to be used as reaction media. A screening experiment was carried out where the ionic liquid 1-ethyl, 3-methylimidizaleum hydrogen sulfate [EMIM][HSO_4], which contains the HSO_4^-anion,was slowly heated and stirred. Periodic samples of the headspace vapor were taken and injected into an SRI 8610 GC equipped with an FPD (Flame Photometric Detector) and Agilent GasPro capillary column. Sulfur trioxide was detected at a temperature of 160 ˚C. Retention time for SO_3 was confirmed by a standard SO_3 sample (Sigma Aldrich, USA). This is encouraging in that it shows the feasibility of liberating SO_3 from an ionic liquid medium containing the HSO_4^- anion using only heat swing.

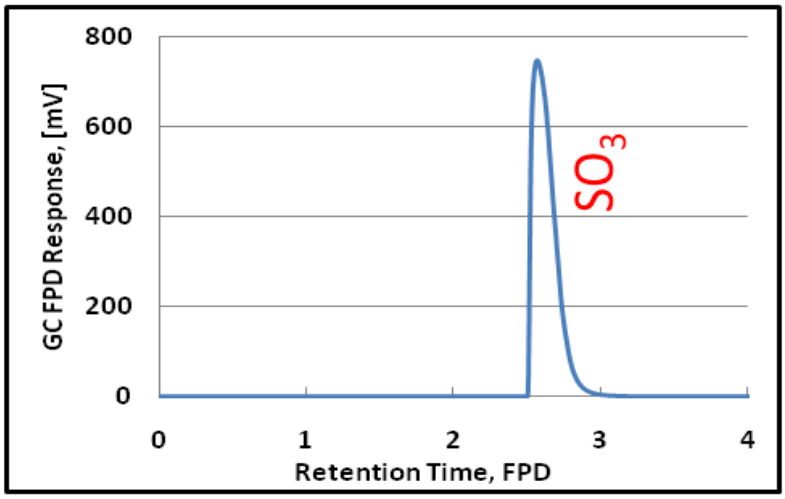

Figure 2.7: Detection of sulfur trioxide in headspace of heated ionic liquid at 160˚C

3 DEMONSTRATION OF STEAM REFORMATION OF H_2S

3.1 Preliminary Proof of Concept

The feasibility of a Sulfur-Sulfur cycle is contingent upon the ability for steam reformation of H_2S to occur:

$$H_2S_{(g)}+2H_2O_{(g)}\leftrightarrow SO_{2(g)}+3H_{2(g)} \qquad \text{Eq. 1.37}$$

From a chemical standpoint, the sulfur in H_2S needs to be oxidized to SO_2. Due to the stoichiometry of the Bunsen reactor side reaction (Eq. 1.1), 75% (3 moles) of the sulfur is retained as H_2SO_4. Since 3 moles of H_2SO_4 (per mole H_2S) need to be thermally decomposed, the energy demand is 3 fold higher than in a normal Sulfur-Iodine or Hybrid Sulfur cycle. As a result, 3 moles of H_2 are required to be produced (per mol of H_2S) in order for this process to be competitive with other cycles. Steam reformation achieves all these goals and conveniently completes a thermochemical cycle. This was the motivation for a preliminary investigation.

3.1.1 Theoretical

The thermodynamics of steam reformation of H_2S are rather discouraging—even at 2000K the Gibbs free energy change is a positive 47 kJ/mol. Thermal decomposition of H_2S is thermodynamically much more favorable (see Figure 3.1). This can be illustrated in Figure 3.2, which shows equilibrium mole fractions of SO_2 much less than those of S_2. However, under favorable circumstances such as high proportions of H_2O and dilution with an inert carrier gas, the actual conversion of H_2S can be higher than under normal circumstances. Being thermodynamically unfavorable, the kinetics of steam reformation have never been investigated.

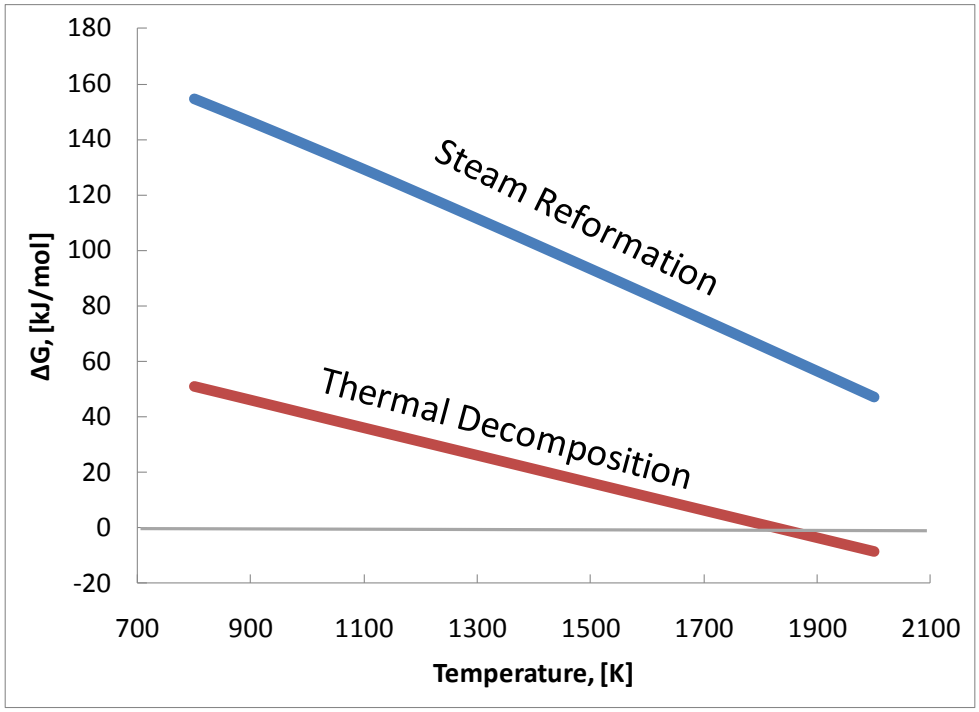

Figure 3.1: Gibbs free energy change, ΔG, from 800-2000K.

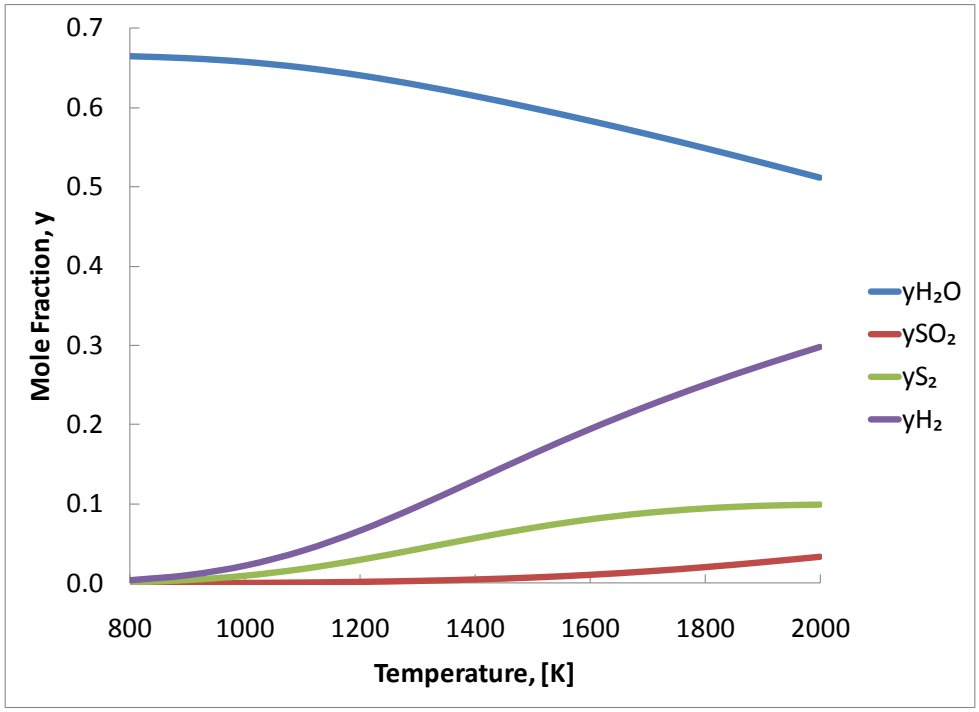

Figure 3.2: Theoretical equilibrium composition of system with feed of 1 mole H_2S and 2 mol H_2O.

3.1.2 Materials and Methods

A 70-cm, stainless steel 304 tube (1/8-in. OD) was used as a tubular reactor and heated to temperatures from 400-800˚C using a tube furnace (see Figure 3.3). Dilute hydrogen sulfide (1% molar) was bubbled through boiling water, then sent to the heated tube. Gas flow rates were measured by rotameter. A cold trap on ice was used to condense any elemental sulfur and unreacted water. Analysis of gaseous products was done via gas chromatography. Hydrogen was monitored via an SRI 8610 GC equipped with a direct-plumbed 1.00 mL injection valve, HID (Helium Ionization Detector), and molecular sieve packed column. Sulfur species (H_2S and SO_2) were monitored by taking syringe samples of 0.20-1.00 mL and manually injecting them into a separate SRI 8610 GC, equipped with an FPD (Flame Photometric Detector) and a 2m Restek Rt-XLSulfur micropacked column.

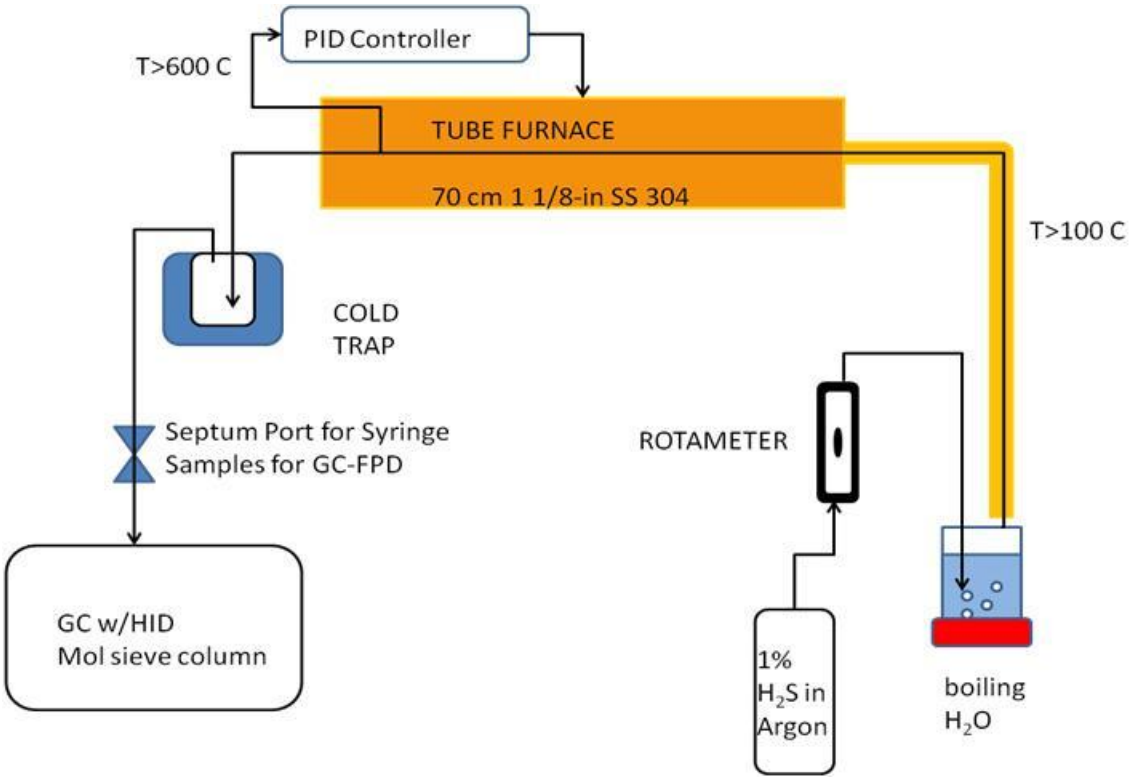

Figure 3.3: Steam reformation apparatus

3.1.3 Results and Discussion

It was assumed that the high temperature reaction between water and hydrogen sulfide only took place only in the heated section of the tube. This was confirmed by runs at lower temperatures, which showed no change in gas composition between inlet and outlet. Water composition was not monitored and assumed in excess. A blank experimental run of bubbling argon through boiling water was done at temperatures up to 800˚C. No measurable hydrogen was detected until the chamber was heated to 700˚C, however an outlet concentration of roughly 0.3 mM hydrogen occurred at 800˚C (see Figure 3.4), indicating some base-level catalytic activity of the stainless steel constituents.

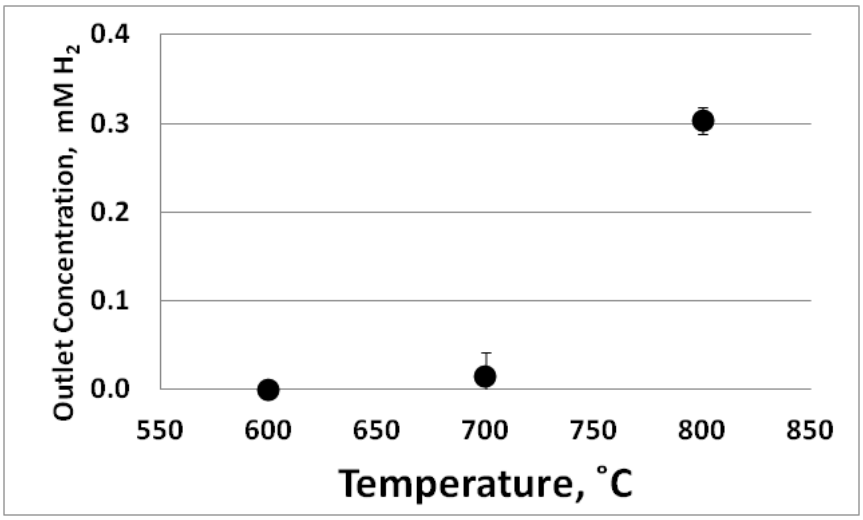

Figure 3.4: Hydrogen evolution from water heated in stainless steel tube at high temperature. No sulfur species were present, reaction tube had no prior usage.

For the steam reformation of hydrogen sulfide investigation, three flow rates and their corresponding residence times (2.4, 3.6, and 7.1 s) were tested at various temperatures (150, 300, 450, 600, 700, 800˚C). As shown in Figure 3.5, at the 700˚C conversion is almost complete at long residence times, and at 800˚C conversion is complete at all residence times. Measureable hydrogen evolution was detected at 600˚C (see Figure 13), and at 700˚C reached a ratio of 3.4 moles of hydrogen to each mole of SO_2 produced, which is in good agreement with the theoretical 3:1 ratio. See Appendix C, Table C. 1 for more detailed results.

Conclusion

This experiment successfully demonstrates the steam reformation of H_2S to SO_2 and H_2 under favorable circumstances. Hydrogen to SO_2 ratios were of the expected order of magnitude. Although adequate for preliminary proof-of-concept, the apparatus and analytic procedures can be improved to give more reliable quantitative results. Water splitting during the blank H_2O runs is likely evidence of metal oxide formation at high temperature. At this point, it is unknown whether the reaction is occurring homogeneously in the gas phase or is surface driven. Further work is needed to determine suitable catalysts and reaction kinetics.

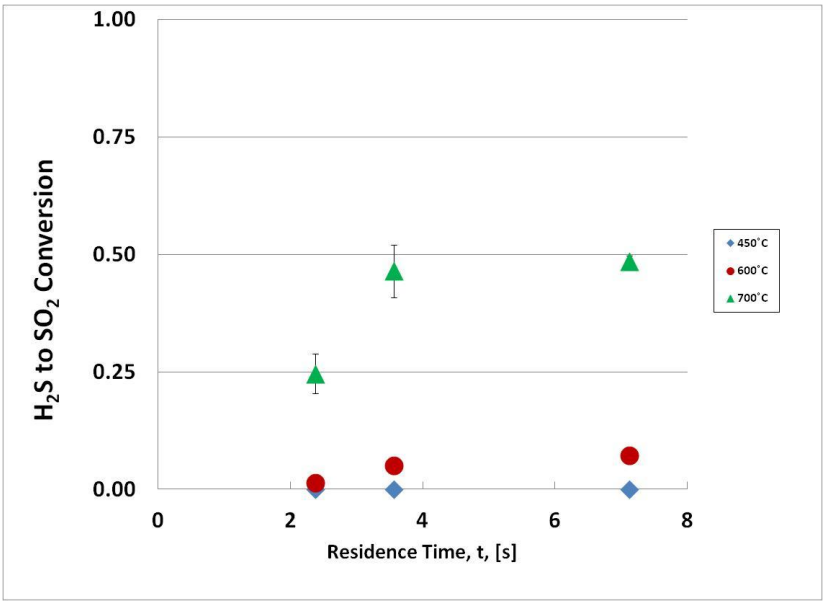

Figure 3.5: Hydrogen sulfide conversion to sulfur dioxide via steam reformation at various temperatures. For temperatures 450˚C and lower, only hydrogen sulfide was detected.

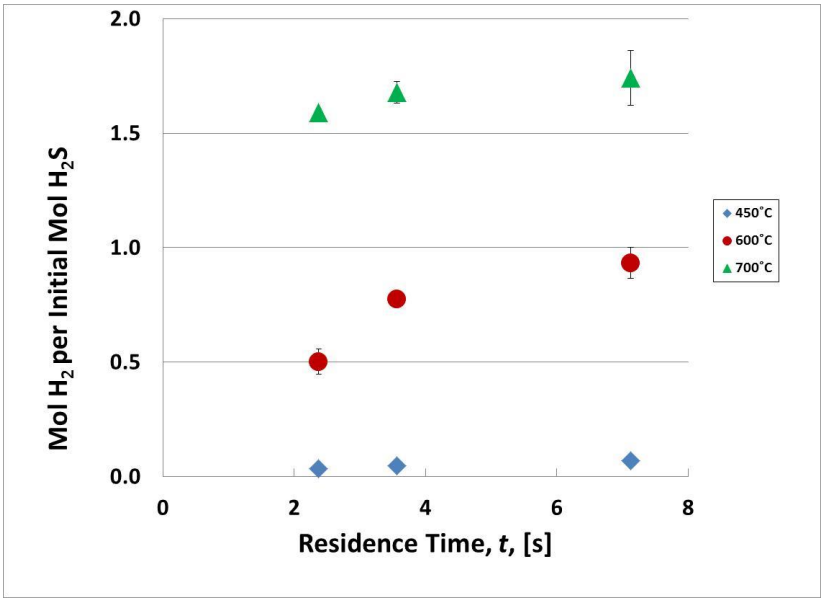

Figure 3.6: Hydrogen production via steam reformation of hydrogen sulfide at various temperatures.

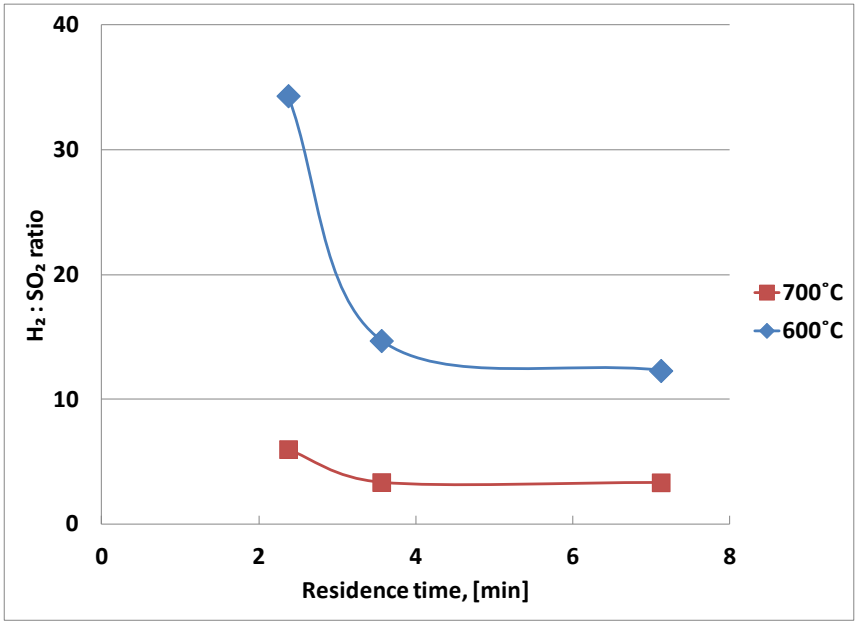

Figure 7: Hydrogen to SO_2 ratio for preliminary steam reformation of hydrogen sulfide trials.

3.2 Investigation of Thermal Splitting of Hydrogen Sulfide in a Quartz Reactor

An experimental apparatus was setup to thermally crack hydrogen sulfide into hydrogen and sulfur both with and without a molybdenum wire in the temperature range of interest (700-900 °C) in a quartz tube. The objectives of this experiment were to

1) Demonstrate H_2S-splitting with a molybdenum catalyst (most likely MoS_2).
2) Determine whether a quartz surface alone would facilitate H_2S splitting

3.2.1 Theoretical

Fukuda et al. propose that the main sulfur product is S_2 for thermal splitting of H_2S above 900 K:[56]

$$H_2S \leftrightarrow H_2 + \tfrac{1}{2} S_2 \qquad \text{Eq. 1.25}$$

At atmospheric pressure, ideal gas behavior is assumed, which corresponds to the following chemical equilibrium:

$$K = \frac{y_{S_2}^{1/2} y_{H_2}}{y_{H_2S}} \qquad \text{Eq. 3.1}$$

Thermodynamic equilibrium calculations were carried out both on the minimization of Gibbs energy, which had excellent agreement with those predicted by Fukuda et al. Due to the diluted (1% molar) state of the H_2S gas used in these experiments, the conversion is higher than if pure H_2S was thermally cracked. Heats of formation and Gibbs energies of formation for all species considered can be found in Appendix A, Tables A.2 and A.3 .

3.2.2 Materials and Methods

A tubular reactor scheme was set up to investigate the thermal splitting of H_2S. A high temperature tube furnace (Mellon, USA) with a 12-in. heated length was used to heat a ¼-in. OD, 4-mm ID fused quartz tube. The assumed reactor volume was 3.83 cm^3. For trials with a catalyst, a 0.04-in. diameter Mo wire with estimated surface area of 0.59 cm^2 (99.95% purity, Thermoshield, USA) was pretreated at 1000°C with a 1% mixture of H_2S in argon (Airgas, USA). Gas flowrate was controlled via a mass flow controller (Horiba STEC SEC-4400). Temperature of the tube furnace was controlled by an external PID controller and a type-K thermocouple place next to the quartz tube. Decomposition runs at three temperatures and performed in triplicate. Each temperature was held until a reasonable steady state had been reached as indicated by measurements of H_2 and H_2S. Concentrations of H_2 and H_2S were measured by gas chromatography using two separate gas chromatographs (both SRI 8610C chassis) equipped with inline sample loops (1 mL and either 10 or 100 uL respectively). Detection of H_2 was done via a Helium Ionization Detector (HID) while H_2S was detected using a Flame Photometric Detector (FPD).

3.2.3 Results and Discussion

Hydrogen production due to H_2S decomposition from the thermal catalytic reaction with residence time 13.7 s are shown in Figure 3.8 and Figure 3.9 respectively. Both H_2 and H_2S measurements agree well with Gibbs equilibrium predictions, showing that the reactor size and catalyst surface area are well matched to the surface kinetics of hydrogen sulfide decomposition. As predicted in the region of temperatures chosen, conversion increased linearly with temperature.

This study also showed that the thermal splitting of H_2S reaction occurs at a rate suitable for the residence times and experimental conditions used. Although the steam reformation of H_2S reaction undoubtedly has a more complicated mechanism, the fact that thermal splitting can occur to the extent that Gibbs equilibrium is reached under the given catalyst surface area, residence time, and temperature here is promising.

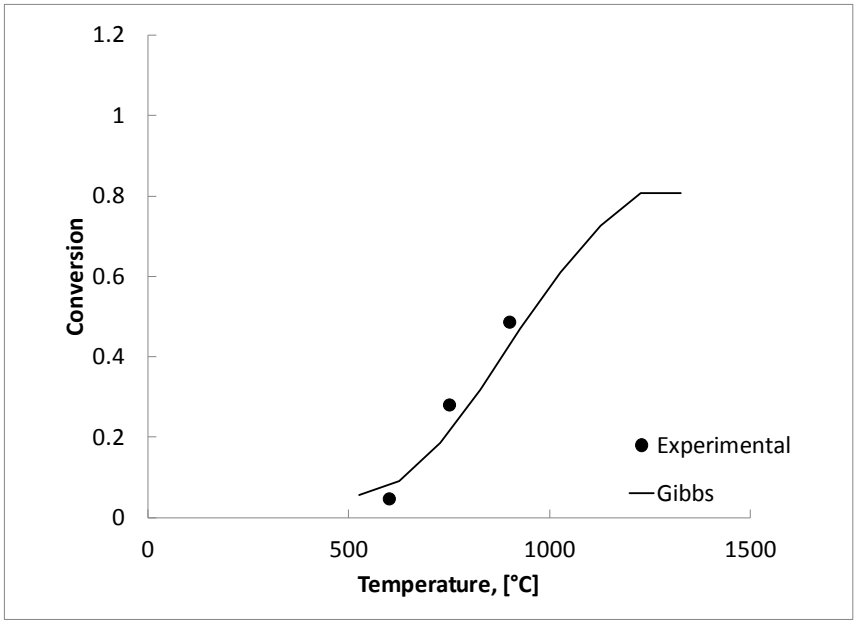

Figure 3.8: Conversion of H_2S to H_2 in quartz tube in presence of Mo wire.

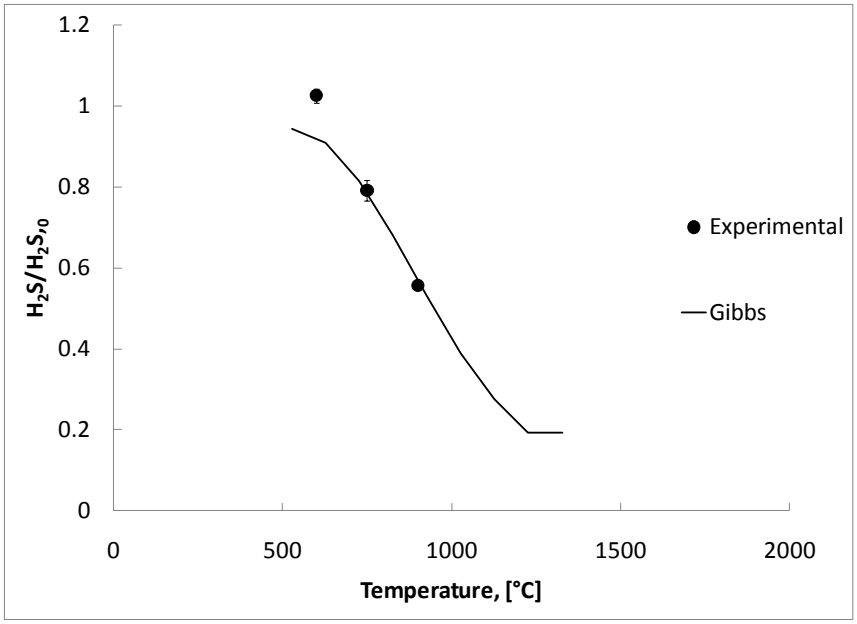

Figure 3.9: Fraction of initial H_2S remaining after thermal decomposition in presence of Mo wire.

Trials without molybdenum catalyst were also carried out albeit at longer residence times and higher temperatures (Figure 3.10 and Figure 3.11). Gibbs equilibrium values for H_2S and H_2 were not reached at 900°C at the residence times studied, however at 1000°C it appears equilibrium was reached at longer durations. These results are evidence that the reaction can be driven forward without intentional (non-metal) catalysis if temperature is sufficiently high.

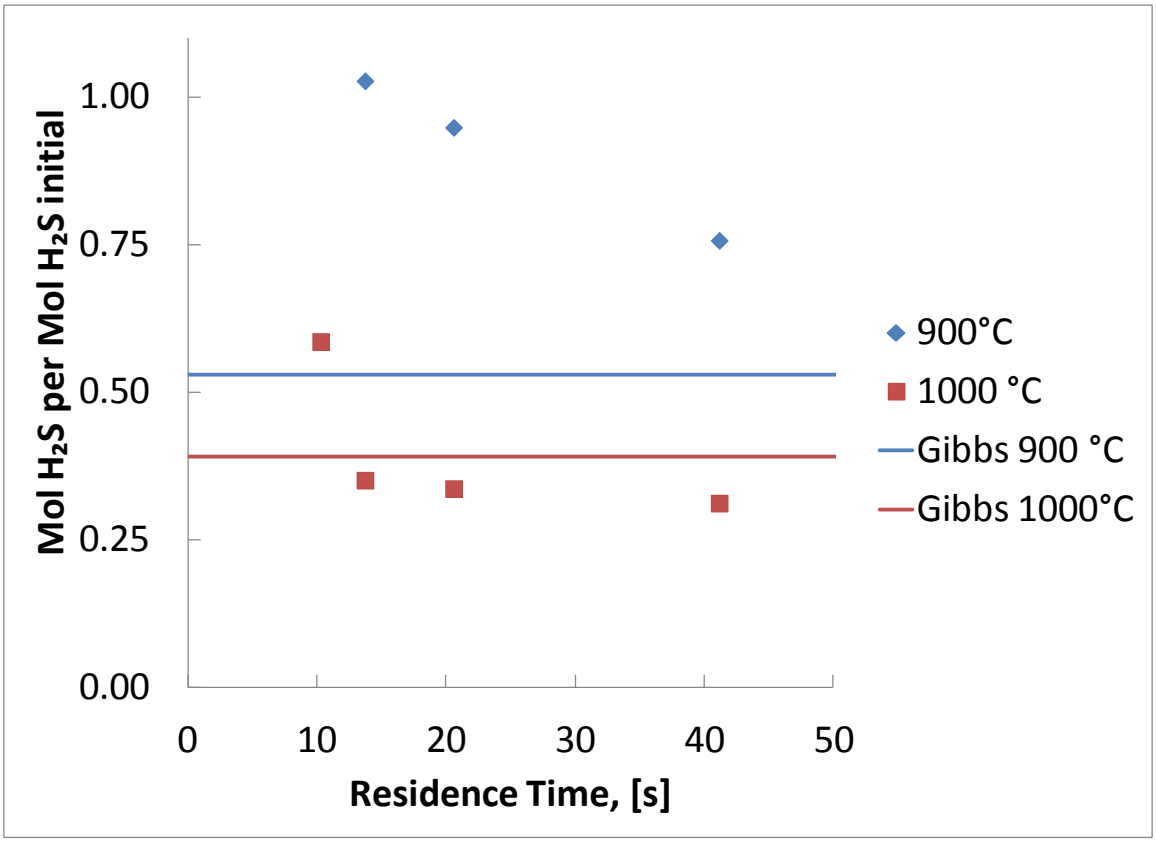

Figure 3.10: Hydrogen sulfide decomposition in quartz reactor

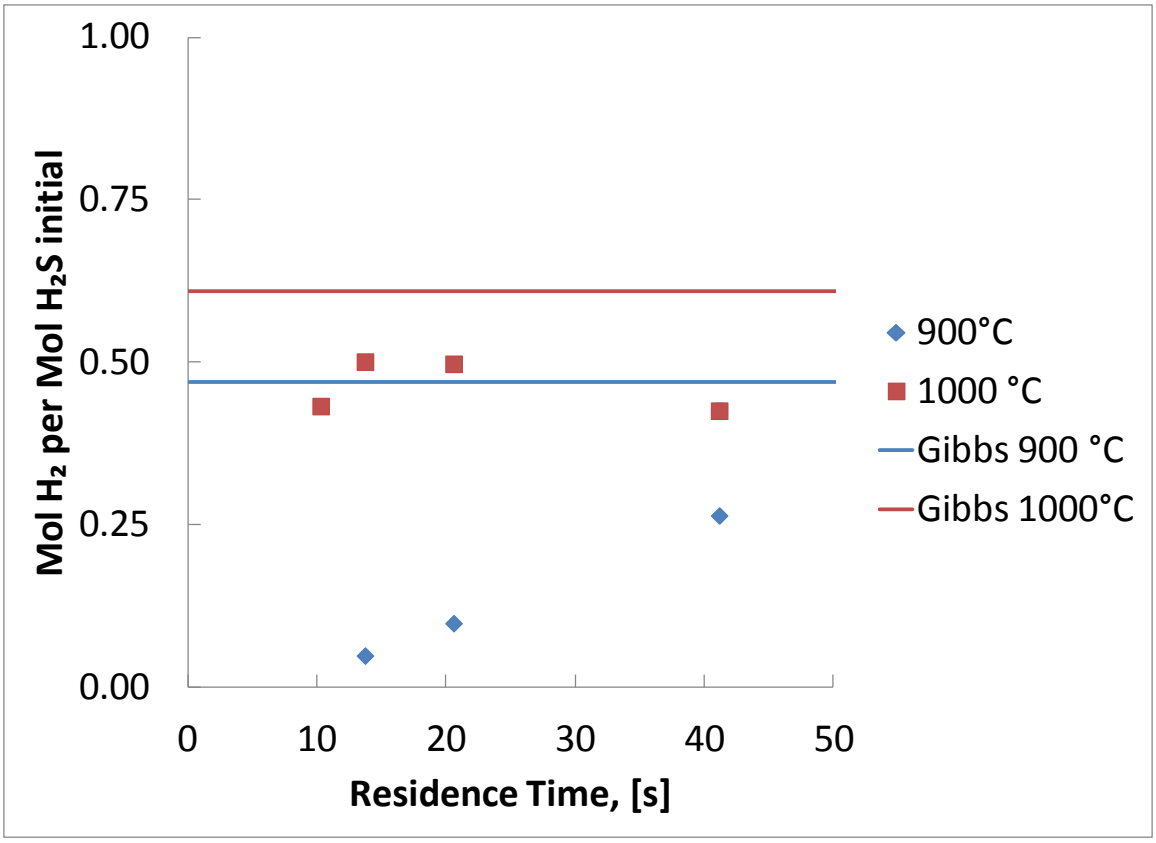

Figure 3.11: Hydrogen production in quartz tube

3.3 Parametric Study of Steam Reformation of Hydrogen Sulfide

In order to close the Sulfur-Sulfur cycle, a final step is needed that achieves two main objectives: 1) SO_2 is produced from H_2S and water, and 2) the reaction can proceed in a forward direction under low enough H_2O:H_2S ratios so that the thermal efficiency is on the order of other thermochemical cycles. Steam reformation of H_2S can accomplish this, although the thermodynamics are rather discouraging: at even 2000 K, the reaction has a positive Gibbs free energy change of +47 kJ/mol and reaction enthalpy change of +233 kJ/mol. Rostrup-Nielsen investigated the steam reformation of sulfur deposited on supported Ni for the purpose of catalyst regeneration in natural gas reforming processes. Regeneration was achieved by treatment of Ni sintered with sulfur with H_2O:H_2 at 700˚C. At H_2O:H_2 ratios less than 250, 60% of the sulfur remained, and at ratios greater than 250 the sulfur remaining quickly decreased to an asymptotic value achieved using pure steam (roughly 15% of the initial amount). Rostrup-Nielson concluded that any H_2 produced via this steam reformation reaction would greatly inhibit the steam reformation reaction.[65]

3.3.1 Theoretical

In the temperature range considered (700-900˚C), both the desired steam reformation reaction and the undesired competing reaction were considered:

$$H_2S_{(g)} \leftrightarrow \tfrac{1}{2}S_{2(g)} + H_{2(g)} \qquad \text{Eq. 1.25}$$

$$H_2S_{(g)} + 2H_2O_{(g)} \leftrightarrow SO_{2(g)} + 3H_{2(g)} \qquad \text{Eq. 1.37}$$

At atmospheric pressure, ideal gas behavior is assumed, which corresponds to the following chemical equilibrium equations:

$$K_1 = \frac{y_{S_2}^{1/2} y_{H_2}}{y_{H_2S}} \qquad \text{Eq. 3.1}$$

$$K_2 = \frac{y_{H_2}^{3} y_{SO_2}}{y_{H_2O}^{2} y_{H_2S}} \qquad \text{Eq. 3.2}$$

Thermodynamic equilibrium calculations were carried out based on the minimization of Gibbs energy using ThermoSolver (version 1.0) software. The simulations took into account H_2S and H_2O as reactants and SO_2, S_2, SO_3, and H_2 as possible products. These Gibbs simulations were then compared to stoichiometric predictions for both the thermal decomposition and steam reformation of hydrogen sulfide reactions outlined above for a reaction occurring with a 20 H_2O:1 H_2S molar ratio (see Figure 3.12). Due to nearly exact matching of these two methods, only the two reactions above were considered. Gibbs energies of formation for all species considered can be found in Appendix A, Table A.3.

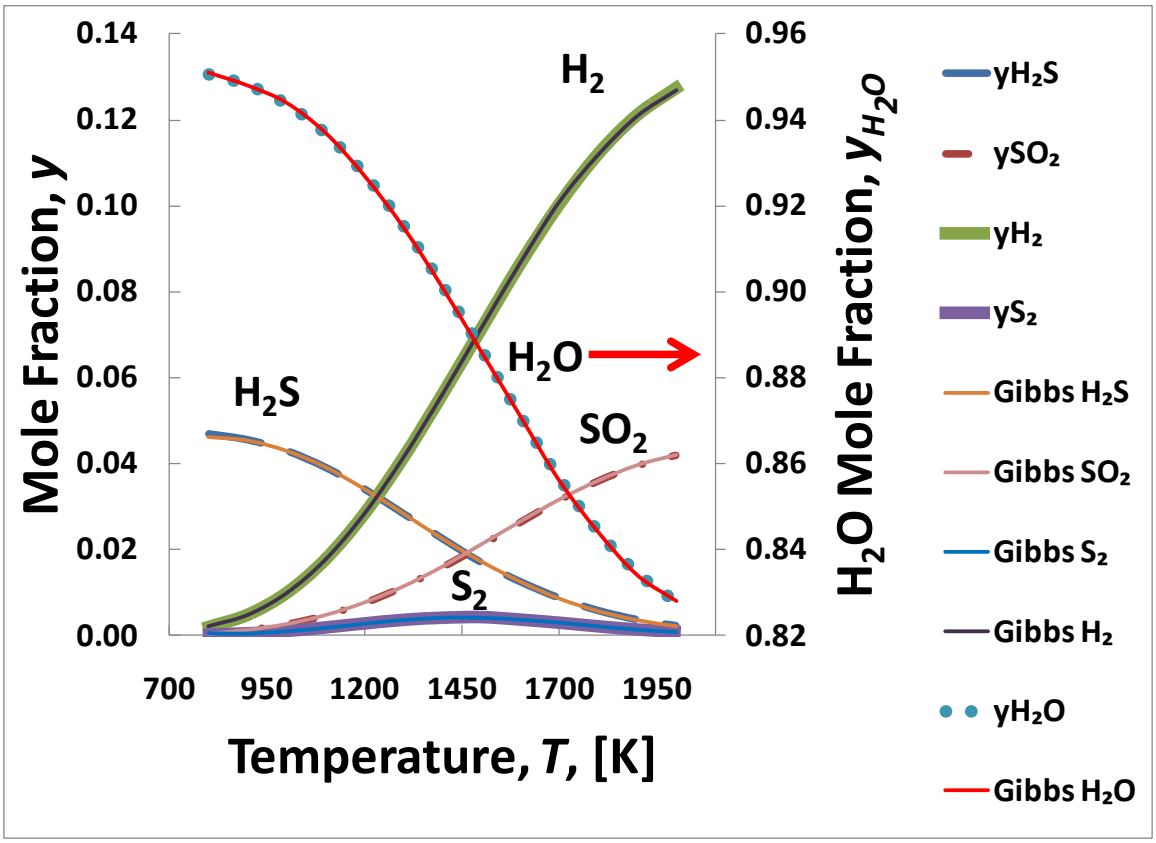

Figure 3.12: Comparison of thermodynamic predictions of equilibrium concentrations based upon minimization of Gibbs Free Energy and stoichiometric methods. Here, H_2O:H_2S ratio = 20:1 (molar). Both approaches give nearly identical results.

Past investigators have speculated that the rate determining step in thermal splitting of hydrogen sulfide is the cleavage of the H-SH bond.[49, 57] Karan et al. fit data from several kinetic studies to determine a rate constant expression for a wide temperature range of 800-3100 ˚C. The rate law used is first order with respect to both H_2S and an inert gas species, M:

$$-r_1=k_1C_MC_{H_2S} \qquad \text{Eq. 1.26}$$

where r_1 is the thermal decomposition reaction, [m^3/kmol-s]; k_1 is the reaction rate constant (1.12±0.11) x10^{11} exp[(28,360±200)/T [m^3/kmol-s]; C_{H_2S} is the concentration of H_2S, [kmol/m^3]; C_M is the concentration of inert gas species, [kmol/m^3].

3.3.2 Materials and Methods

A quartz tube was used a simple reactor for the steam reformation of hydrogen sulfide. A high temperature tube furnace (Mellon, USA) with a 12-in. heated length was used to heat a ¼-in. OD, 4-mm ID quartz tube. The heated reactor volume was 3.83 cm3. A simple catalyst was added in the form of a 0.04-in. diameter Mo wire with estimated surface area of 0.59 cm2 (99.95% purity, Thermoshield, USA) and treated at 1273 K with a 1% mixture of H_2S in argon (Airgas, USA) for a period of 1-15 h. Gas flowrate was controlled via mass flow controllers (Horiba STEC SEC-4400). Temperature of the tube furnace was controlled by an external PID controller and a type-K thermocouple place next to the quartz tube (see Appendix D, Figure D. 1). Trials at three temperatures (700, 800, and 900˚C) were performed in triplicate for trials at different H_2O:H_2S ratios (50:1, 75:1, 100:1, 200:1), as well as residence time (2.86, 4.57 s, 6.86 s, and 13.72 s). Each temperature was held until a reasonable steady state had been reached as indicated by measurements of H_2, H_2S and SO_2. These species were measured by gas chromatography using two separate gas chromatographs (both SRI 8610C chassis) equipped with inline sample loops (1 mL and 100 uL respectively). Detection of H_2 was done via a Helium Ionization Detector (HID) while H_2S and SO_2 were detected using a Flame Photometric (FPD)/Flame Ionization Detector (FID) (see Appendix D, Figure D. 2Figure D. 3 for calibration curves). In cases where the FPD signal had become saturated, the FID signal

was used to quantify the amount of either H_2S or SO_2. The experimental apparatus is shown in Figure 3.14.

3.3.3 Catalyst Preparation

Initial success in promoting the steam reformation reaction was found using an untreated molybdenum wire, however considerable difficulty was encountered in obtaining reproducible results as conversion would decrease after a few hours of operation. Treatment of the wire at high temperature (~1000 ˚C) while flowing H_2O and N_2 failed to produce a working catalyst. Flowing air over the catalyst at 1000˚C resulted in actual diminution of wire near the inlet of the tube, thus this approach was abandoned. Since these treatment most likely formed a MoO_x oxide, the next logical action was to form a sulfide, presumably MoS_2, which was found to be an excellent catalyst choice for Fukuda et al. This was done by flowing a 1% H_2S mixture (in argon) over the wire at flowrates of 0.17-0.42 SCCM in the tube furnace at a temperature of 1000˚C. This treatment was performed initially for 3 h and periodically for durations of 1-15 h as needed or to preserve catalyst integrity during experimental downtime.

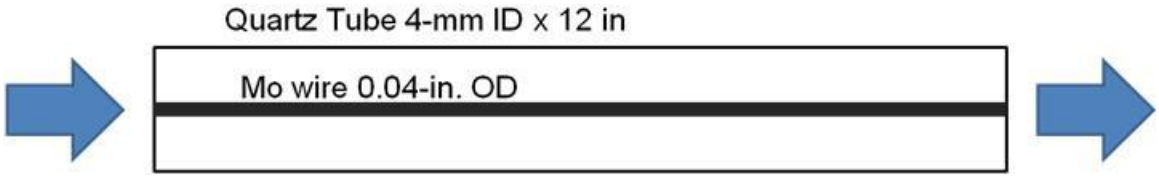

Figure 3.13: Quartz tube reactor with catalyst wire

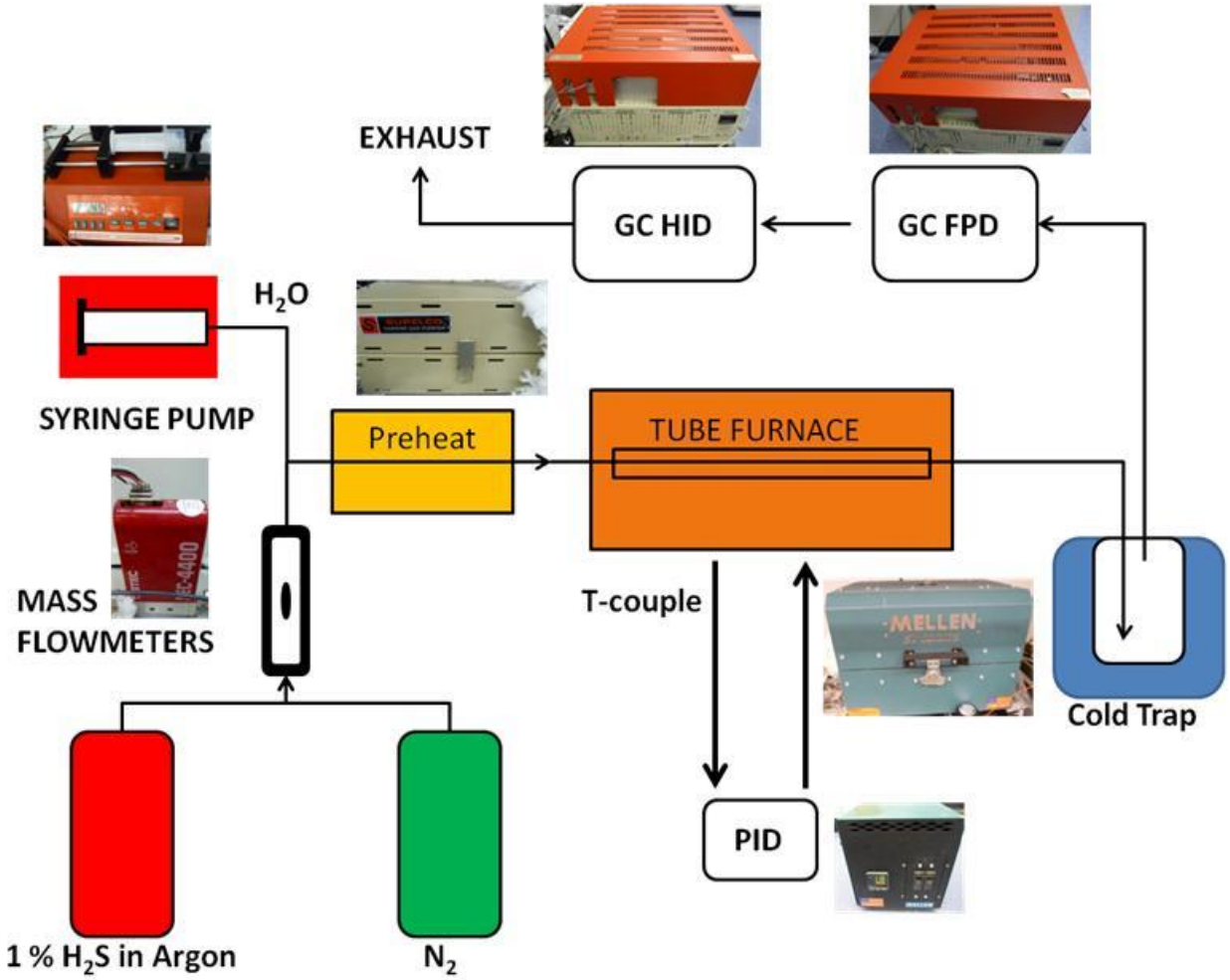

Figure 3.14: Experimental apparatus for steam reformation of H_2S.

3.3.4 Results

The desired reaction between H_2S and H_2O was observed to occur under presence of the molybdenum catalyst. Steam reformation occurred more readily at higher temperatures as expected. Although chemical equilibrium values (based on Gibbs Free Energy) for H_2S were reached, SO_2 and H_2 concentrations were far from reaching predicted equilibrium values, which evidently shows that the steam reformation reaction did not occur to the same extent as the thermal decomposition. Shown below are results pertaining to effects of water ratio and space time on reactor performance.

3.3.4.1 Effects of Water Ratio

Normalized outlet concentrations of H_2, H_2S, and SO_2 are shown below (see Figure 3.15-Figure 3.17). Only H_2S outlet concentrations reach Gibbs equilibrium values, and even slightly exceeded the predicted conversion. Increasing water ratio increases production of SO_2 and H_2 by way of increasing H_2S conversion. When a mass balance of sulfur is performed, the summation of SO_2 and H_2S outlet concentrations leaves a substantial amount of sulfur unaccounted for. This can be explained by estimating the amount of sulfur that could exist as S_2, an unmeasured condensed species, by multiplying the amount of SO_2 measured by a factor of 3 (due to stoichiometry) and subtracting this quantity from the amount of H_2 measured. When this perceived amount of S_2 is included, approximately all sulfur is accounted for (see Figure 3.19). The existence of sulfur as S_2 is highly probable, as condensate showed white and yellow solid formation. Yellow crystals also formed on the end of the reaction tube between the heated reaction zone and the condenser.

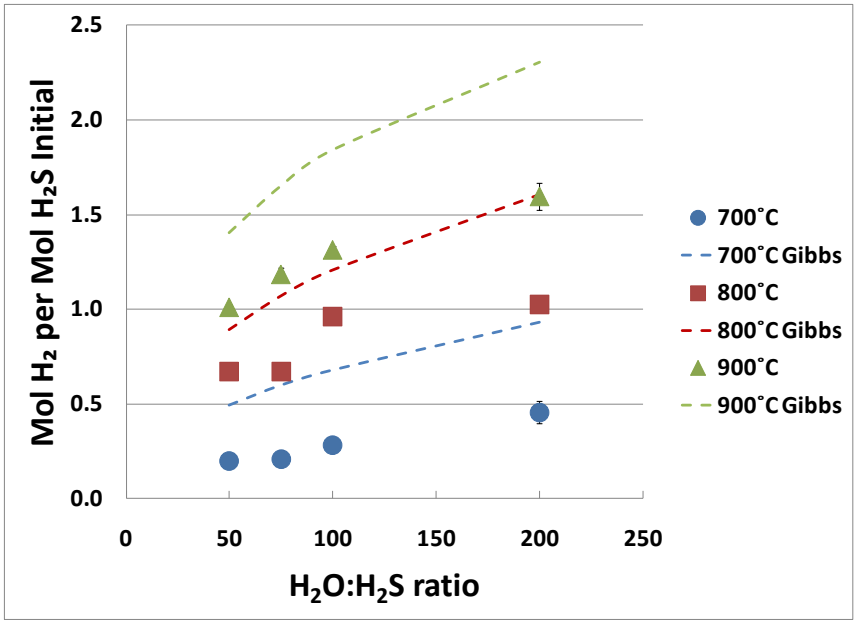

Figure 3.15: Normalized concentrations H_2 at various H_2O:H_2S ratios.

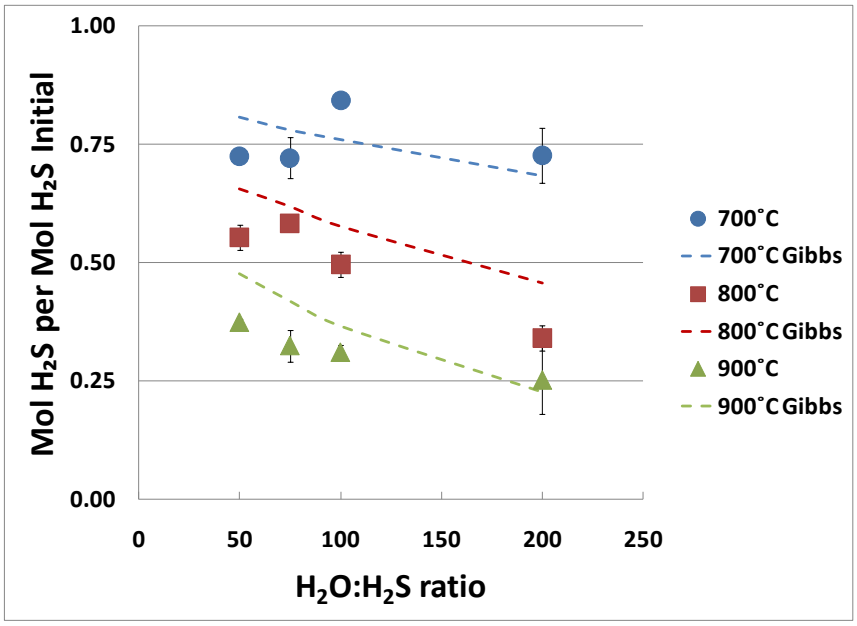

Figure 3.16 Normalized concentrations H_2S at various H_2O:H_2S ratios.

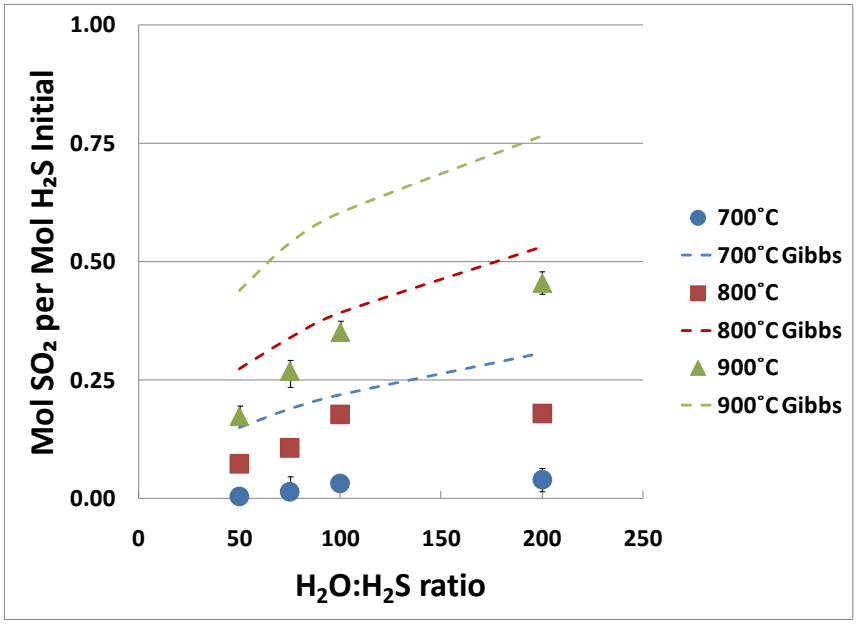

Figure 3.17 Normalized concentrations of SO_2 at various H_2O:H_2S ratios.

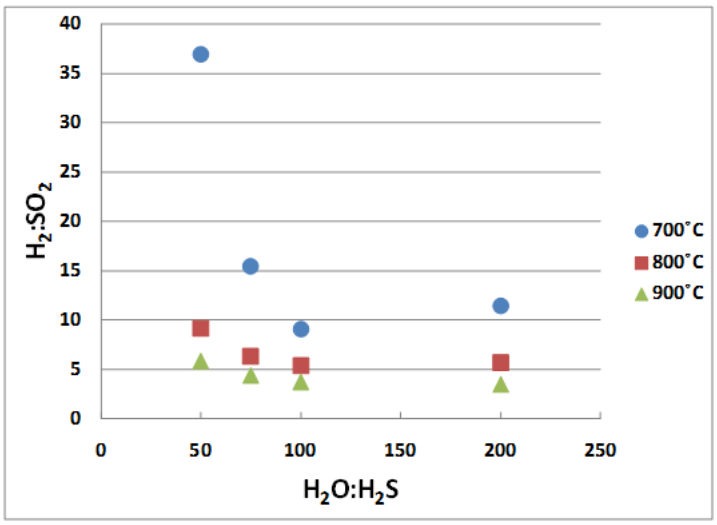

Figure 3.18 H_2:SO_2 ratio at various H_2O:H_2S ratios.

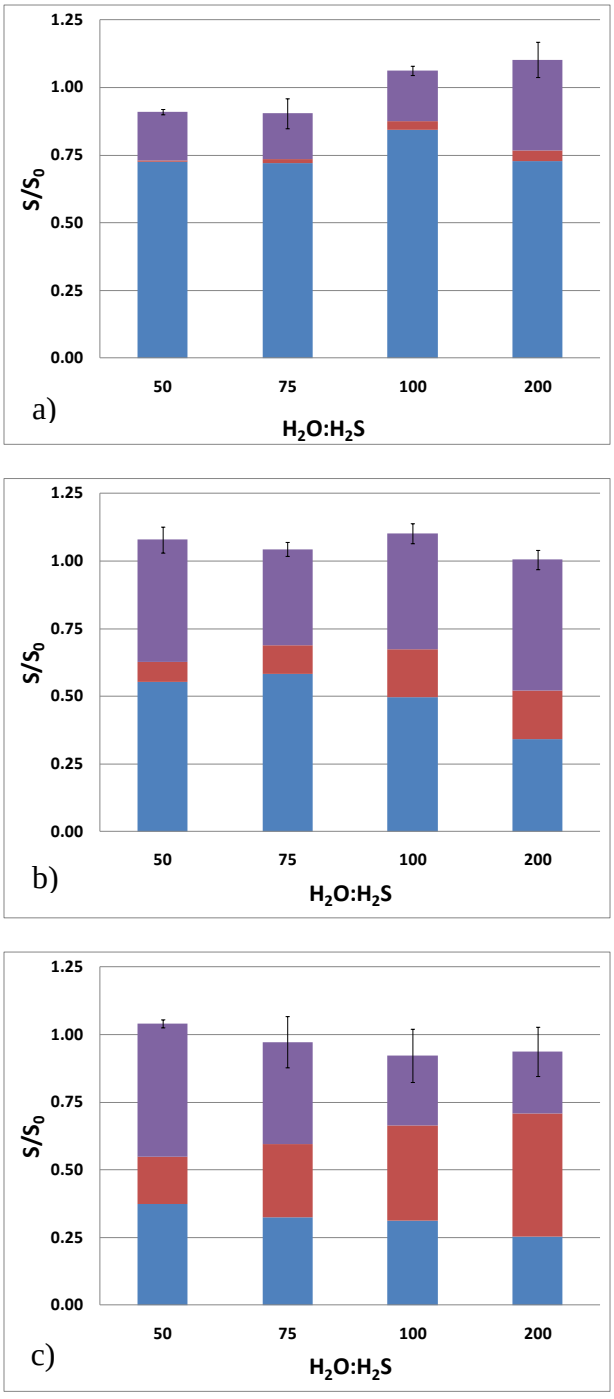

Figure 3.19: Mass Balance on sulfur at various H_2O:H_2S ratios.

a) 700 ˚C , b) 800 ˚C , c) 900 ˚C . ■ H_2S ; ■SO_2 ; ■ S_2.

3.3.4.2 Effect of Residence Time

Trials of three different temperatures (700, 800, 900 ˚C) and three different residence times (4.57, 6.86, 13.72 s) were carried out at a 200:1 H_2O:H_2S ratio. Results for 700 and 800 ˚C show steadily increasing production of SO_2 and H_2 as space time increases, while at 900 ˚C H_2 and SO_2 appear to stagnate (see Figure 3.20-Figure 3.22). The H_2:SO_2 ratio appears to asymptotically approach 3:1 as temperature and space time is increased. Mass balances for sulfur appear in Figure 3.24.

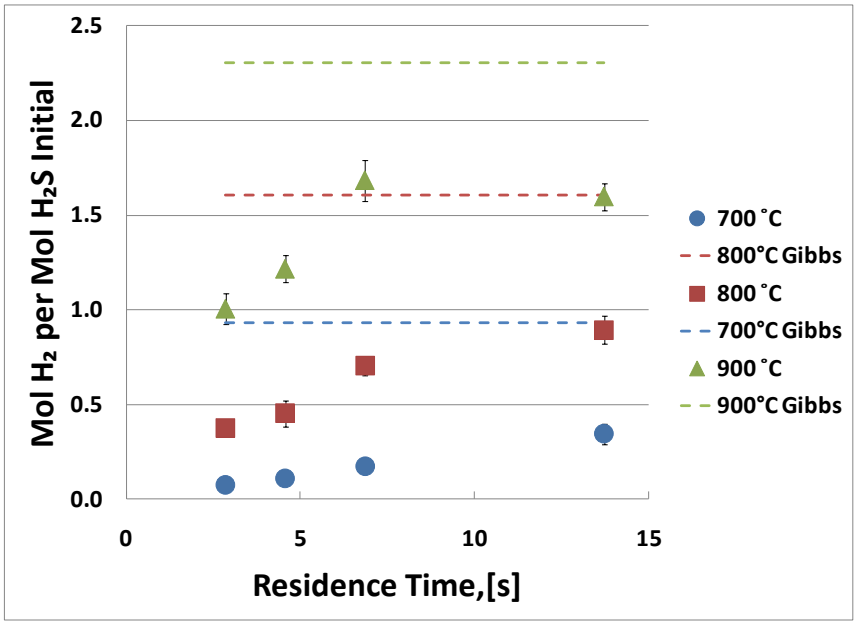

Figure 3.20: Normalized concentration of H_2S at various residence times.

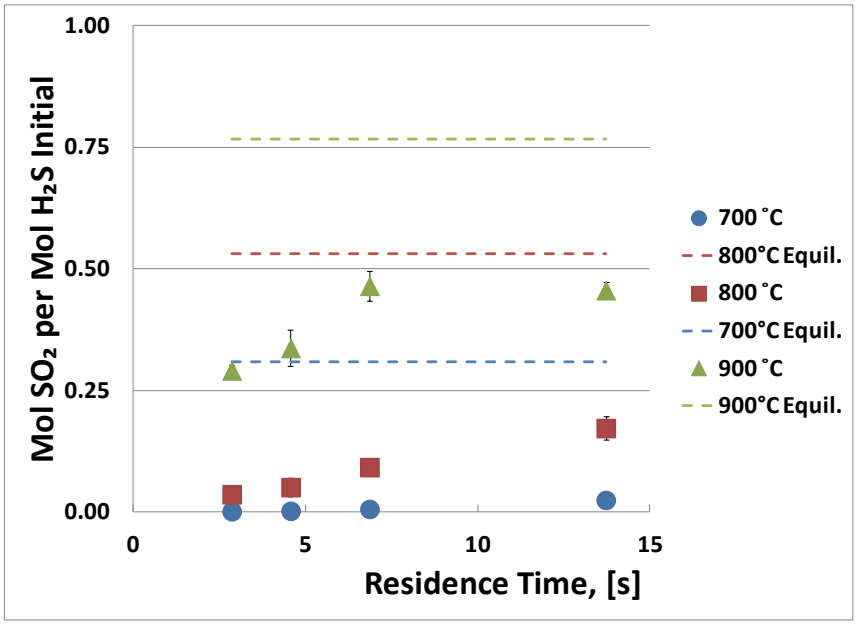

Figure 3.21: Normalized concentration of SO_2 at various residence times.

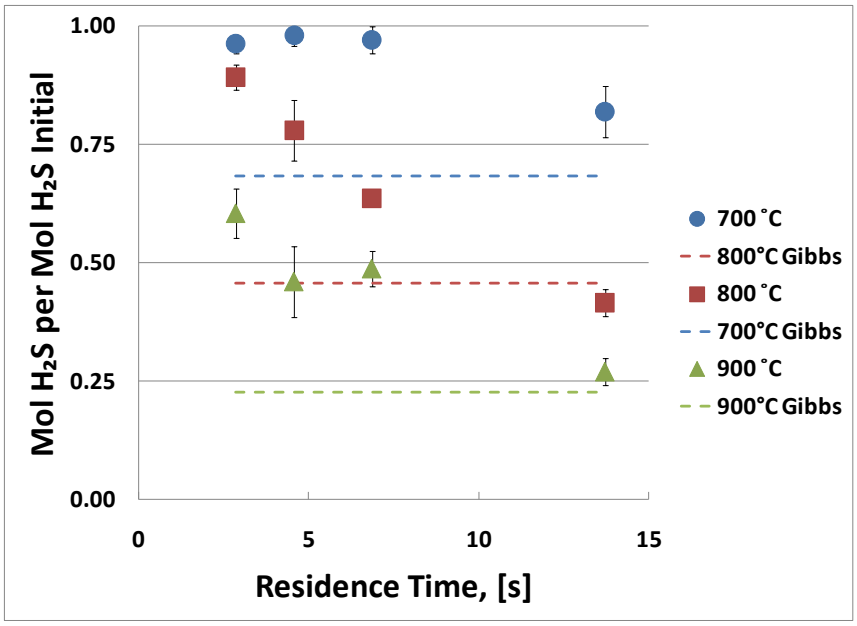

Figure 3.22: Normalized concentration of H_2S at various residence times.

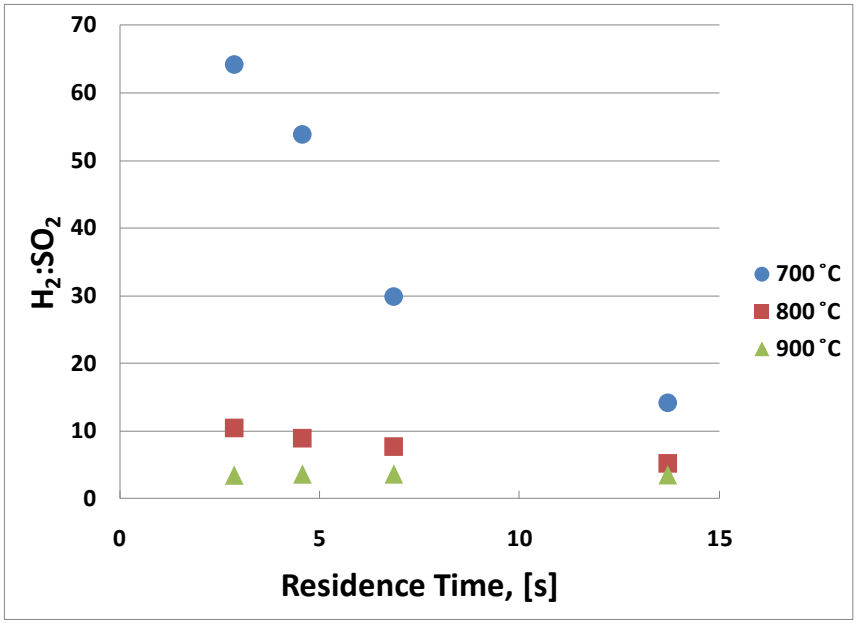

Figure 3.23: H_2:SO_2 ratio at various residence times.

a)

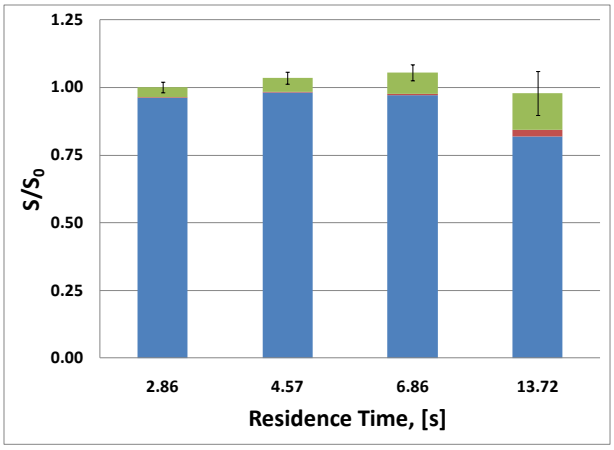

b)

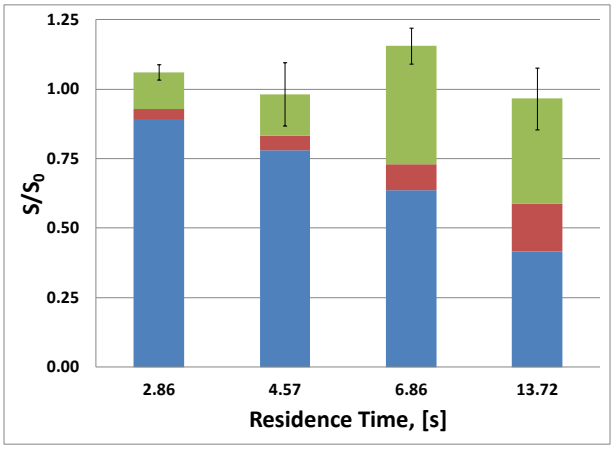

c)

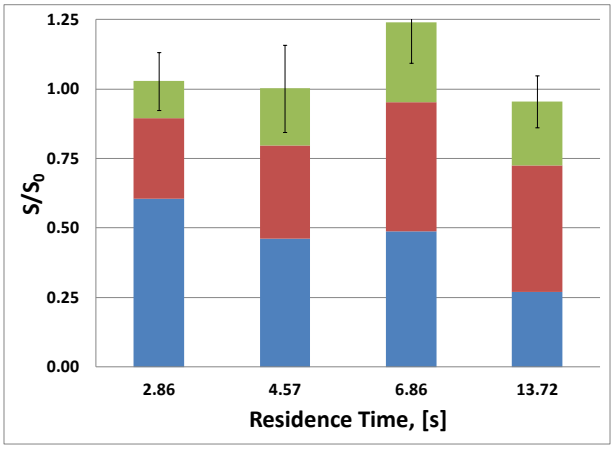

Figure 3.24: Mass balance on sulfur at various residence times.

a) 700 ˚C , b) 800 ˚C , and c) 900 ˚C . H_2S; SO_2; S_2.

3.3.4.3 Influence of surface material

In addition to molybdenum, nichrome (Arcor, USA) was used as a catalyst. The composition was approximately 16.0% chromium, 59.2% nickel, 23.5% iron, and 1% silicon. The preparation and size (18 gauge) was identical to the molybdenum preparation. Yields of H_2 (Figure 3.25) and SO_2 (Figure 3.26) were observed to be comparable to that of molybdenum, though not as high. A quartz tube without a catalyst was also subjected to the same pretreatment methods and tested for steam reformation activity at 900˚ and 1000˚ C. Only at 1000˚C does substantial reaction take place.

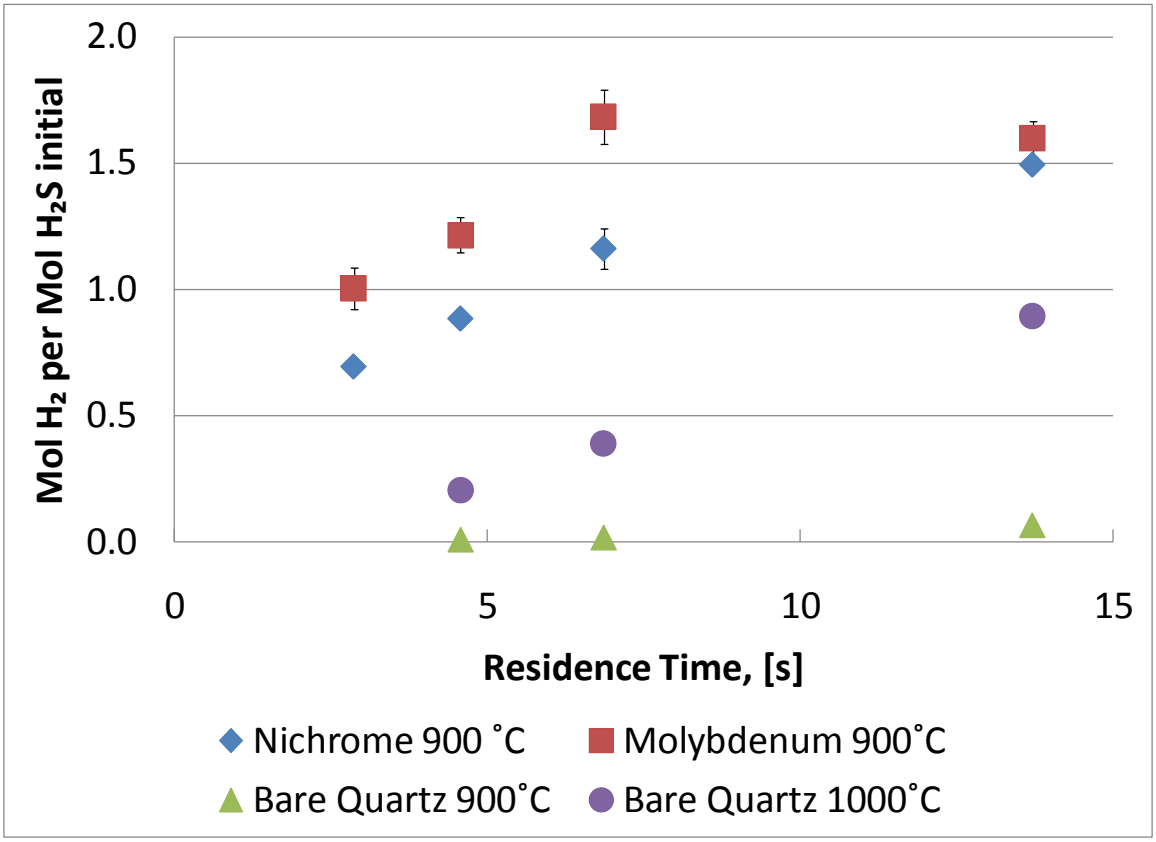

Figure 3.25: Hydrogen yield from steam reformation over other surfaces.

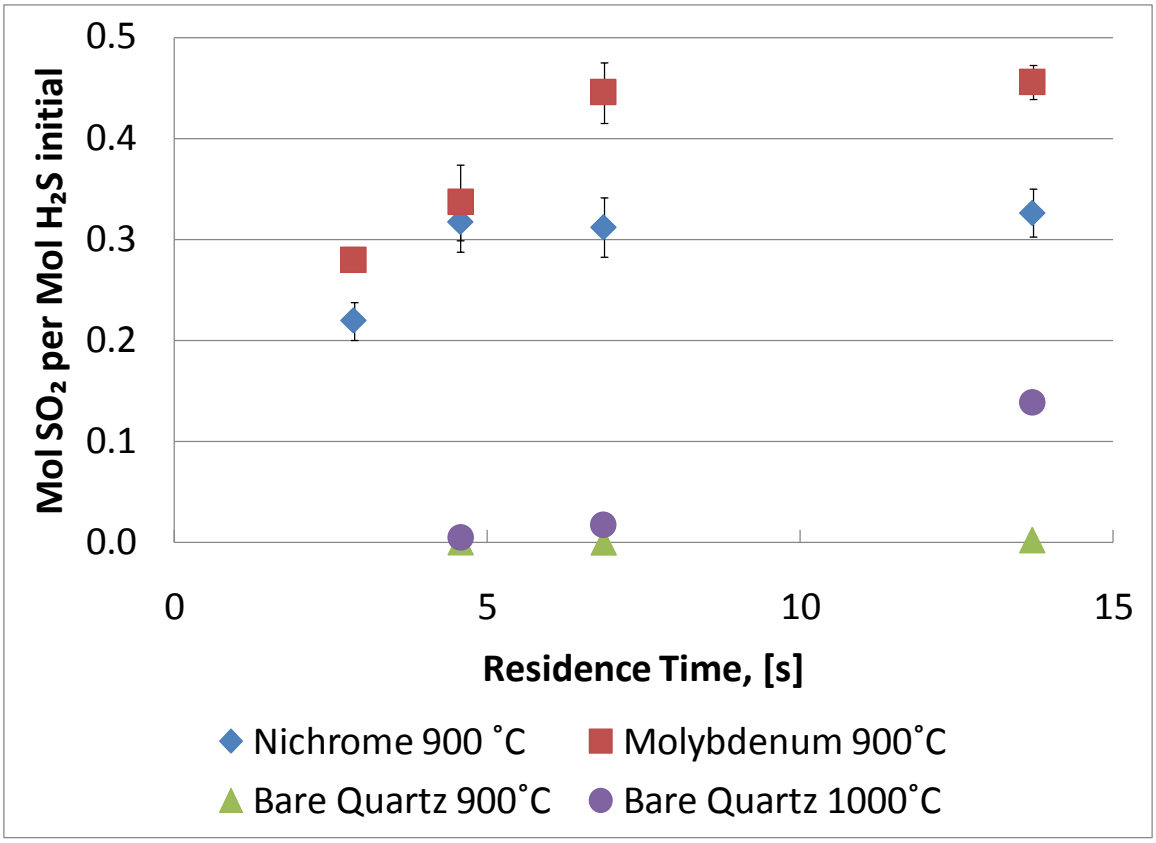

Figure 3.26: Sulfur dioxide yield from steam reformation over other surfaces.

3.3.5 Discussion

In light of competing reactions, the water ratio experiments show increasing selectivity towards steam reformation as water ratio is increased. Inclusion of the implied amount of S_2 formed completes the mass balance. However, although the measured amount of sulfur never exceeds the amount entering, this total amount including S_2 surpasses the inlet amount in certain cases. As H_2O comes into contact with Mo at high temperature, it is possible that a MoO_x is being formed, in effect splitting water and producing H_2. Likewise, another reason for this may be the reverse process, or the replacement of oxygen in MoO_x by sulfur, which would consume H_2S and also produce H_2. Since the amount of S_2 was calculated based on the remainder of H_2 after the subtraction of three times the amount of SO_2, any increase in H_2 would thereby increase the calculated amount of S_2.

Based on previous results of the thermal splitting of H_2S over a molybdenum wire, (see Figure 3.8 and Figure 3.9), it is possible that significant amounts of H_2 and S_2 are being produced via thermal splitting. After long durations, the catalyst did require regeneration with H_2S to redeposit the sulfide layer on the molybdenum catalyst wire. It remains to be seen if this sulfide layer on the catalyst (MoS_2) is being consumed or replaced during the steam reformation reaction. Since the steam reformation reaction works temporarily with an unconditioned catalyst, it would appears that 1) a pre-sulfided layer is not required to facilitate steam reformation and 2) excess water eventually oxidizes the molybdenum catalyst, requiring more conditioning. Future work will have to determine the water proportion and conditioning procedure to extend catalyst viability.

3.3.5.1 Empirical Estimation of Reaction Rate Constants for H_2S-H_2O system at High Temperature

The residence time versus concentration data allowed for apparent kinetic parameter estimation. Reaction rate constants for both the decomposition (reaction 1) and steam reformation (reaction 2) were calculated via a least squares fit of experimental data to proposed rate laws. The rate laws were as follows:

$$r_1 = k_1' C_{H_2S} \qquad \text{Eq. 3.3}$$

$$r_2 = k_2' C_{H_2S} \qquad \text{Eq. 3.4}$$

where $k_1^{'}=k_1\ C_M$ [s^{-1}] (C_M being the concentration of gas species other than H_2S [ppm]) and $k_2^{'}=k_2\ C_{H_2O}$; with k_1 and k_2 as the reaction rate constant of reaction 1 and 2 respectively; and C_{H_2O} being the concentration of H_2O [ppm].

The form of r_2 was chosen since the steam reformation reaction also must undergo cleavage of H-SH bonds, which could very likely be the rate determining step as in thermal decomposition reaction. Since the H_2O concentration, C_{H_2O}, was relatively high, it was assumed that the rate constant, k_2, would carry a constant of proportionality based on the concentration of H_2O in the form of $C_{H_2O}^{n}$, where, n is a constant. For preliminary

estimations, it was further assumed that the reaction order with respect to H_2O is unimolecular, or 1.

The following mathematical model was then derived:

$$\frac{dC_{\mathrm{H_2S}}}{d\tau} = -r_1 - r_2 \; ; \quad C_{\mathrm{H_2S}}(0) = C_{\mathrm{H_2S,0}} \qquad \text{Eq. 3.5}$$

$$\frac{dC_{\mathrm{H_2}}}{d\tau} = r_1 + 3r_2 \; ; \quad C_{\mathrm{H_2}}(0) = 0 \qquad \text{Eq. 3.6}$$

$$\frac{dC_{\mathrm{SO_2}}}{d\tau} = r_2 \; ; \quad C_{\mathrm{SO_2}}(0) = 0 \qquad \text{Eq. 3.7}$$

$$\frac{dC_{\mathrm{S_2}}}{d\tau} = \frac{1}{2} r_1; \quad C_{\mathrm{S_2}}(0) = 0 \qquad \text{Eq. 3.8}$$

The model yields the following analytical solutions:

$$C_{\mathrm{H_2S}}(\tau) = C_{\mathrm{H_2S,0}}[e^{\alpha\,\tau}] \qquad \text{Eq. 3.9}$$

$$C_{\mathrm{H_2}}(\tau) = C_{\mathrm{H_2S,0}}\left[\frac{k_1' + 3k_2'}{\alpha}\right][e^{\alpha\,\tau} - 1] \qquad \text{Eq. 3.10}$$

$$C_{\mathrm{SO_2}}(\tau) = C_{\mathrm{H_2S,0}}\left[\frac{k_2'}{\alpha}\right][e^{\,\alpha\tau} - 1] \qquad \text{Eq. 3.11}$$

$$C_{\mathrm{S_2}}(\tau) = \frac{1}{2} C_{\mathrm{H_2S,0}}\left[\frac{k_1'}{\alpha}\right][e^{\alpha\,\tau} - 1] \qquad \text{Eq. 3.12}$$

where $\alpha = -k_1' - k_2'$, [s^{-1}]; τ is the nominal residence time, [s]; and concentrations, C [ppm], are denoted by a species subscript.

Assuming the temperature dependence of the reaction rate constants can be described by the Arrhenius equation, the pre-exponential terms ($k_{0,i}$) and activation energies ($E_{a,i}$) can be estimated via minimizing a reduced chi-squared (χ_ν^2) objective function that describes the goodness of fit between the model equations for each species and the corresponding experimental data at the three temperatures tested:

$$\text{Reduced chi-squared, } \chi_\nu^2 = \frac{1}{\nu}\sum_{i,j}^{N} \frac{\bar{y}_{i,j} - \bar{C}_i(\tau_j)}{s_{i,j}^2}, \qquad \text{Eq. 3.13}$$

where ν is the degrees of freedom, [dim]; N is the sample size, [dim]; $\bar{y}_i$is the normalized concentration (per mol H_2S initial) of species *i* at data point condition *j*, [dim]; $\bar{C}_i$ is the

normalized model concentration per mol of H_2S initial, [dim]; s is the normalized (per mol of H_2S initial) standard deviation of species *i* under condition *j* [dim]. Since 3 moles of H_2 were possible from the steam reformation reaction, the standard deviation for H_2, (s_{H_2}) was further weighted by a factor of 3 to avoid preferential fitting of the model parameters towards H_2.

The form of the Arrhenius equation used in the model fitting is shown here:

$$k = k_m \exp\left[-\frac{E_a}{R}\left(\frac{1}{T} - \frac{1}{T_m}\right)\right] \qquad \text{Eq. 2.3}$$

where k_m is the pre-exponential term, [s^{-1}]; Ea is the activation energy, [J/mol]; T is temperature, [K]; T_m is a median temperature (in this case 1073 K); R is the ideal gas law constant, 8.314 J-$mol^{-1}K^{-1}$. This form was chosen to avoid correlation between the pre-exponential term and activation energy.[90] Conversion to the more commonly used form of the equation,

$$k = k_0 \exp\left[-\frac{E_a}{RT}\right] \qquad \text{Eq. 2.4}$$

can be accomplished by using the relation:

$$k_0 = k_m \exp\left[-\frac{E_a}{RT}\right], \qquad \text{Eq. 2.5}$$

where k_0 also has units of [s^{-1}]. Using the Arrhenius equation to estimate rate constant, k [s^{-1}], at a given temperature, normalized concentrations for various residence times and temperatures could be predicted. Uncertainties in parameter values were estimated by varying each parameter and observing sensitivity of the reduced chi-squared function to the parameter in question. For experimental data see

Table D. **1** in Appendix D. Plots of model fit can be seen in Figure D.5-Figure D.7 and detailed calculations can be found in Table D. 2 of Appendix D.

Table 3.1: Apparent Arrhenius parameters from steam reformation of H_2S studies in presence of molybdenum wire and thermal splitting of H_2S as determined by Karan et al. without catalyst. Reported variance is ± 1 standard error.

Reaction	**k_0 [s^{-1}]**	**E_a [kJ/mol]**
$H_2S \rightarrow ½\ S_2 + H_2$	$6.57x10^2 \pm 3.97$	82.93 ± 9.48
$H_2S+2H_2O \rightarrow 3H_2+SO_2$	$6.75x10^9 \pm 3.13x10^8$	236.04 ± 5.18
$H_2S \rightarrow ½\ S_2 + H_2$ (Karan et al.)[51]	$5.00x10^9 \pm 4.98x10^8$	236.79 ± 1.66

The minimization of the objective function yielded the Arrhenius parameters shown in

Table 3.1. Activation energy for the thermal splitting of H_2S was considerably lower than that of literature values of Karan et al. which is expected due to use of catalyst in this study. A linearized Arrhenius plot shows that the apparent rate constant for steam reformation begins to overtake that of thermal splitting as temperature is increased. Since the Gibbs equilibrium predictions show increasing prevalence of steam reformation as temperature increases, this kinetic data only further stresses that higher temperatures are beneficial to the process.

3.3.6 Conclusion

In revisiting the initial goals of this study, it appears that the steam reformation of H_2S is indeed possible, although the conversion to desired products of SO_2 and H_2 did not reach predicted values based on Gibbs equilibrium. Fortunately, temperatures of 900 ˚C are at the low end of concentrated solar thermal capabilities, and much is to be gained from simply increasing reaction temperature. For a thermally viable process, the H_2O:H_2S ratio will also have to be decreased to at least 20:1, corresponding to thermal efficiency of roughly 37% based on higher heating value. Preliminary kinetic data yielded Arrhenius parameters for the process and will be useful for sizing of future reactors, and apparent reaction rate constants compared well with literature values. The steam reformation reaction rate constant was found to surpass that of thermal splitting at a temperature between 800-900°C. Molybdenum showed viability as a catalyst and clearly helped increase conversion over non-catalytic trials. The highly endothermic steam reformation of H_2S has been demonstrated, further making a strong case for the Sulfur-Sulfur cycle as a potential hydrogen production method.

4 PROCESS DESIGN OF SULFUR-SULFUR CYCLE

4.1 Estimation of Overall Thermal Efficiency of the Sulfur-Sulfur Cycle

Hydrogen is simply a way to store energy in the form of chemical bonds. While H_2 is relatively easily produced by natural gas reformation, this method is not carbon free as CO_2 is the byproduct. Furthermore, energy in the form of heat is required to drive the reaction at high temperatures, which requires additional natural gas. A higher overall efficiency could be realized if the natural gas had simply been burned to generate thermal energy for heating either buildings or generating steam as in a power plant. As a result, hydrogen production methods must be initially evaluated as to how efficiently they transform primary energy, in this case heat, to chemical energy. As employed by many sources, thermal efficiency of a thermochemical water splitting cycle is defined as follows: [4, 11, 20]

$$\eta = \frac{\Delta H_{f,H_2O}}{Q + W/\eta_R} \qquad \text{Eq. 4.1}$$

Where η is overall thermal efficiency, [dim]; $\Delta H_{f,H_2O}$ is the higher heating value of water, 286 [kJ/mol]; [4, 91] Q is the heat input [kJ/mol]; W is the work input [kJ/mol]; and η_R is an efficiency for electrical production using high temperature nuclear reactors, which is taken to be ~0.5 [dim]. [20]

If a thermochemical cycle is conceptualized as a heat engine, it can be shown that Q=TΔS and W=ΔG= ΔH-TΔS, where T is temperature,[K]; ΔS is the change of enthalpy, [kJ/mol]; ΔG is the change in Gibbs Free Energy, [kJ/mol]; and ΔH is the change in enthalpy, [kJ/mol]. For a process in which all energy input is heat and ΔH-ΔG ≥ 0:

$$Q = \Delta H - \Delta G, \qquad \text{Eq. 4.2}$$

and the total energy input is then:

$$Q + W/\eta_R = \Delta G/\eta_R + (\Delta H - \Delta G). \qquad \text{Eq. 4.3}$$

The estimation of upper-bound thermal efficiency has already been done for the sulfur-iodine cycle by many sources, the most recent of note (51%) by Goldstein et al. The sulfur-sulfur cycle proposed here would eliminate the HI decomposition steps yet add a high temperature steam reformation of H_2S. The Bunsen section and H_2SO_4 decomposition section is assumed to have the same heat and work inputs as outlined by Goldstein et al. The Bunsen section requires 17 kJ/mol of work due for compression of SO_2 to 2 bar.[20] Using the balanced, stoichiometric equations for the Sulfur-Sulfur cycle, an overall thermal efficiency can be calculated. For more detailed calculations see Table D. 3-Table D. 5 in Appendix D. Thermodynamic properties for the species of interest can be found in Appendix A, Table A. 2 and Table A.3.

Table 4.1: Energy inputs for a Sulfur-Sulfur Cycle operating at ~1100 K, with a 2:1 H_2O:H_2S ratio in the steam reformation section.

Section	**$Q+W/\eta_R$ [kJ/mol H_2S]**
Bunsen	4x17 = 68
H_2SO_4 Decomposition (1123 K)	3x352 = 1056
Steam Reformation of H_2S (1100 K)	436
TOTAL	**1560**

As a result of this stoichiometry, the Goldstein estimates of heat input for the decomposition section of H_2SO_4 (352 kJ/mol) are multiplied by 3, and the work input for the Bunsen reaction (17 kJ/mol) is multiplied by 4 (see Table 4.1). For calculating the steam reformation of H_2S, the energy input is the sum of ($Q+W/\eta_R$) for the reaction and the heat of vaporization of the two moles of water added for each mole of H_2S (Goldstein et al. did not include sensible heat addition in their estimation). Using this formulation, the overall thermal efficiency is estimated to range from 55% at a reaction temperature of 1100 K to 58% at 2000 K. The overall thermal efficiency is a strong function of the H_2O:H_2S ratio used in the steam reformation step (see Figure 4.1). At the temperatures of interest, an H_2O:H_2S ratio of 20:1 can still achieve a thermal efficiency of roughly 35% which would be a substantial improvement over any other existing renewable-based

hydrogen production method. On a LHV basis, it would have an efficiency of approximately 32%, which is similar to the 33% figure estimated by Gorensek et al. for PEM electrolysis via a high temperature gas cooled reactor (HTGR).[30] It should be noted, however, that the boundaries of these calculations do not include likely radiative heat losses that might be suffered using solar thermal concentrators, nor do they take into account complications stemming from lower reaction conversion experienced by operating at lower temperatures. Furthermore, an inert sweep gas would be very useful in many sections of the system especially a continuous hydrogen permselective membrane reactor for the steam reformation step. However, separation of inert gas from a stream of H_2, O_2, or air requires separation work, which decreases overall efficiency. If a heat integration scheme cannot supply large enough amounts of sensible heat needed, external heating will be required further decreasing efficiency. Nevertheless, since the proposed Sulfur-Sulfur cycle makes use of ionic liquids with high SO_2 solubilities, the slightly elevated pressures (and work requirements) employed in the Sulfur-Iodine cycle may not be necessary to enable high liquid phase SO_2 concentrations. Appendix D has more detailed calculations involving thermal efficiency.

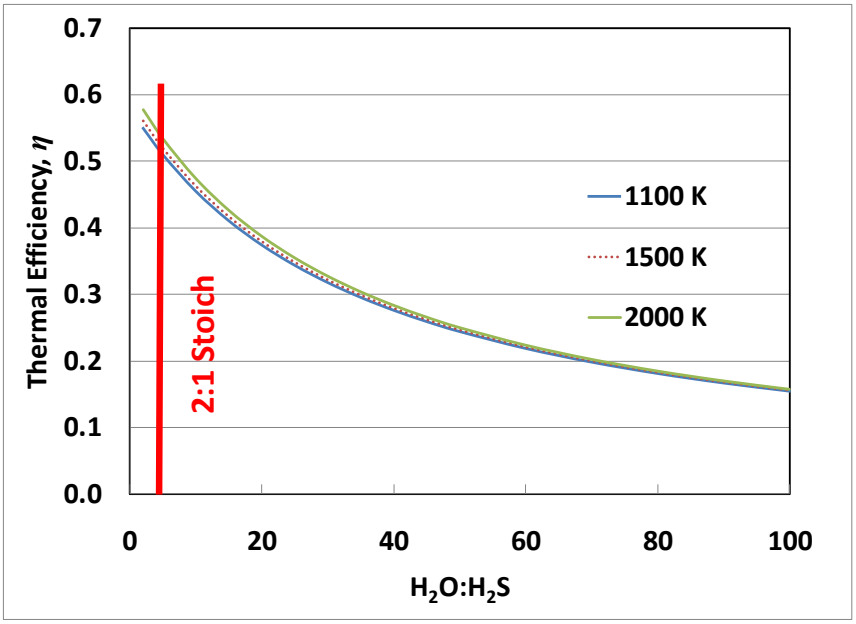

Figure 4.1: Sensitivity of overall thermal efficiency to H_2O:H_2S ratio using in the steam reformation step. Thermal efficiency is based on the HHV of H_2O (286 kJ/mol).

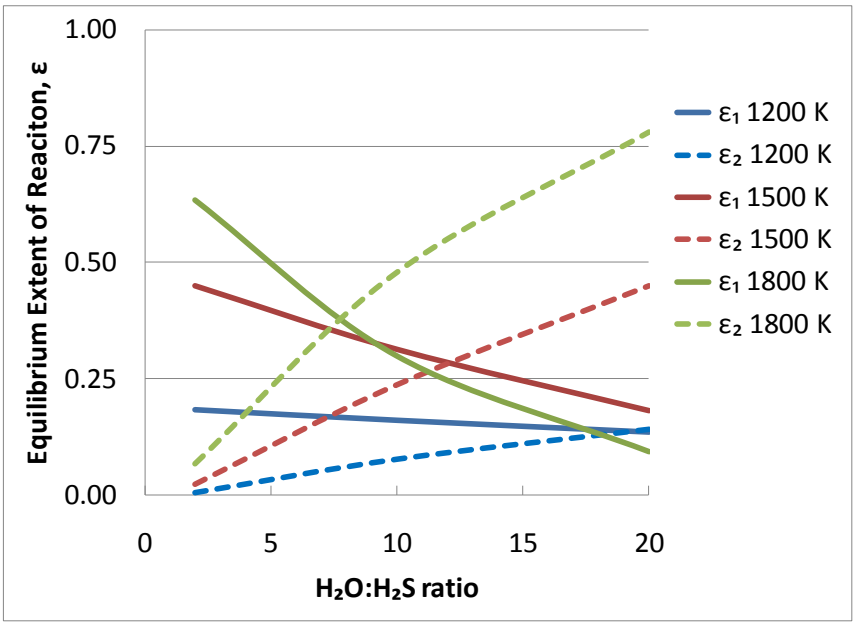

Figure 4.2: Dependence of extent of reaction for both thermal splitting (ε_1) and steam reformation (ε_2) on temperature and H_2O:H_2O ratio.

As shown in the experimental work, the steam reformation of H_2S occurred readily at 1100 K. The thermodynamics, however, show that the reaction is not spontaneous at 1100 K, having a Gibbs free energy change of 129 kJ/mol of H_2S, leading to the conclusion that experimental success was due to severe dilution of H_2S in argon and steam. Even at 2000 K, the Gibbs free energy change for the steam reformation reaction is strongly positive at 47 kJ/mol of H_2S, and the equilibrium constant, K still less than unity (K= 0.0587).

$$K = \frac{y_{H_2}^3 y_{SO_2} P}{y_{H_2S} y_{H_2O}^2} \qquad \text{Eq. 3.2}$$

Adding sufficient excess of steam to achieve complete conversion would require so much heat to vaporize H_2O that the overall thermal efficiency would decrease to near zero. It is therefore desired to use a modest excess of water, an inert, diluting gas, or a continuous product separation scheme. For example, if steam and inert gas are added at a 20:1 molar ratio to H_2S at 2000 K, an equilibrium conversion of 92% can be reached (see Appendix D). There are many other routes to producing H_2 from H_2S,[49, 56, 60-62, 92] yet since the stoichiometry requires the decomposition of 3 moles of H_2SO_4 for each mole of H_2S, it is imperative that 3 moles of H_2 are produced (per mole of H_2S); otherwise the cycle would be thermally handicapped. Steam reformation is the most straightforward method of producing a sufficient amount of hydrogen and regenerating SO_2.

4.2 Process Considerations

An overall conceptual design of the sulfur-sulfur cycle is shown below in Figure 4.3. The initial reactions (Bunsen + H_2S generation reaction) occur in a gas-liquid contacting column, where an ionic liquid stream with dissolved I_2 and H_2O absorbs SO_2. This reactor will facilitate both reactions, so that I_2 is regenerated and can be recycled. The gas product stream is then mixed with water and enters the high temperature decomposition section where H_2S is reformed to H_2 and SO_2. The liquid products from the reactor undergo heat swing to vaporize the H_2SO_4/SO_3 species, which then undergo high temperature decomposition to form O_2, SO_2, and H_2O.

Separation of both H_2 and O_2 from SO_2 is done by passing the gas streams through an ionic liquid absorbent to use their high solubility for SO_2 as a separating mechanism. The SO_2-saturated ionic liquid is then sent to a liquid stripper where it undergoes heating to release the SO_2 for recycle. A steam reformation reaction carried out in a hydrogen-selective ceramic membrane may offer an alternative way to separate the SO_2-H_2 mixture while simultaneously increasing conversion.

Due to material availability issues associated with iodine,[5, 93] it may also be of interest to explore using bromine in place of iodine.[94] In 2010, annual global production of bromine was 380,000 tons compared to 29,000 tons of iodine. There are reportedly 11 million tons of bromine reserves in the United States, and perhaps 1 billion tons in the Dead Sea.[95]

Another issue is storage of H_2S produced in a dark reaction (reaction carried out when solar heat is not available). Though H_2S is a toxic gas, its presence is ubiquitous in the petroleum and natural gas production industries, and safety items such as low level H_2S gas sensors are widely available. Vast amounts of knowledge on keeping workers safe under these conditions are available. Further, its low olfactory recognition threshold of 0.025 ppm makes its presence easy to recognize, at least upon first exposure.[96] Storage of the intermediate product from the reaction during dark periods, simple pressurization of the H_2S in an enclosed, heavy double wall tank may be adequate.

A more advanced option would involve absorption of the H_2S gas in a storage medium such as an ionic liquid such as 1-butyl-methylimidazolium tetrafluoroborate [BMIM][BF_4], for which mole fractions of up to 0.7 are reported.[74] This could also double as a pressure swing separator for any SO_2 entrained in the product stream. During periods of solar intensity, pressure could be decreased until H_2S vaporizes, leaving the residual SO_2 behind in the liquid matrix.

Whereas the Sulfur-Iodine and Hybrid Sulfur cycles have traditionally been designed for use with high temperature nuclear reactors, a whole host of other cycles have been proposed for solar thermal utilization. The most promising involve 2-step metal oxide reduction schemes composed of a high temperature step that could be done during the day, and a low temperature step that could be accomplished at night.[5] Although these cycles have been proven, they are challenged due to the use of solid reactants and their associated lifetime issues. Furthermore, the temperatures required for many of the metal oxide reductions make reactor material selection quite difficult.[3] The fluidic nature of all Sulfur-Sulfur species makes the Sulfur-Sulfur cycle much easier to implement.

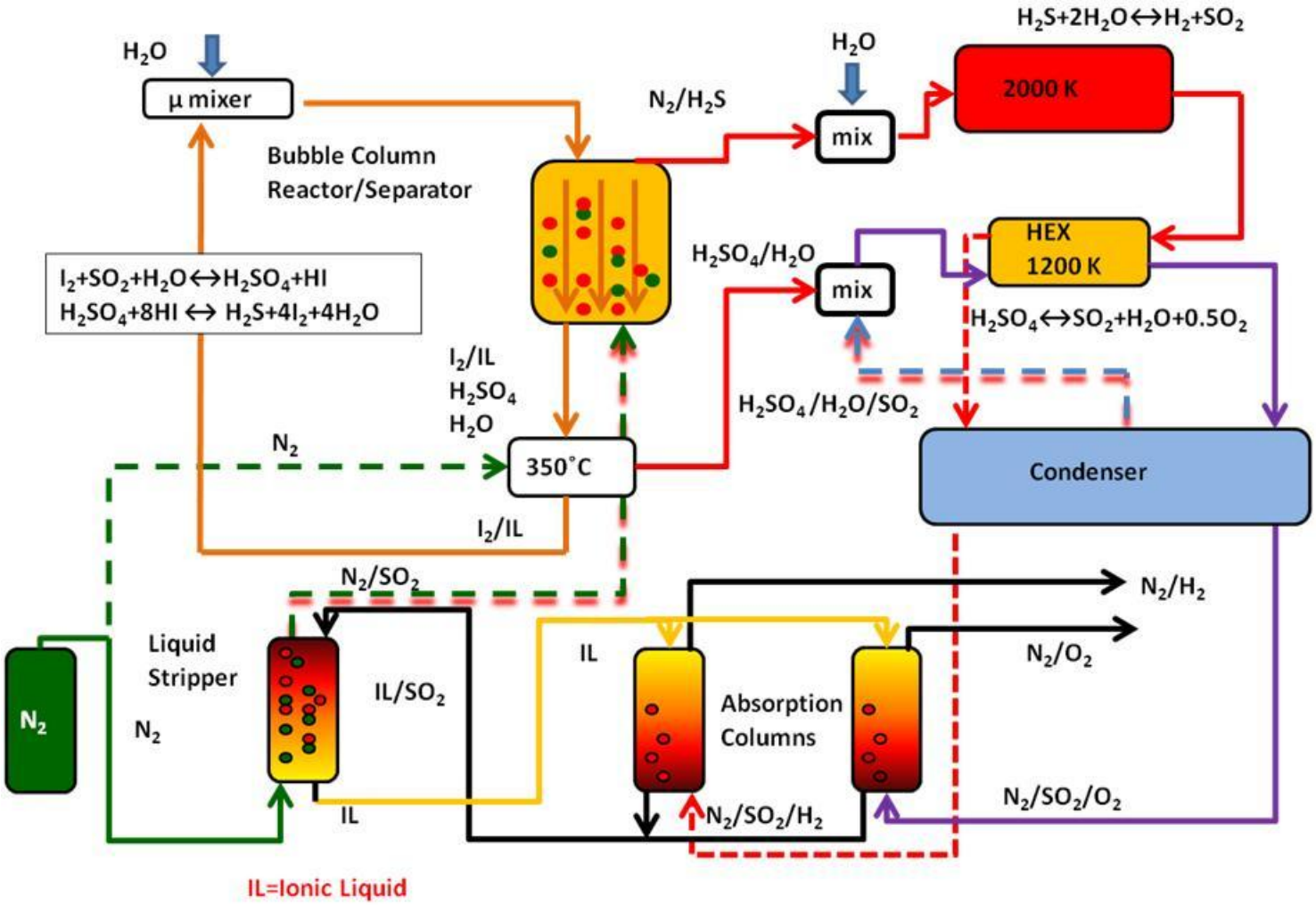

Figure 4.3: Conceptual Diagram of Sulfur-Sulfur Cycle Process

5 CONCLUSION AND FUTURE WORK

5.1 Conclusion

Sustainable hydrogen production from water using thermochemical methods has been an elusive goal for the last 40 years. Difficult separations, involvement of solid phase species, and material compatibility issues have held back significant development of any thermochemical cycle. This is especially true of the Sulfur-Iodine cycle.

The work presented here has made important modifications to this most heavily studied cycle. Using an ionic liquid such as [BMIM][OTf] as an alternative reaction medium led to the production of H_2S, not HI, as originally hypothesized. All Bunsen reactants (I_2, SO_2, H_2O) readily dissolve in the imidazolium-based hydrophilic ionic liquids and the Bunsen reaction was shown to occur in ionic liquid [BMIM][OTf]. The Arrhenius pre-exponential term, k_0, and activation energy, E_a, estimated from directly fitting were found to be 61,500 ± 4900 s^{-1} and 32.9 ± 3.0 kJ-mol^{-1} respectively.

Attempts to release HI vapor from the liquid matrix were unsuccessful, however, the evolution of significant (i.e. ~5% SO_2 conversion) H_2S under conditions of high temperature and excess water lead to the development of an alternative approach to thermochemical water splitting using sulfur and iodine. Since the side reaction that produces H_2S also conveniently regenerates I_2, iodine can remain in the liquid phase.

This new Sulfur-Sulfur Cycle requires a steam reformation step in order to close the cycle and generate sufficient H_2. Steam reformation was successfully done at a preliminary proof-of-concept experiment in a stainless steel tube heated in a tube furnace. A more quantitative experiment was then performed with a molybdenum wire inserted into quartz tubing. At the highest temperature tested (900°C) and maximum dilution by water (200:1), maximum yields of roughly 1.5 moles H_2 and 0.5 moles of SO_2 per initial mole of H_2S were observed. As expected, preference to steam reformation over thermal splitting is seen as H_2O:H_2S ratio increases. A mass balance that includes unmeasured S_2 accounts for all sulfur. During times of declining activity, the molybdenum wire was successfully regenerated in H_2S at 1000˚C, which gives evidence that the effective

catalyst is presumably MoS_2. Nichrome wire had slightly less activity than molybdenum. A kinetics investigation determined the apparent Arrhenius parameters for both the steam reformation reaction and thermal splitting reaction of H_2S and agreed well with past literature.[51]

Thermodynamic calculations show that a modest H_2O:H_2S molar ratio of 20:1 would still yield an upper bound thermal efficiency of roughly 37% (based on HHV), which is a significant improvement over any currently existing renewable hydrogen production method. Ionic liquids could also play a vital role in separation/recovery processes due to their high capabilities for physical absorption of SO_2, which has already been suggested in previous studies.[97] Overall upper-bound efficiency is estimated to be 59%, making the Sulfur-Sulfur cycle a viable candidate for thermochemical water-splitting.

5.2 Future Work

5.2.1 Hydrogen Sulfide Generation

Based upon preliminary experiments showing H_2S generation via a side reaction of the Bunsen products, a reactor will be constructed. The reactor will be capable of absorbing SO_2 from a gas stream, carrying out the two liquid phase reactions, and releasing H_2S vapors from one outlet and an ionic liquid/I_2 mixture from the other outlet. Since preliminary experiments suggest relatively slow kinetics, substantial understanding into the timeframes associated with the reaction on a batch scale is required before sizing and design of a flow reactor is done.

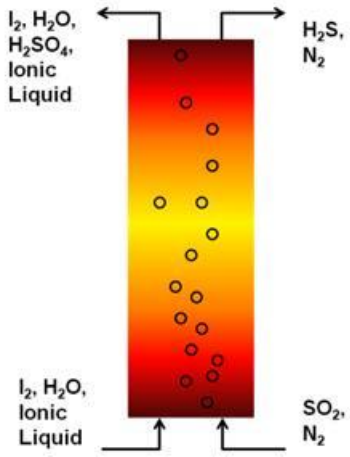

Figure 5.1: Gas-liquid contacting reactor for H_2S production

5.2.2 Steam Reformation

From a preliminary thermodynamic analysis, it appears that there is excellent potential for steam reformation at temperatures higher than those used in this work. Future efforts should utilize heat sources capable of temperatures up to at least 2000 K. Figure 5.3 shows that the predicted residence times required by a reactor operating under a 20:1 H_2O: H_2S ratio at 1500°C to reach nearly full conversion can be quite short, on the order of 0.02 s.

While this work presents preliminary screening of suitable catalysts such as molybdenum and chromium, a suitable high temperature catalyst support in the form of a packed bed or porous network should be used to improve catalyst surface area and stability. Molybdenum sulfide has a melting point of roughly 1185°C, and that of chromium sulfide is slight higher (1350°C). Temperatures stability, surface area, and selectivity of catalysts towards steam reformation can all be improved to promote higher yields.

To further improve the extent of the steam reformation reaction, the reaction channel can be lined with a hydrogen selective membrane. This membrane can continuously remove H_2, thereby increasing conversion of H_2S via mass action, which

has previously been demonstrated by Edlund and Pledger in thermal splitting of H_2S.[58] A membrane reactor would also greatly improve downstream SO_2/H_2 separation, as most H_2 will have already been separated from the SO_2 stream into the permeate stream. As a result, the downstream separation process may require less ionic liquid absorbent or maybe unnecessary altogether.

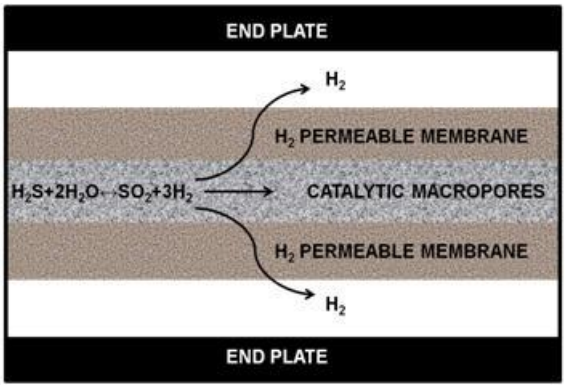

Figure 5.2: Conceptual diagram of membrane reactor

5.2.3 Process Simulation

Once rough estimates of real reactor performance for both H_2S generation and steam reformation can be determined, it is recommended that a process flowsheet be constructed. This flowsheet can test metrics such as thermal efficiency for their sensitivity towards reactant ratios, temperature, pressure, and flow rates. Such a flowsheet will also aid in making strategic decisions regarding scheduling of process steps based on the diurnal solar cycle. Heat integration will also be assessed, which will shed light on the realistic thermal efficiencies to expect.

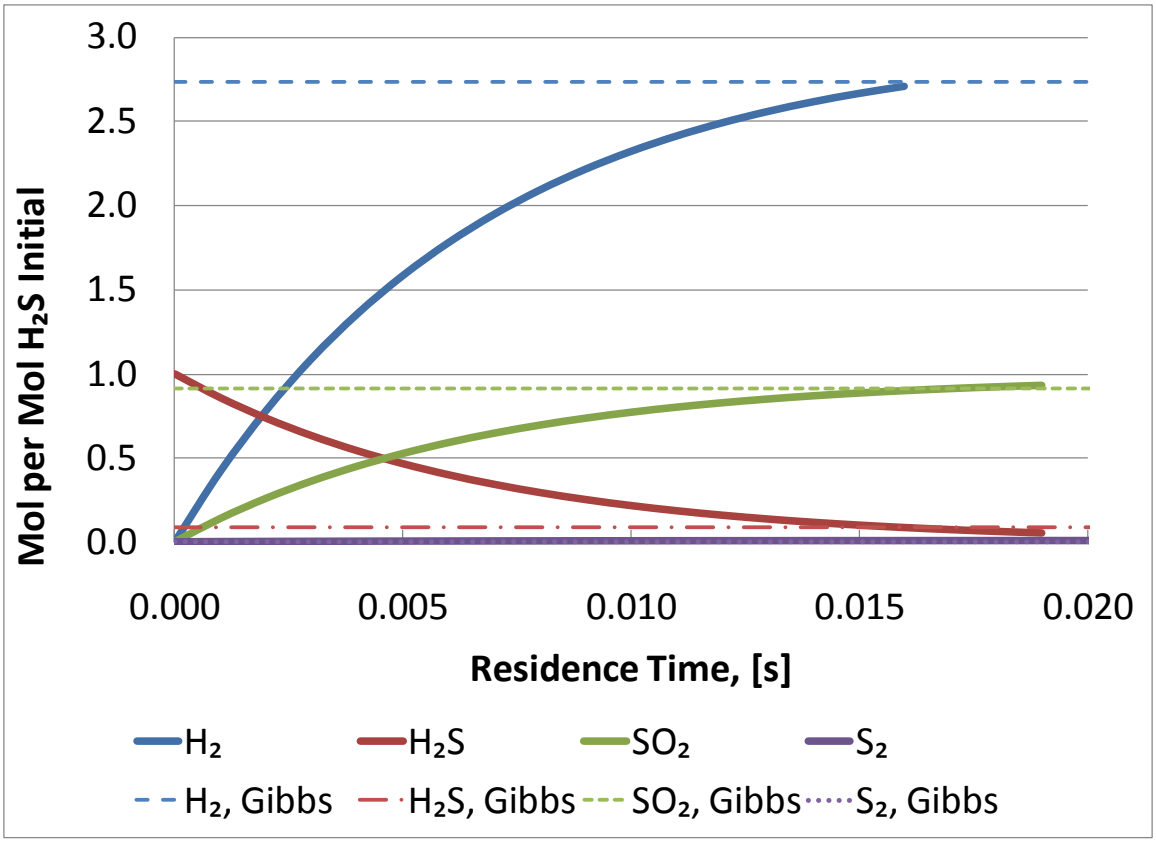

Figure 5.3: Predicted outlet composition from steam reformation reactor operating at 1500°C with a 20:1 H_2O:H_2S ratio, based on kinetic parameters obtained in this work.

BIBLIOGRAPHY

1. Lutz, A. E.; Larson, R. S.; Keller, J. O., Thermodynamic comparison of fuel cells to the Carnot cycle. International Journal of Hydrogen Energy 2002, 27 (10), 1103-1111.

2. Perkins, C.; Weimer, A. W., Likely near-term solar-thermal water splitting technologies. International Journal of Hydrogen Energy 2004, 29 (15), 1587-1599.

3. Licht, S., Thermochemical solar hydrogen generation. Chemical Communications (Cambridge) 2005, 4635-4646.

4. Funk, J. E. In Thermochemical Production of Hydrogen via Multistage Water Splitting Processes, Hydrogen Energy Fundamentals, Miami, Florida, Veziroglu, T. N., Ed. University of Miami: Miami, Florida, 1975; pp S2-3-S2-27.

5. Perkins, C.; Weimer, A. W., Solar-Thermal Production of Renewable Hydrogen. AIChe Journal 2009, 55 (2), 286-293.

6. Giaconia, A.; Caputo, G.; Ceroli, A.; Diamanti, M.; Barbarossa, V.; Tarquini, P.; Sau, S., Experimental study of two phase separation in the Bunsen section of the sulfur–iodine thermochemical cycle. International Journal of Hydrogen Energy 2007, 32 (5), 531-536

7. Holbrey John, D.; Turner Megan, B.; Rogers Robin, D., Selection of Ionic Liquids for Green Chemical Applications. In Ionic Liquids as Green Solvents, American Chemical Society: Washington, DC, 2003; pp 2-12.

8. Russell, J. L.; McCorkle, K. H.; Norman, J. H.; Porter, J. T.; Roemer, T. S.; Schuster, J. R.; Sharp, R. S. In Water Splitting-A Progress Report, 1st World Hydrogen Energy Conference, Miami Beach, Florida, March 1-3, 1976; Veziroglu, T. N., Ed. The School of Continuing Studies, University of Miami: Miami Beach, Florida, 1976; pp 1A-105-1A-125.

9. Steinfeld, A., Solar hydrogen production via a two-step water-splitting thermochemical cycle based on Zn/ZnO redox reactions. International Journal of Hydrogen Energy 2002, 27 (6), 611-619.

10. Bhosale, R. R.; Shende, R. V.; Puszynski, J. A., Thermochemical water-splitting for H2 generation using sol-gel derived Mn-ferrite in a packed bed reactor. International Journal of Hydrogen Energy In Press, Corrected Proof.

11. Funk, J. E.; Reinstrom, R. M., Energy Requirements in Production of Hydrogen from Water. Industrial and Engineering Chemistry Process Design and Development 1966, 5 (3), 336-342.

12. Barnert, H.; Schulten, R. In Nuclear Water Splitting and High Temperature Reactors, Hydrogen Energy, Miami, Veziroglu, T. N., Ed. Plenum Press: Miami, 1974; pp 115-136; Quade, R. N.; McMain, A. T. In Hydrogen Production with a High-Temperature Gas-Cooled Reactor (HTGR), Hydrogen Energy, Miami, Veziroglu, T. N., Ed. Plenum Press: Miami, 1974; pp 137-154; Balcomb, J.; Booth, L. In High Temperature Nuclear Reactors as an Energy Source for Hydrogen Production, Hydrogen Energy, Miami, Veziroglu, T. N., Ed. Plenum Press: Miami, 1974; pp 129-136.

13. Harth, R. E.; Hoehlein, B. In Hydrogen Production Process by Means of Nuclear Energy, 1st World Hydrogen Energy Conference, Miami Beach, Florida, March 1-3, 1976; Veziroglu, T. N., Ed. The School of Continuing Studies, University of Miami: Miami Beach, Florida, 1976; pp 1A-3-1A18.

14. Hildebrandt, A. F.; Vant-Hull, L. L. In A Tower-Top Point Focus Solar Energy Conversion, Hydrogen Energy, Miami, Veziroglu, T. N., Ed. Plenum Press: Miami, 1974; pp 35-44; HAHM, T.; SCHMIDT–TRAUB, H.; LEßMANN, B., A CONE CONCENTRATOR FOR HIGH-TEMPERATURE SOLAR CAVITYRECEIVERS. Solar Energy 1999, 65 (1), 33-41.

15. Steinfeld, A., Solar thermochemical production of hydrogen—a review. Solar Energy 2005, 78, 603-615.

16. Sakurai, M.; Bilgen, E.; Tsutsumi, A.; Yoshida, K., Solar UT-3 thermochemical cycle for hydrogen production. Solar Energy 1996, 57 (1), 51-58.

17. Funk, J. E., Thermochemical hydrogen production: past and present. International Journal of Hydrogen Energy 2001, 26, 185-190.

18. BROWN, L. C.; FUNK, J. F.; SHOWALTER, S. K. INITIAL SCREENING OF THERMOCHEMICAL WATER-SPLITTING CYCLES FOR HIGH EFFICIENCY GENERATION OF HYDROGEN FUELS USING NUCLEAR POWER; University of Kentucky Sandia National Laboratory General Atomics: April 2000, 2000.

19. Huang, C.; T-Raissi, A., Analysis of sulfur–iodine thermochemical cycle for solar hydrogen production. Part I: decomposition of sulfuric acid. Solar Energy 2005, 78, 632-646.

20. Goldstein, S.; Borgard, J.-M.; Vitart, X., Upper bound and best estimate of the efficiency of the iodine sulphur cycle. International Journal of Hydrogen Energy 2005, 30 619 - 626.

21. Vitart, X.; Le Duigou, A.; Carles, P., Hydrogen production using the sulfur–iodine cycle coupled to a VHTR: An overview. Energy Conversion and Management 2006 47, 2740-2747.

22. Kubo, S.; Nakajima, H.; Kasahara, S.; Higashi, S.; Masaki, T.; Abe, H.; Onuki, K., A demonstration study on a closed-cycle hydrogen production by the thermochemical

water-splitting iodine–sulfur process. Nuclear Engineering and Design 2004, 233, 347-354.

23. Sakurai, M.; Nakajimaa, H.; Amirb, R.; Onukia, K.; Shimizua, S., Experimental study on side-reaction occurrence condition in the iodine±sulfur thermochemical hydrogen production process. International Journal of Hydrogen Energy 2000, 25, 613-619.

24. Lee, B. J.; NO, H. C.; Yoon, H. J.; Kim, S. J.; Kim, E. S., An optimal operating window for the Bunsen process in the I–S thermochemical cycle. International Journal of Hydrogen Energy 2008, 11.

25. Goldstein, S.; Borgard, J.-M.; Vitart, X., Upper bound and best estimate of the efficiency of the iodine sulphur cycle. International Journal of Hydrogen Energy 2005, 30, 619 - 626.

26. Norman, J. H.; Mysels, K. J.; D.R., O. K.; Stowell, S. A.; Williamson, D. G. In Chemical Studies on the General Atomic Sulfur-Iodine Thermochemical Water-Splitting Cycle, 2nd World Hydrogen Energy Conference, Zurich, Switzerland, August 21-24, 1978; Vezirolglu, N.; Seifritz, W., Eds. Pergamon Press Inc.: Zurich, Switzerland, 1978; pp 513-543.

27. Wong, B.; Buckingham, R. T.; Brown, L. C.; Russ, B. E.; Besenbruch, G. E.; Kaiparambil, A.; Santhanakrishnan, R.; Roy, A., Construction materials development in sulfur-iodine thermochemical water-splitting process for hydrogen production. International Journal of Hydrogen Energy 2007, 32 (4), 497-504.

28. Nomura, M.; Kasahara, S.; Okuda, H.; Nakao, S.-i., Evaluation of the IS process featuring membrane techniques by total thermal efficiency. International Journal of Hydrogen Energy 2005, 30 1465 - 1473.

29. Barbarossa, V.; Brutti, S.; Diamanti, M.; Sau, S.; De Maria, G., Catalytic thermal decomposition of sulphuric acid in sulphur-iodine cycle for hydrogen production. International Journal of Hydrogen Energy 2006, 31 (7), 883-890.

30. Gorensek, M. B.; Summers, W. A., Hybrid sulfur flowsheets using PEM electrolysis and a bayonet decomposition reactor. International Journal of Hydrogen Energy 2009, 34 (9), 4097-4114.

31. Cedergren, A., Determinatin of kinetics of the Karl Fischer Reaction Bsed on Coulometry and True Potentiometry. ANALYTICAL CHEMISTRY 1996, 68 (5), 784-791.

32. Grunke, S.; Wunsch, G., Kinetics and Stoichiometry in the Karl Fischer solution. Fresenius J. Anal. Chem. 2000, 368, 139-147.

33. Sherman, F. B., DETERMINATION OF WATER WITH A MODIFIED KARL-FISCHER-REAGENT - STABILITY AND THE MECHANISM OF REACTION WITH WATER. Talanta 1980, 27 (12), 1067-1072.

34. Fischer, W.; Beil, S.; Krenn, K. D., KARL-FISCHER MECHANISM AND BUNSEN REACTION. Analytica Chimica Acta 1992, 257 (1), 165-171.

35. Stewart, F. F.; Orme, C. J.; Jones, M. G., Membrane processes for the sulfur–iodine thermochemical cycle. International Journal of Hydrogen Energy 2007, 32, 457 – 462.

36. Mason, C. F. V.; Bowman, M. G. In Reactions for Improving Efficiencies in Thermochemical Cycles Related to the Sulfur Dioxide-Iodine Process, 4th World Hydrogen Energy Conference, Pasadena, Switzerland, June 13-17, 1982; Vezirolglu, N.; Van Vorst, W. D.; Kelley, J. H., Eds. Pergamon Press Inc.: Pasadena, Switzerland, 1982; pp 665-674.

37. Giaconia, A.; Caputo, G.; Sau, S.; Prosini, P. P.; Pozio, A.; De Francesco, M.; Tarquini, P.; Nardi, L., Survey of Bunsen reaction routes to improve the sulfur-iodine thermochemical water-splitting cycle. International Journal of Hydrogen Energy 2009, 34 (9), 4041-4048.

38. Ammon, R. L. In Status of Materials Evaluation for Sulfuric Acid Vaporization and Decomposition Applications, 4th World Hydrogen Energy Conference, Pasadena, Switzerland, June 13-17, 1982; Vezirolglu, N.; Van Vorst, W. D.; Kelley, J. H., Eds. Pergamon Press Inc.: Pasadena, Switzerland, 1982; pp 623-649.

39. De Beni, G.; Pierini, G.; Spelta, B., The reaction of sulphur dioxide with water and a halogen. The case of iodine: reaction in presence of organic solvents. International Journal of Hydrogen Energy 1980, 5 (2), 141-149.

40. De Beni, G.; Pierini, G.; Spelta, B. In The Reaction of Sulfur Dioxide with Water and a Halogen. The Cases of Bromine and Iodine, 2nd World Hydrogen Energy Conference, Zurich, Switzerland, August 21-24, 1978; Vezirolglu, N.; Seifritz, W., Eds. Pergamon Press Inc.: Zurich, Switzerland, 1978; pp 617-648.

41. Taylor, M.; Styring, P.; Allen, R. W. K. In Novel Organic Solvents for the Bunsen Reaction, American Institute of Chemical Engineers, Philadelphia, PA., Philadelphia, PA., 2008.

42. Farbman, G. H.; Brecher, L. E. In Hydrogen Production by Water Decomposition using a Combined Electrolytic-Thermochemical Cycle, 1st World Hydrogen Energy Conference, Miami Beach, Florida, March 1-3, 1976; Veziroglu, T. N., Ed. The School of Continuing Studies, University of Miami: Miami Beach, Florida, 1976; pp 9A-29-9A-52.

43. Graf, D.; Monnerie, N.; Roeb, M.; Schmitz, M.; Sattler, C., Economic comparison of solar hydrogen generation by means of thermochemical cycles and electrolysis. International Journal of Hydrogen Energy 2008, 33 (17), 4511-4519.

44. Hinkley, J. T.; O'Brien, J. A.; Fell, C. J.; Lindquist, S.-E., Prospects for solar only operation of the hybrid sulphur cycle for hydrogen production. International Journal of Hydrogen Energy In Press, Corrected Proof.

45. Villasmil, W.; Steinfeld, A., Hydrogen production by hydrogen sulfide splitting using concentrated solar energy - Thermodynamics and economic evaluation. Energy Conversion and Management 2010, 51 (11), 2353-2361.

46. Pieplu, A.; Saur, O.; Lavalley, J. C.; Legendre, O.; Nedez, C., Claus catalysis and H_2S selective oxidation. Catalysis Reviews-Science and Engineering 1998, 40 (4), 409-450.

47. Baykara, S. Z.; Figen, E. H.; Kale, A.; Nejat Veziroglu, T., Hydrogen from hydrogen sulphide in Black Sea. International Journal of Hydrogen Energy 2007, 32 (9), 1246-1250.

48. Zaman, J.; Chakma, A., Production of hydrogen and sulfur from hydrogen sulfide. Fuel Processing Technology 1995, 41 (2), 159-198.

49. Kaloidas, V. E.; Papayannakos, N. G., Kinetic studies on the catalytic decomposition of hydrogen sulfide in a tubular reactor. Industrial & Engineering Chemistry Research 1991, 30 (2), 345-351.

50. Woiki, D.; Roth, P., Kinetics of the High-Temperature H2S Decomposition. The Journal of Physical Chemistry 1994, 98 (49), 12958-12963.

51. Karan, K.; Mehrotra, A. K.; Behie, L. A., On reaction kinetics for the thermal decomposition of hydrogen sulfide. Aiche Journal 1999, 45 (2), 383-389.

52. Bishara, A.; Salman, O. A.; Khraishi, N.; Marafi, A., Int. J. Hydrogen Energy 1987, 12 (null), 679.

53. Harvey, W. S.; Davidson, J. H.; Fletcher, E. A., Thermolysis of Hydrogen Sulfide in the Temperature Range 1350−1600 K. Industrial & Engineering Chemistry Research 1998, 37 (6), 2323-2332.

54. Tesner, P. A.; Nemirovskii, M. S.; Motyl, D. N., KINETICS OF THE THERMAL-DECOMPOSITION OF HYDROGEN-SULFIDE AT 600-1200-DEGREES-C. Kinetics and Catalysis 1990, 31 (5), 1081-1083; Kappauf, T.; Murray, J. P.; Palumbo, R.; Diver, R. B.; Fletcher, E. A., Hydrogen and sulfur from hydrogen sulfide--IV. Quenching the effluent from a solar furnace. Energy 1985, 10 (10), 1119-1137.

55. Raymont, M. E. D., Hydrocarbon Process. 1975, 54, 139.

56. Fukuda, K.; Dokiya, M.; Kameyama, T.; Kotera, Y., Catalytic Decomposition of Hydrogen Sulfide. Industrial & Engineering Chemistry Fundamentals 1978, 17 (4), 243-248.

57. Adesina, A. A.; Meeyoo, V.; Foulds, G., Thermolysis of hydrogen sulphide in an open tubular reactor. International Journal of Hydrogen Energy 1995, 20 (10), 777-783.

58. Edlund, D. J.; Pledger, W. A., Thermolysis of hydrogen sulfide in a metal membrane reactor. Journal of membrane Science 1993, 77, 255-264.

59. Kotera, Y.; Todo, N.; Fukuda, N. Process for Production of Hydrogen and Sulfur from Hydrogen Sulfide as Raw Material. US3962409, 1976.

60. Yang, B. L.; Kung, H. H., Hydrogen Recovery from Hydrogen Sulfide by Oxidation and by Decomposition. Industrial & Engineering Chemistry Research 1994, 33 (5), 1090-1097.

61. Herrington, D. R. B., OH), Kuch, Philip L. (Aurora, OH) Thermochemical method for producing hydrogen from hydrogen sulfide. 1984.

62. Bowman, M. G. W. B. D., Pleasant View, UT, 84404) Thermochemical cycle for splitting hydrogen sulfide. 1991.

63. Huang, C.; T-Raissi, A., Liquid hydrogen production via hydrogen sulfide methane reformation. Journal of Power Sources 2008, 175, 464-472.

64. Wang, H., Hydrogen production from a chemical cycle ofH2S splitting. International Journal of Hydrogen Energy 2007.

65. Rostrupn.Jr, SOME PRINCIPLES RELATING TO REGENERATION OF SULFUR-POISONED NICKEL CATALYST. Journal of Catalysis 1971, 21 (2), 171-&.

66. Brennecke, J. F.; Maginn, E. J., Ionic Liquids: Innovative Fluids for Chemical Processing. AIChe Journal 2001, 47 (11), 2384-2389.

67. Comminges, C.; Barhdadi, R.; Laurent, M.; Troupel, M., Determination of viscosity, ionic conductivity, and diffusion coefficients in some binary systems: Ionic liquids plus molecular solvents. J. Chem. Eng. Data 2006, 51 (2), 680-685.

68. Blanchard, L. A.; Brennecke, J. F., Recovery of organic products from ionic liquids using supercritical carbon dioxide. Industrial & Engineering Chemistry Research 2001, 40 (1), 287-292.

69. Jork, C.; Kristen, C.; Pieraccini, D.; Stark, A.; Chiappe, C.; Beste, Y. A.; Arlt, W., Tailor-made ionic liquids. J. Chem. Thermodyn. 2005, 37, 537-558.

70. Jiang, Y.-Y.; Zhou, Z.; Jiao, Z.; Li, L.; Wu, Y.-T.; Zhang, Z.-B., SO2 Gas Separation Using Supported Ionic Liquid Membranes. The Journal of Physical Chemistry B 2007, 111 (19), 5058-5061.

71. Anderson, J. L.; Dixon, J. K.; Maginn, E. J.; Brennecke, J. F., Measurement of SO2 Solubility in Ionic Liquids. Journal of Physical Chemistry B 2006, 110, 15059-15062.

72. Lee, K. Y.; Taek Gonga, G.; Songb, K. H.; Kima, H.; Junga, K.-D.; Kima, C. S., Use of ionic liquids as absorbents to separate SO2 in

SO2/O2 in thermochemical processes to produce hydrogen. International Journal of Hydrogen Energy 2008.

73. Huang, J.; Riisager, A.; Wasserscheid, P.; Fehrmann, R., Reversible physical absorption of SO2 by ionic liquids. Chem. Commun. 2006, (38), 4027-4029.

74. Pomelli, C. S.; Chiappe, C.; Vidis, A.; Laurenczy, G. b.; Dyson, P. J., Influence of the Interaction between Hydrogen Sulfide and Ionic Liquids on Solubility: Experimental and Theoretical Investigation. The Journal of Physical Chemistry B 2007, 111 (45), 13014-13019.

75. Shokouhi, M.; Adibi, M.; Jalili, A. H.; Hosseini-Jenab, M.; Mehdizadeh, A., Solubility and Diffusion of H2S and CO2 in the Ionic Liquid 1-(2-Hydroxyethyl)-3-methylimidazolium Tetrafluoroborate. Journal of Chemical & Engineering Data 2009.

76. Jou, F. Y.; Mather, A. E., Solubility of hydrogen sulfide in bmim PF6. International Journal of Thermophysics 2007, 28 (2), 490-495.

77. Rebelo, L. P. N.; Lopes, J. N. C.; Esperancüa, J. M. S. S.; Filipe, E., On the Critical Temperature, Normal Boiling Point, and Vapor Pressure of Ionic Liquids. Journal of Physical Chemistry B 2005, 109, 6040-6043.

78. Van Valkenburg, M. E.; Vaughn, R. L.; Williams, M.; Wilkes, J. S., Thermochemistry of ionic liquid heat-transfer fluids. Thermochim. Acta 2005, 425 (1-2), 181-188.

79. Taylor, A. W.; Lovelock, K. R. J.; Deyko, A.; Licence, P.; Jones, R. G., High vacuum distillation of ionic liquids and separation of ionic liquid mixtures. PCCP 2010, 12 (8), 1772-1783.

80. MacFarlane, D. R.; Pringle, J. M.; Johansson, K. M.; Forsyth, S. A.; Forsyth, M., Lewis base ionic liquids. Chemical Communications (Cambridge) 2006.

81. Robert, T.; Magna, L.; Olivier-Bourbigou, H.; Gilbert, B., A Comparison of the Acidity Levels in Room-Temperature Ionic Liquids. J. Electrochem. Soc. 2009, 156 (9), F115-F121.

82. D'Anna, F.; La Marca, S.; Noto, R., p-Nitrophenolate: A Probe for Determining Acid Strength in Ionic Liquids. J. Org. Chem. 2009, 74 (5), 1952-1956.

83. Thomazeau, C.; Olivier-Bourbigou, H.; Magna, L.; Luts, S.; Gilbert, B., Determination of an Acidic Scale in Room Temperature Ionic Liquids. J. Am. Chem. Soc. 2003, 125 (18), 5264-5265.

84. Mason, C. F. V.; Bowman, M. G. In Reactions for Improving Efficiencies in Thermochemical Cycles Related to the Sulfur Dioxide-Iodine Process, 4th World Hydrogen Energy Conference, Pasadena, Switzerland, June 13-17, 1982; Vezirolglu, N.; Van Vorst, W. D.; Kelley, J. H., Eds. Pergamon Press Inc.: Pasadena, Switzerland, 1982; pp 665-674.

85. Dillon, R. T.; Young, W. G., THE PREPARATION OF ANHYDROUS HYDROGEN IODIDE1. J. Am. Chem. Soc. 1929, 51 (8), 2389-2391.

86. Earle, M. J.; Gordon, C. M.; Plechkova, N. V.; Seddon, K. R.; Welton, T., Decolorization of Ionic Liquids for Spectroscopy. ANALYTICAL CHEMISTRY 2007, 79 (2), 758-764.

87. Cedergren, A., Reaction Rates Between Water and Some Modified Rapidly-Reacting Karl Fischer Reagents. Talanta 1978, 25, 229-232; Wunsch, G.; Schoffski, K., Die Iodierende Nebenreaktion im Karl-Fischer-System. Analytica Chimica Acta 1990, 239, 283-290; Wunsch, G.; Seubert, A., Stochiometrie und Kinetik der Karl-Fischer-Reaktion in Methanol als Reaktionsmedium. Fresenius Z Anal Chem 1989, 334, 16-21; Wunsch, G.; Seubert, A., Nebenreaktionen in Karl-Fischer-Reagentien. Fresenius Z Anal Chem 1989, 334, 256-260.

88. Keefer, R. M.; Allen, T. L., Absorption Spectra of I2 and I4 in CCl4 solution. The Journal of Chemical Physics 1956, 25 (5), 1059-1061; Bower, J. G.; Scott, R. L., The Solubility and Absorption Spectrum of Iodine in Sulfuric Acid Solutions. J. Am. Chem. Soc. 1953, 75 (14), 3583-3585.

89. Awtrey, A. D.; Connick, R. E., The Absorption Spectra of I_2, I_3-, I-, IO_3-,$S_40_6^{2-}$ and $S_2O_3^-$. Heat of the Reaction I3- =I2 + I. J. Am. Chem. Soc. 1951, 73 (4), 1842-1843; Licht, S.; Myung, N., Aqueous Polyiodide Spectroscopy and Equilibria and Its Effect on n-WSe2 Photoelectrochemistry. J. Electrochem. Soc. 1995, 142 (3), 845-849; Hayakawa, K.; Nakamura, S., The determination of the Formation Constants of the Triiodide Ion in Water-Alcohol Mixed Solvents at Various Temperatures. Bull. Chem. Soc. Jpn. 1977, 50 (3), 566-569.

90. Rawlings, J. B.; Ekerdt, J. G., Chemical Reactor Analysis and Design Fundamentals Nob Hill Publishing: Madison, WI, 2009.

91. Kasahara, S.; Hwang, G.-J.; Nakajima, H.; Choi, H.-S.; Onuki, K.; Nomura, M., Effects of Process Parameters of the IS Process on Total Thermal Efficiency to Produce Hydrogen from Water. Journal of Chemical Engineering of Japan 2003, 36 (7), 887-899.

92. Baykara, S. Z.; Figena, E. H.; Kaleb, A.; Veziroglu, T. N., International Journal of Hydrogen Energy 2007 32, 1246 - 1250; Cox, B. G.; Clarke, P. F.; Pruden., B. B., Economics of Thermal Dissociation of H2S to Produce Hydrogen. International Journal of Hydrogen Energy 1998, 23, 531-544; Wang, H., Hydrogen production from a chemical cycle ofH2S splitting. International Journal of Hydrogen Energy 2007, 32, 3907-3914; Yu, G.; Wang, H.; Chuang, K. T., Upper Bound for the Efficiency of a Novel Chemical Cycle of H2S Splitting for H2 Production. Energy & Fuels 2009, 23 (4), 2184-2191.

93. Iodine; U.S. Geological Survey: January 2011; Vitart, X.; Carles, P.; Anzieu, P., A general survey of the potential and the main issues associated with the sulfureiodine thermochemical cycle for hydrogen production using nuclear heat. Progress in Nuclear Energy 2008, 50, 402-410.

94. De Beni, G.; Pierini, G.; Spelta, B. In The Reaction of Sulfur Dioxide with Water and a Halogen. The Cases of Bromine and Iodine, 2nd World Hydrogen Energy Conference, Zurich, Switzerland, August 21-24, 1978; Vezirolglu, N.; Seifritz, W., Eds. Pergamon Press Inc.: Zurich, Switzerland, 1978; pp 617-648.

95. Ober, J. A. Bromine; 2011.

96. Hirsch, A. R.; Zavala, G., Long Term Effects on the Olfactory System of Exposure to Hydrogen Sulphide. Occupational and Environmental Medicine 1999, 56 (4), 284-287.

97. Lee, K. Y.; Taek Gonga, G.; Songb, K. H.; Kima, H.; Junga, K.-D.; Kima, C. S., Use of ionic liquids as absorbents to separate SO_2 in SO_2/O_2 in thermochemical processes to produce hydrogen. International Journal of Hydrogen Energy 2008.

98. Barin, I., Thermochemical data of pure substances. 2nd ed.; Weinheim, Federal Repubic of Germany: New York, 1993; Vol. 1-2.

APPENDICES

LIST OF FIGURES

Figure B.1: Calibration curve for absorbance of iodine in ionic liquid [BMIM][OTf] at 294 nm diluted in dichloromethane……...95

Figure B.2: Difference in absorbance measurements between 22 and 100°C at various concentrations. 96

Figure B. 3: Pseudo-first order plot for reaction at 50˚C 98

Figure B. 4: Pseudo-first order plot for reaction at 70˚C 98

Figure B. 5: Pseudo-first order plot for reaction at 100˚C 99

Figure B. 6: Damkohler number variation with excess proportion of SO_2 and H_2O and space time in PFR 100

Figure B. 7: SO_2, H_2O, and space time requirements to meet conversion of 90%. Points above the curve exceed 90% conversion. 100

Figure C. 1: Calibration curve for SO_2 using GC-FPD during H_2S generation experiments……..102

Figure C. 2: Calibration curve using GC-FPD during H_2S generation experiments. …..102

Figure C. 3: Calibration curve for H_2 using GC-FPD during H_2S generation experiments. 102

Figure D. 1: Temperature distribution inside quartz reaction tube under conditions of 20 SCCM gas flow……103

Figure D. 2: Calibration curve for Helium Ionization Detector (GC-HID) used in measuring H_2 concentration in steam reformation parametric study. 104

Figure D. 3: Calibration curve for sulfur species (per mole sulfur) for Flame Photometric Detector (GC-FPD) used in steam reformation parametric study. 104

Figure D.4: Arrhenius parameters as reconciled by Karan et al. from several literature reports.[51] compared to apparent values obtained in this investigation. 108

Figure D.5: Model fit to data at 700°C, 200:1 H_2O:H_2S molar ratio. 109

Figure D.6: Model fit to data at 800°C, 200:1 H_2O:H_2S molar ratio. 110

Figure D.7: Model fit to data at 900°C, 200:1 H_2O:H_2S molar ratio. 111

Figure D.8: Normal probability plots for a) H_2; b)H_2S; c) SO_2; d) All. 112

LIST OF TABLES

Table A. 1: Boiling Points of Bunsen Species 93

Table A. 2: Heat of Formation, ΔH_f, [kJ/mol] for Steam Reformation Species at 1 atm.[98] 94

Table A.3: Gibbs Energy of Formation, ΔG_f, [kJ/mol] for Steam Reformation Species at 1 atm.[98] 94

Table B. 1: Data and model fitting for Bunsen reaction in ionic liquid……97

Table C. 1: Experimental data showing normalized (per $H_2S_{,0}$) averages of triplicate runs at each temperature and residence time……...101

Table D. 1: Data for kinetic investigation into steam reformation of H_2S…….105

Table D. 2: Model fitting of Arrhenius parameters to data. 106

Table D. 3: Theoretical thermal load on steam reformation section..... 112

Table D. 4: LHV overall thermal efficiency estimates at various H_2O:H_2S ratios..... 113

Table D. 5: HHV overall thermal efficiency estimates at various H_2O:H_2S ratios 113

APPENDIX A: Physical and Chemical Properties of Sulfur-Sulfur Cycle Species

Table A. 1: Boiling Points of Bunsen Species

Species	Boiling Point (˚C)
Hydrogen Sulfide (H_2S)	-82
Hydrogen Iodide (HI)	-35.4
Sulfur Dioxide (SO_2)	-10.1
Sulfur Trioxide (SO_3)	44.7
Iodine (I_2)	184.3
Sulfuric Acid (H_2SO_4)	337
Ionic Liquids	~250 to 500

Table A. 2: Heat of Formation, ΔH_f, [kJ/mol] for Steam Reformation Species at 1 atm.[98]

Temperature [K]	H_2S	H_2O	SO_2	H_2, S_2	SO_3
1100	-90.25	-248.46	-361.79	0.00	-406.13
1200	-90.39	-249.00	-361.64	0.00	-460.08
1300	-90.46	-249.48	-361.47	0.00	-459.59
1400	-90.47	-249.90	-361.30	0.00	-459.05
1500	-90.44	-250.27	-361.11	0.00	-458.48
1600	-90.37	-250.59	-360.93	0.00	-457.88
1700	-90.27	-250.88	-360.74	0.00	-457.26
1800	-90.16	-251.14	-360.56	0.00	-456.64
1900	-90.02	-251.37	-360.38	0.00	-456.02
2000	-89.88	-251.58	-360.21	0.00	-455.40

Table A.3: Gibbs Energy of Formation, ΔG_f, [kJ/mol] for Steam Reformation Species at 1 atm.[98]

Temperature [K]	H_2S	H_2O	SO_2	H_2, S_2	SO_3
1100	-36.03	-187.17	-281.32	0.00	-321.95
1200	-31.09	-181.57	-274.01	0.00	310.20
1300	-26.15	-175.93	-266.72	0.00	-293.57
1400	-21.20	-170.26	-259.43	0.00	-277.00
1500	-16.25	-164.56	-252.16	0.00	-260.47
1600	-11.31	-158.83	-244.91	0.00	-243.99
1700	-6.37	-153.09	-237.66	0.00	-227.56
1800	-1.44	-147.33	-230.43	0.00	-211.18
1900	3.49	-141.56	-223.20	0.00	-194.83
2000	8.41	-135.77	-215.99	0.00	-178.53

APPENDIX B: Kinetics of the Bunsen Reaction

As described in Chapter 2, monitoring I_2 via UV-visible spectroscopy presented challenges in terms of temperature stability. The absorbance measured is that of the peak at 294 nm. Small volumes (10 uL) of a concentrated I_2-IL solution at either 22 or 100˚C were immediately injected into a cuvette containing 2.0 mL of dichloromethane at 22˚C and stirred. The peak at 294 nm was relatively stable with increase in temperature. Figure B.1 shows the relative similarity in the absorbance at 294 nm between samples of I_2 in ionic liquid [BMIM][OTf] at 22 and 100°C. Peaks at 265 and 365 nm were tracked as well, and Figure B.2 shows the square of the difference in absorbance between 22 and 100°C among the peaks in question.

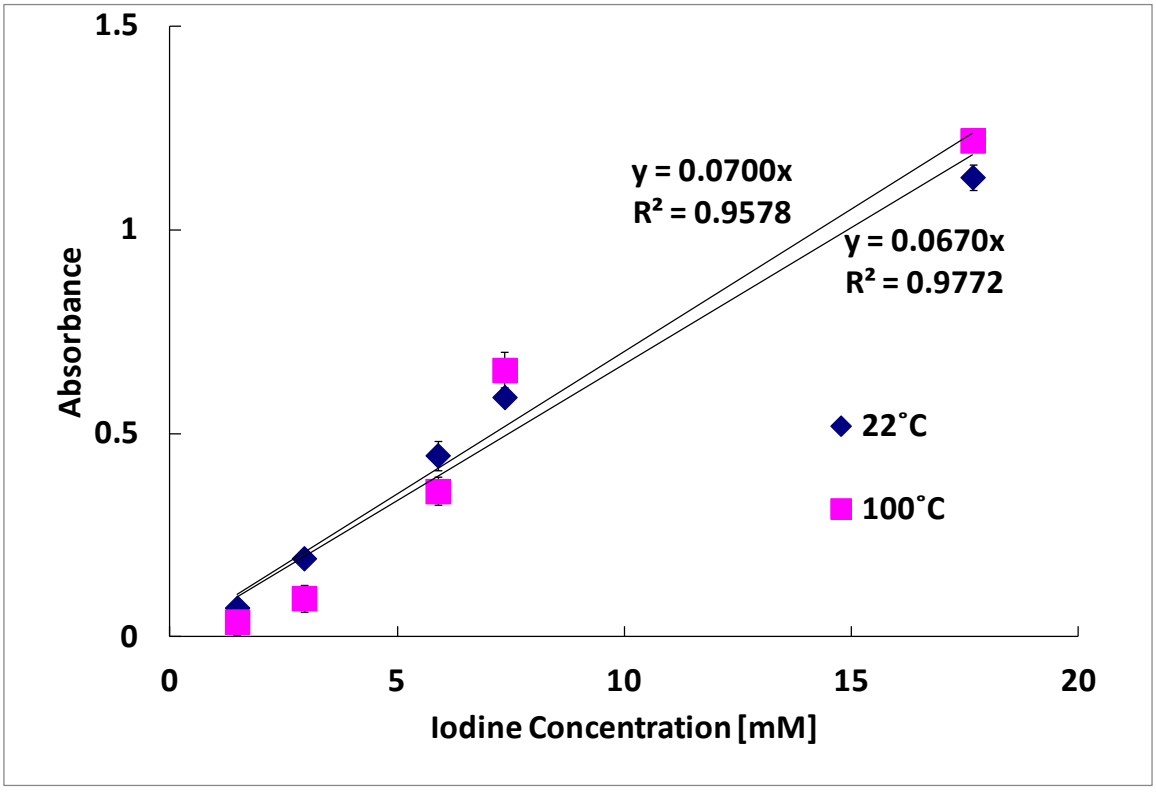

Figure B.1: Calibration curve for absorbance of iodine in ionic liquid [BMIM][OTf] at 294 nm diluted in dichloromethane.

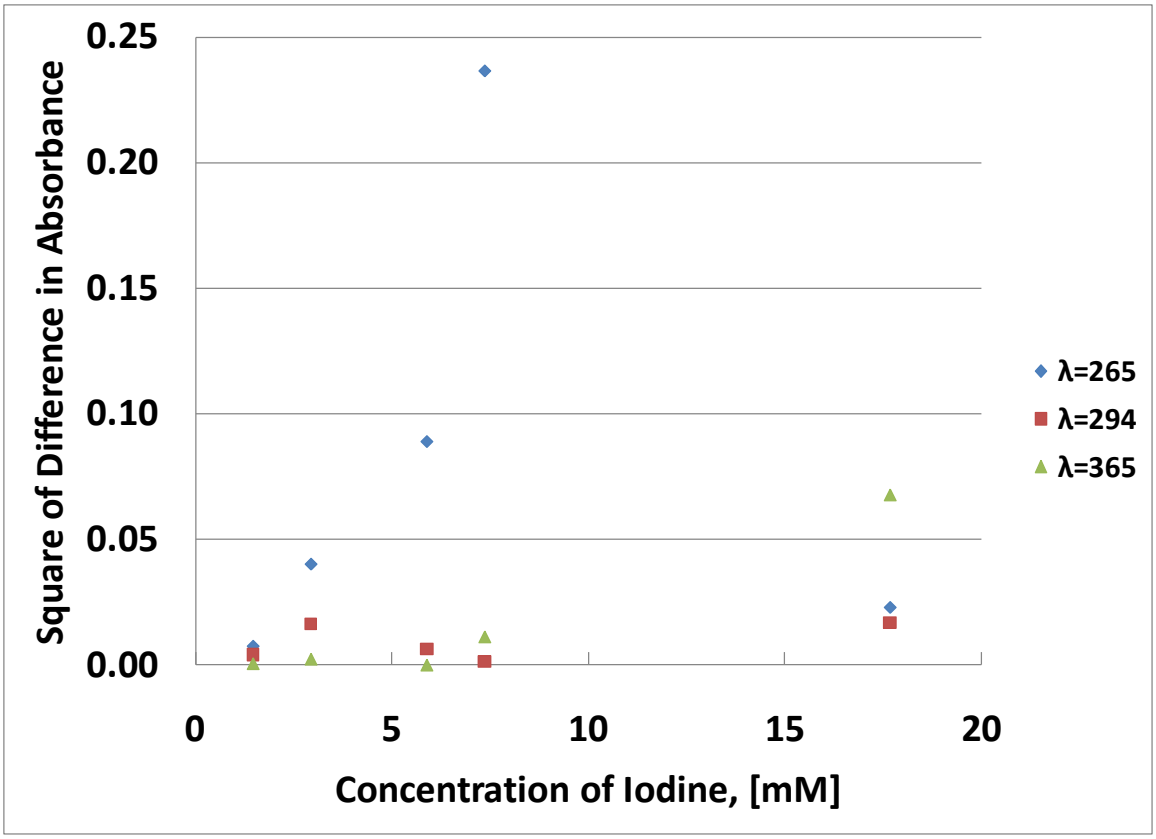

Figure B.2: Difference in absorbance measurements between 22 and 100°C at various concentrations.

First-order approximation reaction data:

If the rate law for the Fischer reaction is used (first order with respect to all reactants H_2O and SO_2), the pseudo first order reaction rate constant can be approximated by plotting logarithmic concentration versus time. These linearizations and the regression values are shown in Table B. 1 and Figure B. 3-Figure B. 5. Model A is direct fitting of Arrhenius parameters by non-linear regression without finding rate constant, k values. Model B is based on the determination of rate constants via graphical means. Model C is based on explicit determination of the rate constant from data. Data points were only included up to the point in time where the reaction velocity (i.e. the disappearance of iodine) decreased.

Table B. 1: Data and model fitting for Bunsen reaction in ionic liquid.

	A	SSE =	0.16	B	SSE =	0.39	C	SSE =	0.18
T	k'	k	ln k	k'	k	ln k	k avg	k	ln k
K	min^{-1}	$min^{-1}M^{-2}$		min^{-1}	$min^{-1}M^{-2}$			$min^{-1}M^{-2}$	
323	0.38	6.93	-2.16	0.30	5.46	-2.40	0.38	7.00	-2.18
343	0.77	14.16	-1.44	0.53	9.65	-1.83	0.81	14.82	-1.46
373	1.96	35.85	-0.52	1.03	18.90	-1.16	1.51	27.67	-0.86

			A		B		C	
T	time	DATA	MODEL	MODEL	MODEL	MODEL	MODEL	MODEL
	t	C/C_o	C/C_o	SE	C/C_o	SE	C/C_o	SE
	[min]							
50 ˚C	0.0	1.00	1.00	0.00E+00	1.00	0.00E+00	1.00	0.00E+00
50 ˚C	0.0	1.00	1.00	0.00E+00	1.00	0.00E+00	1.00	0.00E+00
50 ˚C	0.0	1.00	1.00	0.00E+00	1.00	0.00E+00	1.00	0.00E+00
50 ˚C	1.0	0.75	0.68	4.05E-03	0.74	4.00E-05	0.74	1.39E-05
50 ˚C	1.0	0.56	0.68	1.58E-02	0.74	3.34E-02	0.74	3.44E-02
50 ˚C	1.2	0.61	0.64	1.24E-03	0.71	9.71E-03	0.71	1.03E-02
50 ˚C	2.5	0.30	0.39	7.59E-03	0.47	3.01E-02	0.48	3.16E-02
50 ˚C	3.0	0.36	0.32	1.62E-03	0.41	2.25E-03	0.41	2.67E-03
50 ˚C	3.9	0.26	0.23	8.05E-04	0.31	3.10E-03	0.32	3.60E-03
50 ˚C	4.3	0.19	0.20	7.09E-05	0.28	8.10E-03	0.29	8.87E-03
50 ˚C	5.3	0.25	0.14	1.31E-02	0.21	1.81E-03	0.21	1.49E-03
50 ˚C	6.0	0.14	0.10	1.55E-03	0.17	6.06E-04	0.17	7.92E-04
70 ˚C	0.0	1.00	1.00	0.00E+00	1.00	0.00E+00	1.00	0.00E+00
70 ˚C	0.0	1.00	1.00	0.00E+00	1.00	0.00E+00	1.00	0.00E+00
70 ˚C	0.0	1.00	1.00	0.00E+00	1.00	0.00E+00	1.00	0.00E+00
70 ˚C	0.5	0.54	0.68	2.05E-02	0.77	5.39E-02	0.73	3.84E-02
70 ˚C	0.5	0.55	0.68	1.72E-02	0.77	4.85E-02	0.73	3.39E-02
70 ˚C	0.5	0.73	0.68	2.50E-03	0.77	1.53E-03	0.73	8.17E-06
70 ˚C	2.3	0.25	0.18	5.17E-03	0.31	3.37E-03	0.25	2.45E-06
70 ˚C	2.3	0.22	0.16	2.58E-03	0.29	5.93E-03	0.23	3.26E-04
70 ˚C	3.8	0.15	0.05	9.55E-03	0.13	2.79E-04	0.09	3.33E-03
100 ˚C	0.0	1.00	1.00	0.00E+00	1.00	0.00E+00	1.00	0.00E+00
100 ˚C	0.0	1.00	1.00	0.00E+00	1.00	0.00E+00	1.00	0.00E+00
100 ˚C	0.0	1.00	1.00	0.00E+00	1.00	0.00E+00	1.00	0.00E+00
100 ˚C	0.5	0.33	0.38	1.67E-03	0.60	6.86E-02	0.56	5.01E-02
100 ˚C	0.5	0.33	0.38	1.68E-03	0.60	6.87E-02	0.56	5.02E-02
100 ˚C	0.5	0.40	0.38	4.28E-04	0.60	4.02E-02	0.56	2.63E-02
100 ˚C	2.0	0.12	0.02	9.55E-03	0.13	8.60E-05	0.10	4.08E-04
100 ˚C	2.0	0.14	0.02	1.38E-02	0.13	1.12E-04	0.10	1.60E-03
100 ˚C	2.3	0.17	0.01	2.62E-02	0.10	5.79E-03	0.07	1.03E-02
No SO_2, 100 ˚C	0.0	1.00						
blank	0.5	0.99						
blank	2.2	0.94						
blank	4.5	0.99						
blank	7.0	1.01						
blank	20.0	1.00						

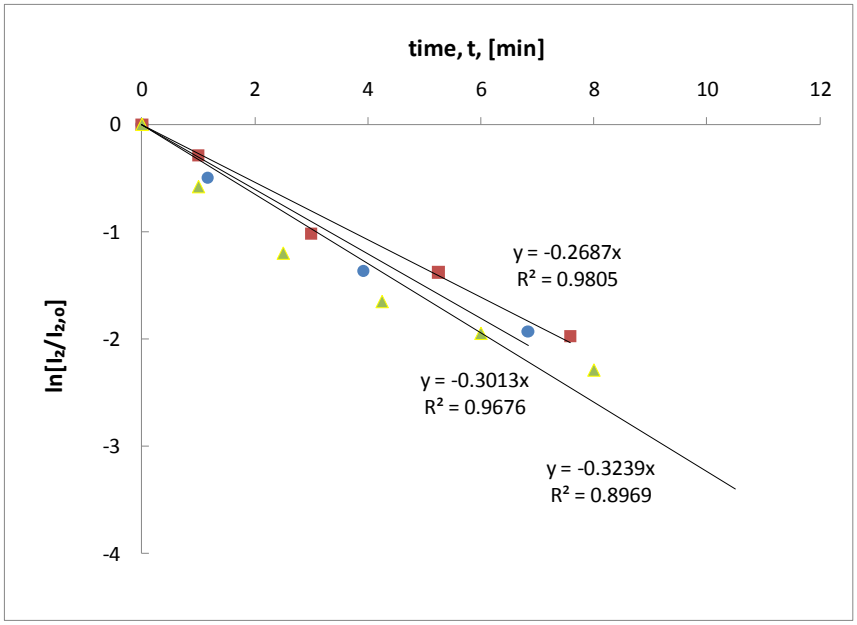

Figure B. 3: Pseudo-first order plot for reaction at 50˚C

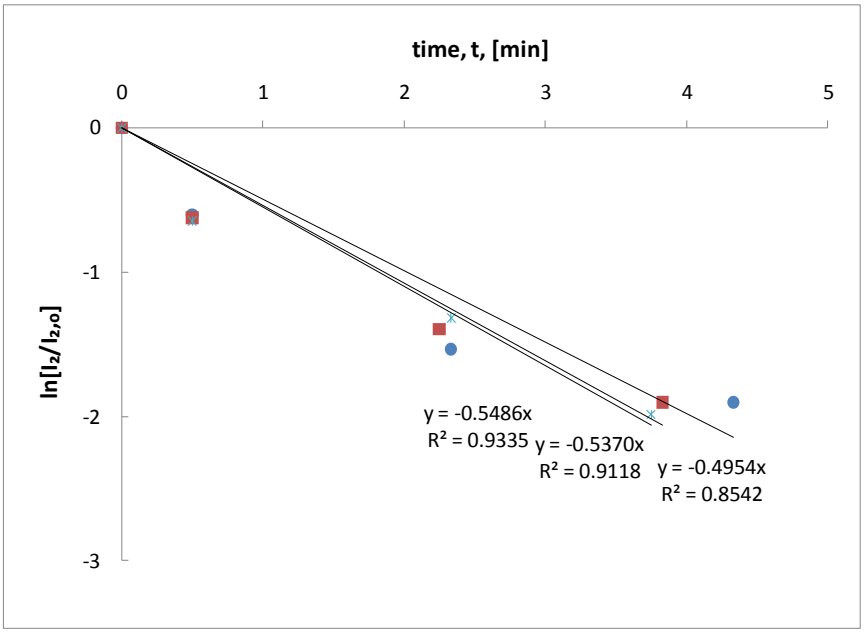

Figure B. 4: Pseudo-first order plot for reaction at 70˚C

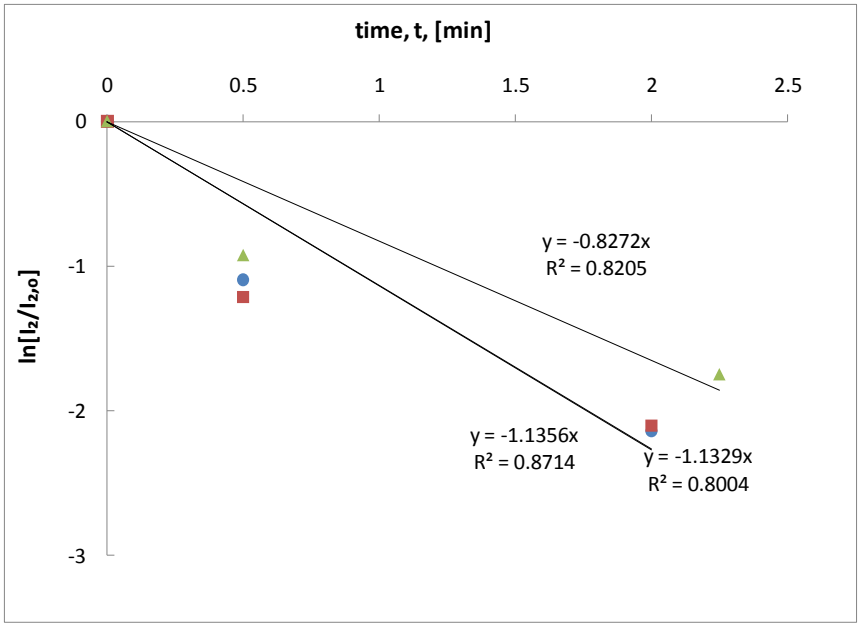

Figure B. 5: Pseudo-first order plot for reaction at 100˚C

The determination of the Arrhenius parameters allow for sizing of a tubular flow reactor. Reactor performance is characterized using the Damkohler number, which compares the reaction rate with the convection rate in a continuous reactor. Since conversion increases with increasing Damkohler number, it is a useful metric for comparing reactors of differing size or flowrate. For a first order (or in this case pseudo first-order) reaction, the Damkohler number is described as follows:

$$Da = k'\tau \qquad \text{Eq. 0.1}$$

where Da is the dimensionless Damkohler number and τ is the residence time, [s]. Using the same initial concentration of iodine as the batch reactions (0.018 M), a 3-D surface is created to compare relative excesses of SO_2 and H_2O (with respect to I_2) as well as different space times (see Figure 5). A Da of 10 or greater corresponds to a conversion of 90% or greater, and all the combinations of excess ratio and space time that lie above the curve in Figure B. 6 would satisfy this requirement.

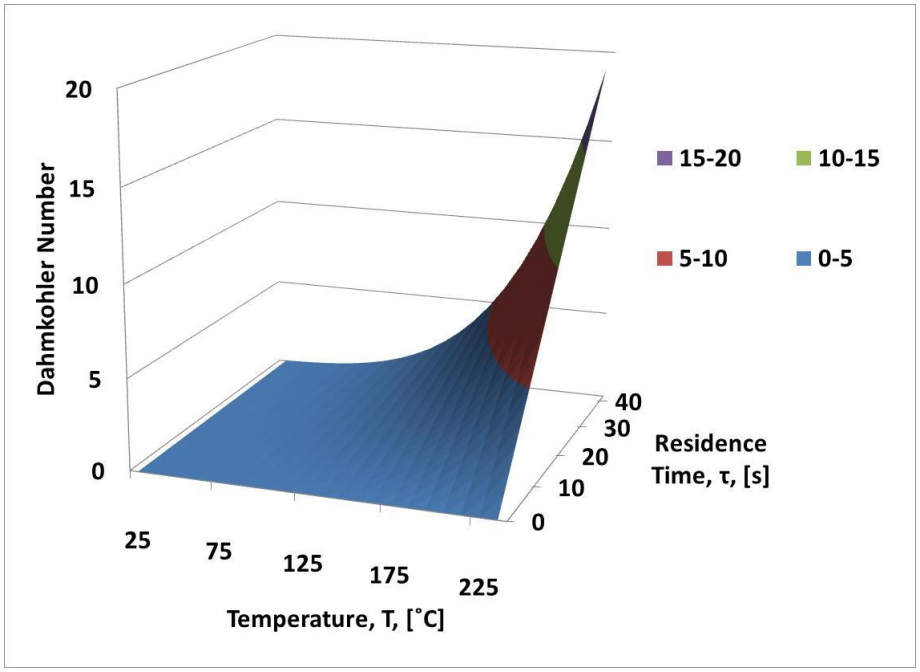

Figure B. 6: Damkohler number variation with excess proportion of SO_2 and H_2O and space time in PFR

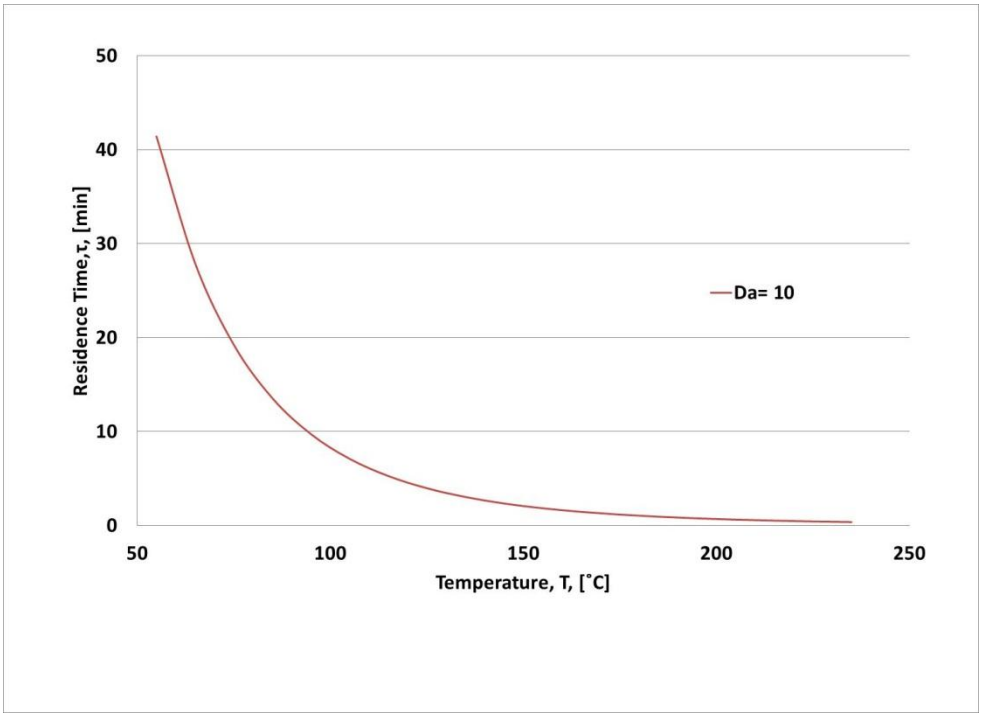

Figure B. 7: SO_2, H_2O, and space time requirements to meet conversion of 90%. Points above the curve exceed 90% conversion.

APPENDIX C: Preliminary Investigation into Steam Reformation of Hydrogen Sulfide

Table C. 1: Experimental data showing normalized (per $H_2S_{,0}$) averages of triplicate runs at each temperature and residence time.

	Res Time	$H_2S/H_2S_{,o}$	$H_2S/H_2S_{,o}$	$SO_2/H_2S_{,o}$	$SO_2/H_2S_{,o}$	$S/H_2S_{,o}$	H_2	H_2	$H_2/H_2S_{,o}$	$H_2/H_2S_{,o}$	H_2:SO_2
	s						mM	mM			
		avg	std	avg	std		avg	std	avg	std	
150˚C	**7.13**	0.67	0.08	0.00	0.00	0.67	0.00	0.00	0.00	0.00	-
	3.56	0.66	0.56	0.00	0.00	0.66	0.00	0.00	0.00	0.00	-
	2.38	0.27	0.15	0.00	0.00	0.27	0.00	0.00	0.00	0.00	-
300˚C	**2.38**	0.27	0.14	0.00	0.00	0.27	0.00	0.00	0.00	0.00	-
	7.13	0.15	0.09	0.00	0.00	0.15	0.00	0.00	0.00	0.00	-
	3.56	0.26	0.14	0.00	0.00	0.26	0.00	0.00	0.00	0.00	-
450˚C	**3.56**	0.34	0.21	0.00	0.00	0.34	0.05	0.01	0.05	0.01	-
	7.13	0.34	0.18	0.00	0.00	0.34	0.07	0.00	0.07	0.00	-
	2.38	0.25	0.28	0.00	0.00	0.25	0.03	0.00	0.03	0.00	-
600˚C	**2.38**	0.94	0.22	0.01	0.00	0.95	0.48	0.11	0.50	0.11	34.3
	3.56	0.68	0.14	0.05	0.03	0.73	0.74	0.02	0.77	0.02	14.7
	7.13	0.68	0.10	0.07	0.03	0.75	0.89	0.16	0.93	0.17	12.3
700˚C	**2.38**	0.19	0.14	0.25	0.08	0.43	1.47	0.03	1.59	0.03	6.0
	7.13	0.04	0.02	0.48	0.02	0.53	1.62	0.23	1.74	0.24	3.3
	3.56	0.28	0.01	0.46	0.10	0.74	1.56	0.09	1.68	0.09	3.4

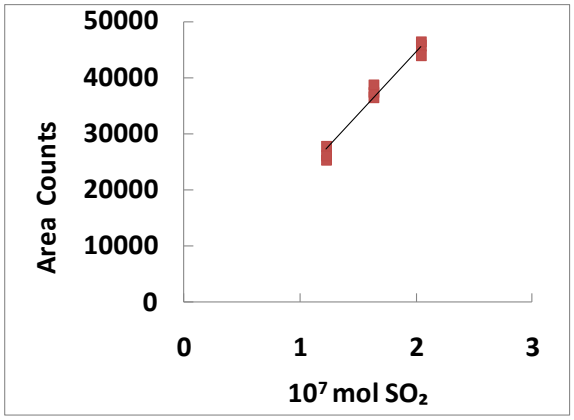

Figure C. 1: Calibration curve for SO_2 using GC-FPD during H_2S generation experiments.

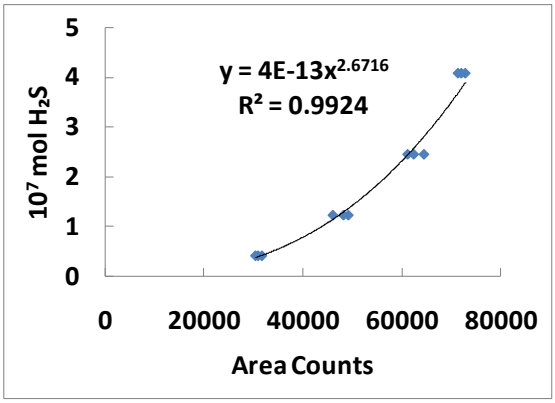

Figure C. 2: Calibration curve using GC-FPD during H_2S generation experiments.

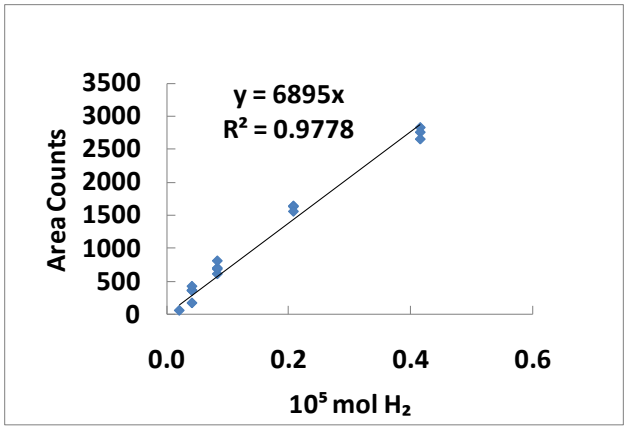

Figure C. 3: Calibration curve for H_2 using GC-FPD during H_2S generation experiments.

APPENDIX D: Steam Reformation of Hydrogen Sulfide

Measurements were made inside 20 SCCM nitrogen flow to estimate temperature in actual stream (see Figure D. 1). During experimental reaction trials, temperature was only measured at surface of tube in order avoid unintentionally catalyzing the reaction with SS 316 thermocouple tip. Tubing between heated zone and condenser was not insulated in order to facilitate more rapid condensation, the reason being again to avoid unintentional catalysis with stainless steel piping.

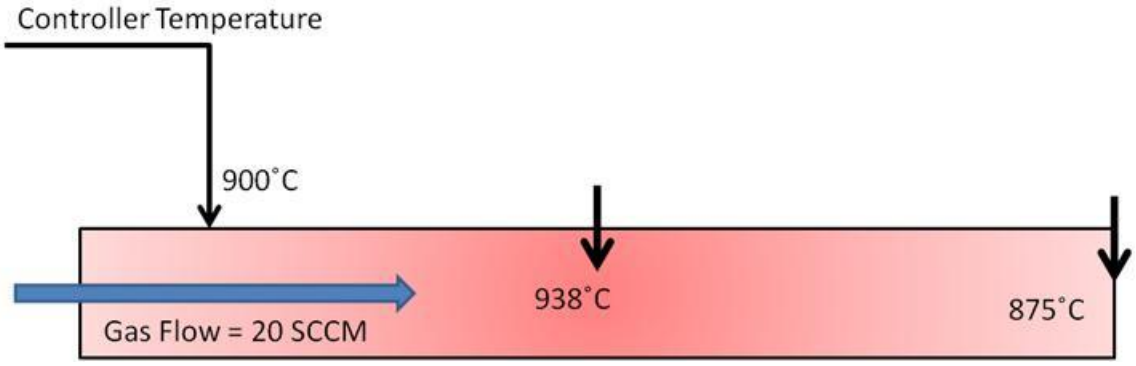

Figure D. 1: Temperature distribution inside quartz reaction tube under conditions of 20 SCCM gas flow.

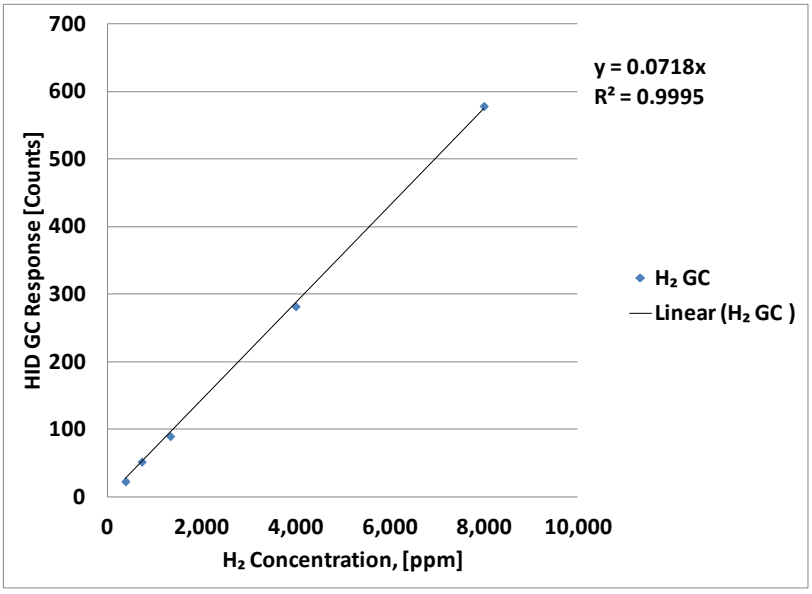

Figure D. 2: Calibration curve for Helium Ionization Detector (GC-HID) used in measuring H_2 concentration in steam reformation parametric study.

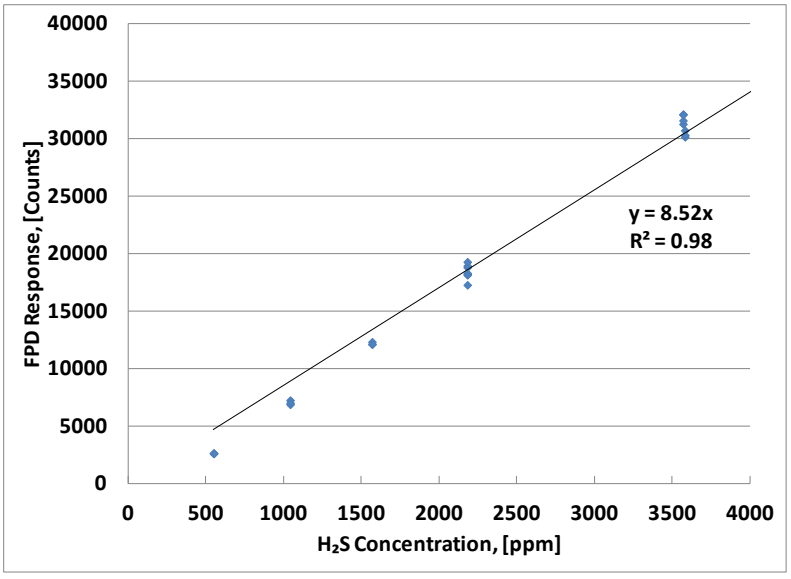

Figure D. 3: Calibration curve for sulfur species (per mole sulfur) for Flame Photometric Detector (GC-FPD) used in steam reformation parametric study.

Table D. 1: Data for kinetic investigation into steam reformation of H_2S.

	CONCENTRATION						NORMALIZED DATA					STANDARD ERROR		
	t	CH_2	CH_2S	CSO_2	CS_2		CH_2	CH_2S	CSO_2	CS_2		CH_2	CH_2S	CSO_2
973 K	[s]	[ppm]	[ppm]	[ppm]	[ppm]									
	2.86	252	3209	4	120		0.08	0.96	0.00	0.04		0.004	0.019	0.000
	4.57	372	3269	7	176		0.11	0.98	0.00	0.05		0.006	0.022	0.001
	6.86	769	3142	36	330		0.23	0.94	0.01	0.10		0.006	0.029	0.002
	13.72	1519	2422	133	560		0.46	0.73	0.04	0.17		0.090	0.089	0.013
1073 K	**2.86**	1262	2919	127	440		0.38	0.88	0.04	0.13		0.004	0.027	0.003
	4.57	1508	2594	169	500		0.45	0.78	0.05	0.15		0.070	0.064	0.020
	6.86	2348	2122	307	714		0.70	0.64	0.09	0.21		0.049	0.014	0.013
	13.72	3411	1345	599	808		1.02	0.40	0.18	0.24		0.122	0.047	0.040
1173 K	**2.86**	3350	1377	932	277		1.01	0.41	0.28	0.08		0.083	0.052	0.009
	4.57	4051	1286	1123	341		1.22	0.39	0.34	0.10		0.071	0.075	0.038
	6.86	5608	1267	1485	577		1.68	0.38	0.45	0.17		0.123	0.044	0.035
	13.72	5322	841	1520	382		1.60	0.25	0.46	0.11		0.103	0.036	0.026

Table D. 2: Model fitting of Arrhenius parameters to data. Note: S_2 was modeled but residuals of S_2 fit were not factored into the objective function since S_2 was not actually measured.

		MODEL						WEIGHTED SSE						
		CH_2 model	CH_2S model	CSO_2 model	CS_2 model			CH_2 model	CH_2S model	CSO_2 model	CS_2 model		OVERALL	
973 K	**t**						**Weight:**	**3 s.d.**	**1 s.d.**	**1 s.d.**	**N/A**		**SSE**	**0.43**
	2.86	0.07	0.93	0.00	0.03			0.040	0.764	7.557	1.537		**Wt SSE**	**85.2894**
	4.57	0.11	0.90	0.00	0.05			0.001	4.979	1.503	0.228		χ_ν^2	**2.7513**
	6.86	0.16	0.85	0.01	0.07			4.134	3.521	3.459	14.862			
	13.72	0.30	0.72	0.01	0.14			0.106	0.003	1.578	0.151			
1073 K	**2.86**	0.27	0.81	0.04	0.08			26.029	2.179	0.026	51.296			
	4.57	0.40	0.71	0.06	0.12			0.020	0.371	0.025	0.180			
	6.86	0.56	0.60	0.08	0.16			0.337	2.476	0.398	0.967			
	13.72	0.89	0.36	0.12	0.26			0.044	0.300	0.626	0.011			
1173 K	**2.86**	1.09	0.46	0.28	0.13			0.040	0.269	0.061	0.420			
	4.57	1.44	0.29	0.36	0.17			0.361	0.550	0.161	0.385			
	6.86	1.71	0.16	0.43	0.21			0.002	8.791	0.055	0.058			
	13.72	1.97	0.02	0.50	0.24			0.492	13.143	0.889	1.227			

Kinetic Parameters Estimation

Figure D.4 shows the apparent Arrhenius parameters determined in this work to those reconciled by Karan et al. for thermal splitting of H_2S. The apparent pre-exponential term for thermal splitting of H_2S, or frequency factor, is much less than the literature value. Similarly, the apparent activation energy is orders of magnitude less, which is expected due to exposure of ~0.59 cm^2 of catalytic molybdenum surface area.

Interestingly enough, both the activation energies and pre-exponential terms for thermal splitting (designating as reaction 1) by Karan et al. and steam reformation (designated as reaction 2) in this work are nearly identical. This is evident in the closeness of the curves in Figure D.4.

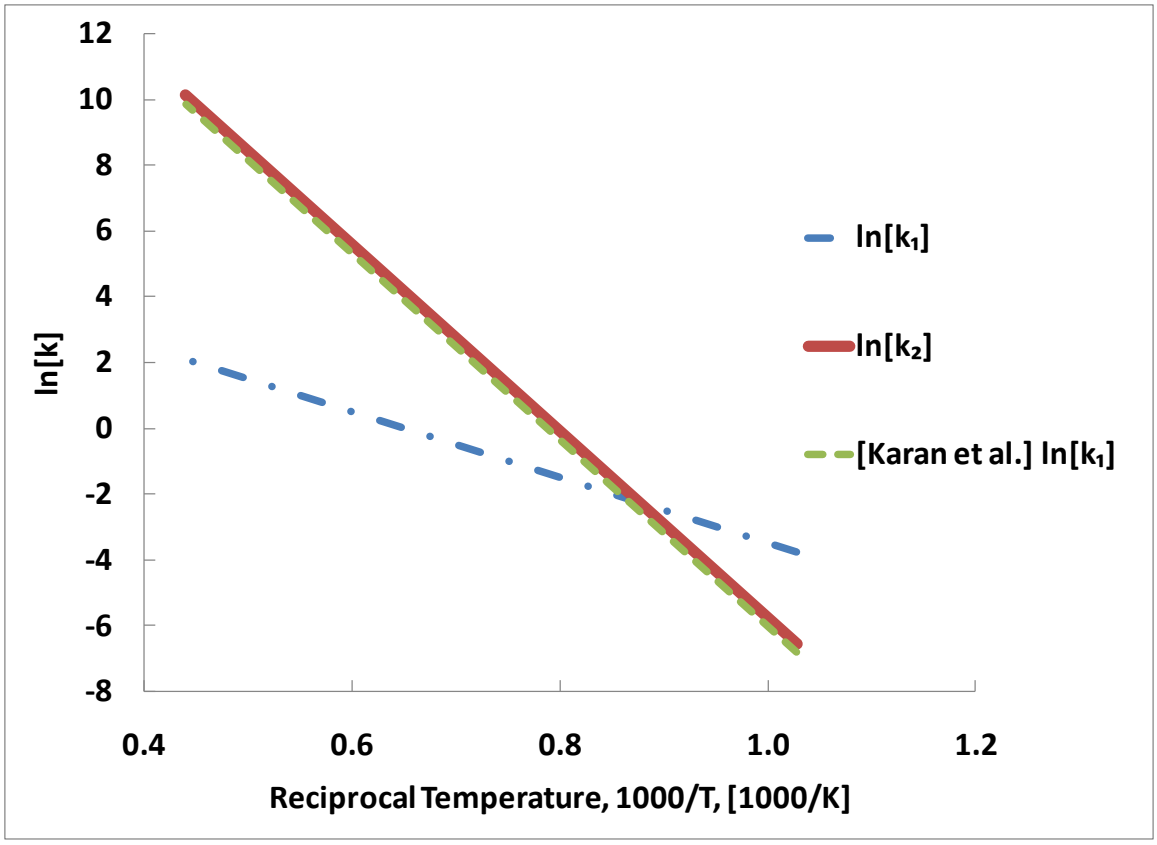

Figure D.4: Arrhenius parameters as reconciled by Karan et al. from several literature reports.[51]compared to apparent values obtained in this investigation.

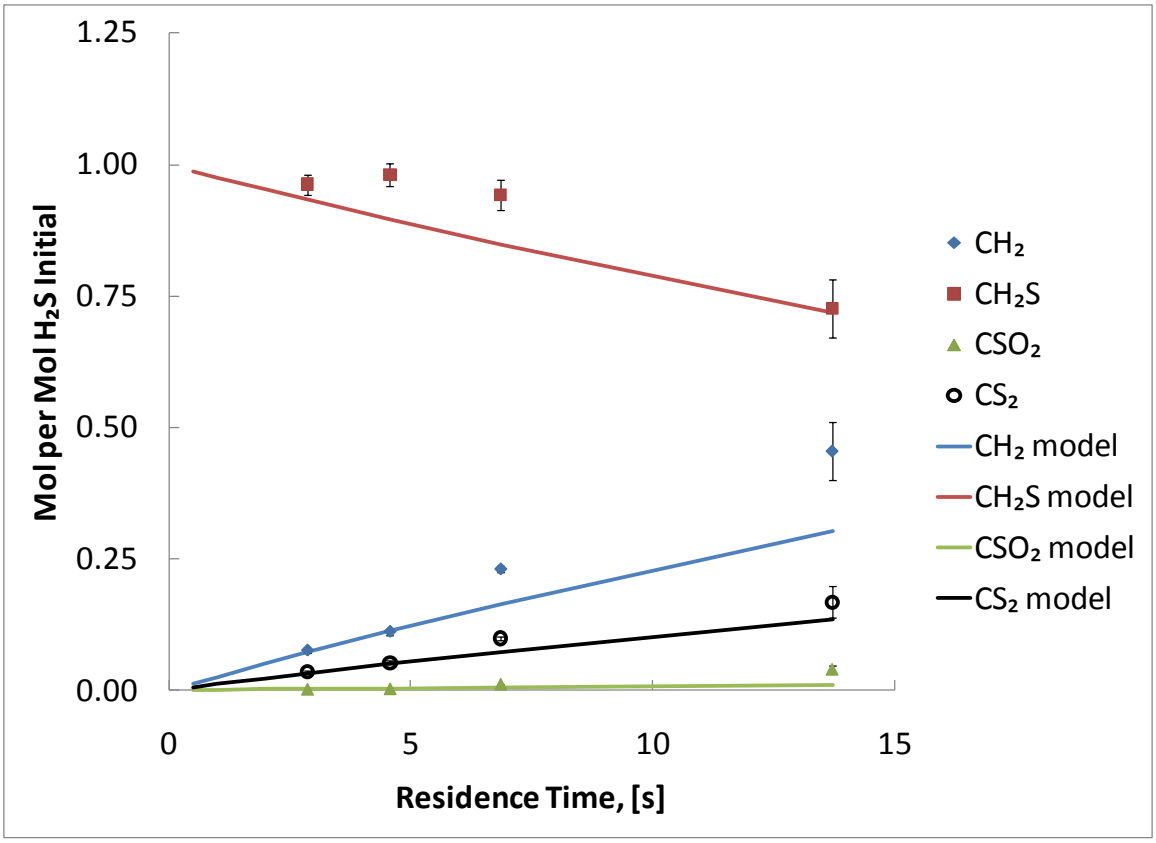

Figure D.5: Model fit to data at 700°C, 200:1 H_2O:H_2S molar ratio.

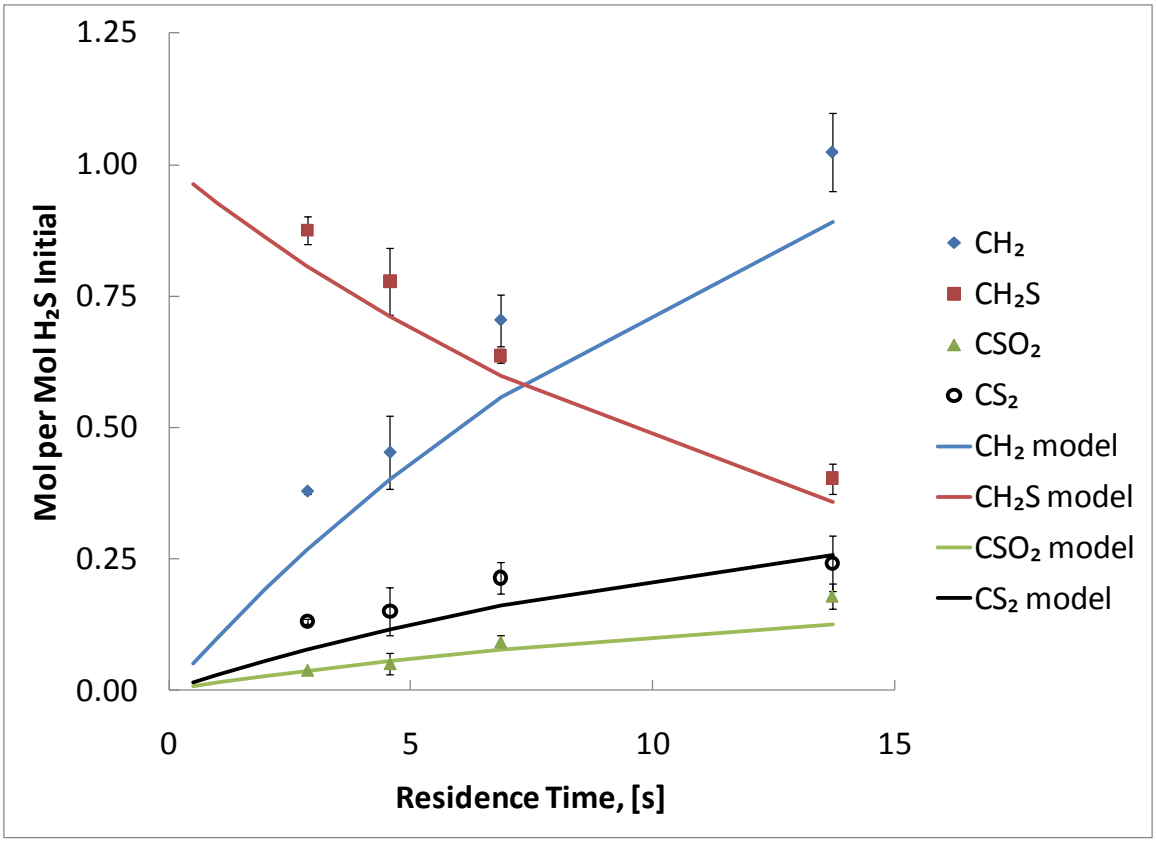

Figure D.6: Model fit to data at 800°C, 200:1 H_2O:H_2S molar ratio.

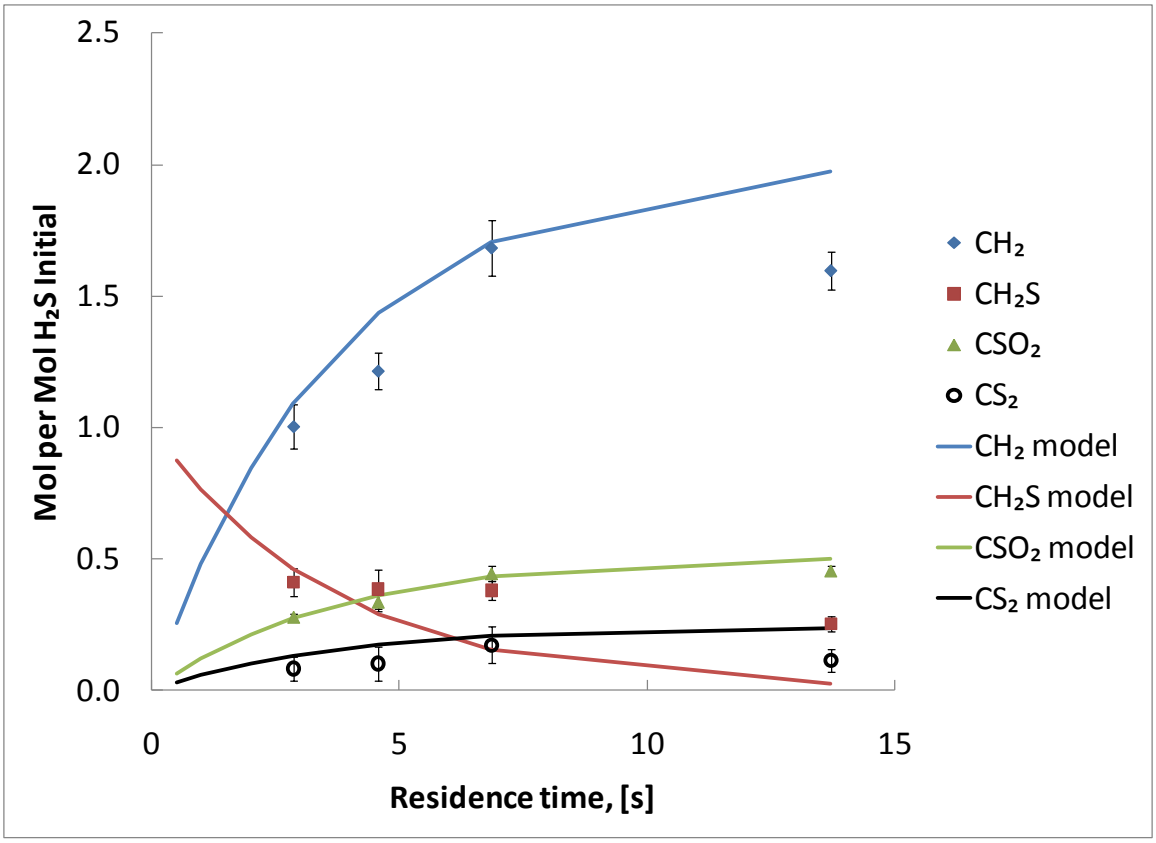

Figure D.7: Model fit to data at 900°C, 200:1 H_2O:H_2S molar ratio.

As described in Chapter 3, parameters were fit using a reduced chi-squared (χ_v^2) objective function. The residuals between the model and actual data can be used to construct normal probability plots (see Figure D.8) to ascertain whether or not the residuals are normally distributed and gain insight into how well a model describes the data by how linearity of the Z value-residuals plot. From the data below, it appears that the residuals are somewhat linear, however there is some skewness, especially in the combined plot of all species residuals. This is evidence that the model could use more complexity, which should be no surprise considering it has been simplified to only consider irreversible, pseudo-first order reactions. Before increasing complexity, however, more data and more importantly, a faster, more convenient means of measuring gas concentrations is required.

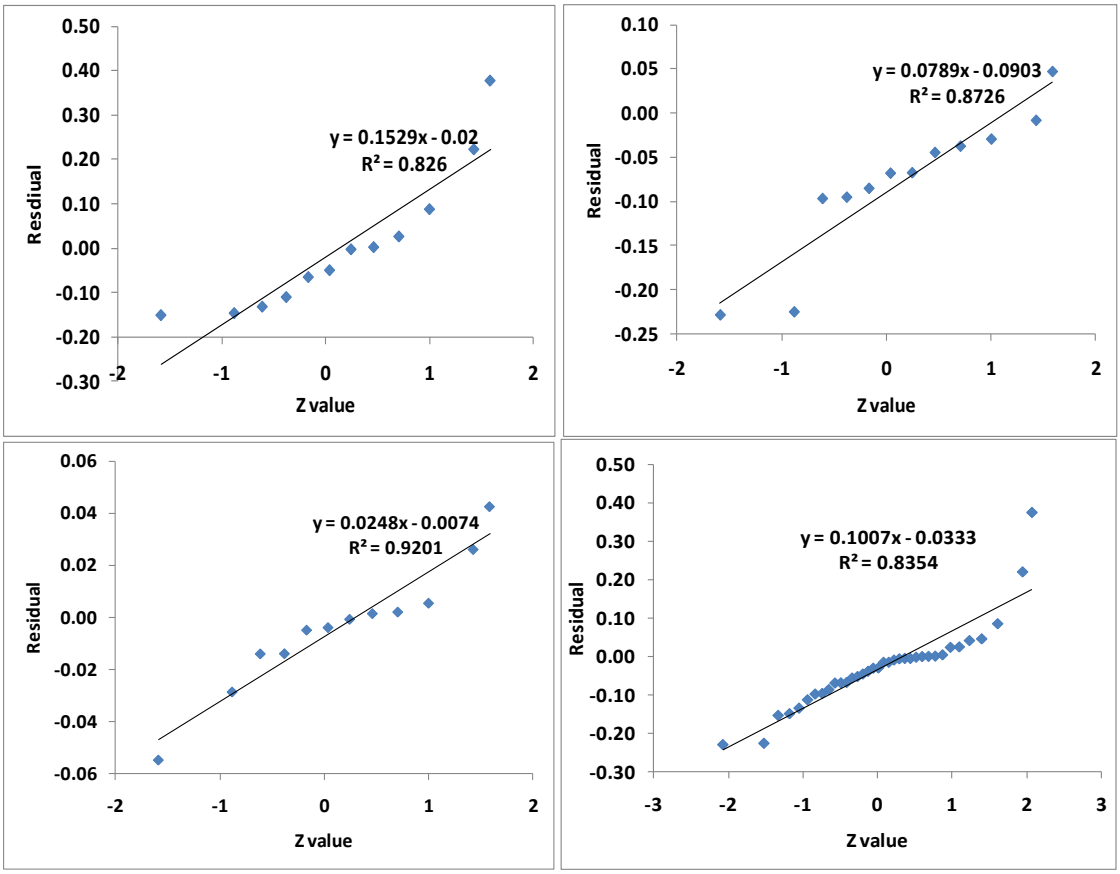

Figure D.8: Normal probability plots for a) H_2; b)H_2S; c) SO_2; d) All.

Table D. 3: Theoretical thermal load on steam reformation section.

T	ΔHrxn	ΔGrxn	ΔG/ηr+ΔH-ΔG	ΔH-ΔG	
[K]	[kJ/mol]	[kJ/mol]	[kJ/mol]	[kJ/mol]	K_2
1100	225	129	354	96	7.45E-07
1200	227	120	347	107	5.84E-06
1300	228	111	339	117	3.37E-05
1400	229	102	331	127	1.53E-04
1500	230	93	323	137	5.68E-04
1600	231	84	315	147	1.80E-03
1700	231	75	306	156	5.00E-03
1800	232	66	298	166	1.24E-02
1900	232	56	289	176	2.81E-02
2000	233	47	280	186	5.87E-02

Table D. 4: LHV overall thermal efficiency estimates at various H_2O:H_2S ratios

For 3 mol H_2 basis								
Energy Output	242	kJ/mol						
ηr	0.5							
Sulfuric Decomposition	352	kJ/mol						
Compression of SO_2	17	kJ/mol						
ΔHvap	40.65	kJ/mol						
H_2O:H_2S ratio:	2	5	10	15	20	25	30	35
T steam reformation step	η							
[K]								
1100	0.47	0.43	0.39	0.35	0.32	0.29	0.27	0.25
1200	0.47	0.43	0.39	0.35	0.32	0.29	0.27	0.25
1300	0.47	0.44	0.39	0.35	0.32	0.29	0.27	0.25
1400	0.47	0.44	0.39	0.35	0.32	0.29	0.27	0.25
1500	0.48	0.44	0.39	0.35	0.32	0.29	0.27	0.25
1600	0.48	0.44	0.39	0.35	0.32	0.30	0.27	0.25
1700	0.48	0.44	0.40	0.36	0.32	0.30	0.27	0.25
1800	0.48	0.45	0.40	0.36	0.32	0.30	0.27	0.26
1900	0.49	0.45	0.40	0.36	0.33	0.30	0.28	0.26
2000	0.49	0.45	0.40	0.36	0.33	0.30	0.28	0.26

Table D. 5: HHV overall thermal efficiency estimates at various H_2O:H_2S ratios

For 3 mol H_2 basis								
Energy Output	286	kJ/mol						
ηr	0.5							
Sulfuric Decomposition	352	kJ/mol						
Compression of SO_2	17	kJ/mol						
ΔHvap	40.65	kJ/mol						
H_2O:H_2S ratio:	2	5	10	15	20	25	30	35
T steam reformation step	η							
[K]								
1100	0.55	0.51	0.46	0.41	0.37	0.34	0.32	0.30
1200	0.55	0.51	0.46	0.41	0.38	0.34	0.32	0.30
1300	0.56	0.51	0.46	0.41	0.38	0.35	0.32	0.30
1400	0.56	0.52	0.46	0.42	0.38	0.35	0.32	0.30
1500	0.56	0.52	0.46	0.42	0.38	0.35	0.32	0.30
1600	0.56	0.52	0.46	0.42	0.38	0.35	0.32	0.30
1700	0.57	0.53	0.47	0.42	0.38	0.35	0.32	0.30
1800	0.57	0.53	0.47	0.42	0.38	0.35	0.32	0.30
1900	0.57	0.53	0.47	0.42	0.39	0.35	0.33	0.30
2000	0.58	0.53	0.47	0.43	0.39	0.35	0.33	0.30